



UNIVERSIDADE FEDERAL DO RIO GRANDE DO SUL
Instituto de Biociências
Programa de Pós-Graduação em Ecologia



UNIVERSIDADE FEDERAL DO RIO GRANDE DO SUL
INSTITUTO DE BIOCIÊNCIAS
PROGRAMA DE PÓS-GRADUAÇÃO EM ECOLOGIA

Tese de Doutorado

Modelo de simulação da dinâmica de vegetação em paisagens de coexistência campo-floresta
no sul do Brasil

CAROLINA CASAGRANDE BLANCO

Porto Alegre, setembro de 2011

Modelo de simulação da dinâmica de vegetação em paisagens de coexistência campo-floresta no sul do Brasil

Carolina Casagrande Blanco

Tese de Doutorado apresentada ao Programa de Pós-Graduação em Ecologia, do Instituto de Biociências da Universidade Federal do Rio Grande do Sul, como parte dos requisitos para obtenção do título Doutor em Ciências com ênfase em Ecologia.

Orientador: Prof. Dr. Valério De Patta Pillar

Comissão Examinadora

Prof. Dr. Gerhard Ernst Overbeck (UFRGS)
Prof. Dr. Manoel Ferreira Cardoso (CCST-INPE)
Profa. Dra. Vânia Regina Pivello (USP)

Porto Alegre, setembro de 2011

AGRADECIMENTOS

Os objetivos mais difíceis de serem alcançados tornam-se possíveis quando somos conduzidos sobre os ombros de gigantes e sob o amparo do amor. Agradeço a todos que fizeram parte desta minha caminhada para o amadurecimento pessoal e profissional:

Ao meu orientador Valério Pillar, pelo exemplo humano e profissional de motivação e compreensão e por ter proporcionado todo o apoio e a estrutura necessários para a realização deste trabalho.

Ao meu colega e amigo Enio Sosinski, pelo apoio profissional e pessoal para o desenvolvimento deste trabalho e por gentilmente disponibilizar o código fonte da estrutura inicial e o auxílio necessário para a construção do modelo bidimensional apresentado neste trabalho.

Ao colega Simon Scheiter e ao professor Steven Higgins, que gentilmente me receberam na Universidade Técnica de Munique, Alemanha (TUM), disponibilizando o código fonte do Modelo Adaptativo Global de Dinâmica de Vegetação (aDGVM) e fornecendo o auxílio necessário para a implementação do mesmo no modelo apresentado nesta tese.

Ao colega Guilherme Flach e ao professor Marcelo Johann, do Instituto de Informatics/UFRGS, pelo apoio técnico incondicional durante o processo de espacialização do aDGVM e para a operacionalização e bom funcionamento da configuração final do modelo bidimensional desenvolvido neste trabalho (2D-aDGVM).

Aos professores Roger Cousens (Universidade de Melbourne, Austrália) e Pedro Jordano (Estação Biológica de Doñana, Espanha) e ao colega Paul Caplat (Universidade de Queensland, Austrália) pelas discussões e apoio durante a implementação da equação que descreve os padrões de dispersão de sementes.

Ao colega Eliseu Weber, do Laboratório de Geoprocessamento/UFRGS, pelas discussões e apoio durante a implementação dos algoritmos para ajuste da radiação solar incidente para superfícies inclinadas.

À colega e amiga Ana Luiza Matte por gentilmente disponibilizar os mapas da área de estudo e pela serenidade e profissionalismo durante a preparação dos mesmos para utilização no modelo desenvolvido neste trabalho.

Aos queridos amigos e colegas (muitos quase irmãos), do Laboratório de Ecologia Quantitativa, em especial Sandra Müller, Alessandra Fidelis, Letícia Dadalt, Rafael Machado e Rodrigo Bergamin, Cláudia Porto, Melina dos Santos e Juliano Oliveira, pela parceria nos vários momentos inesquecíveis e pelo apoio incondicional nos momentos difíceis.

À coordenação do PPG-Ecologia/UFRGS e especialmente à Silvana, pela compreensão, serenidade e disposição nos momentos necessários.

À banca examinadora do exame de qualificação, professores Fernando Gertum Becker (UFRGS), Gerhard Overbeck (UFRGS) e José Pedro Pereira Trindade (EMBRAPA), pelas sugestões no primeiro e segundo capítulos desta tese.

Aos professores Gerhard Overbeck (UFRGS), Manoel Ferreira Cardoso (CCST-INPE) e Vânia Regina Pivello (USP), pelo pronto aceite em participar da banca examinadora da defesa desta tese. Antecipadamente, agradeço também pelas sugestões e críticas sobre o trabalho apresentado.

Ao Interamerican Institute for Global Change Research (IAI) pelo financiamento da maior parte deste trabalho através do projeto *From Landscape to Ecosystem: Across-scales Functioning in changing environments (LEAF)*, e à CAPES, pela bolsa de estudos concedida no período de finalização desta tese.

Ao companheiro Átila da Rosa, pela parceira, amizade e amor que vivemos ao longo de vários anos.

À minha querida família, início e pilar de tudo, tornando os momentos difíceis suportáveis. Meu eterno incentivo, apoio e inspiração à vida. Obrigada!

RESUMO

Uma questão que ainda instiga discussões na literatura ecológica é como explicar a ocorrência dinâmica e milenar de formações florestais e campestres sob um mesmo regime climático que tende a favorecer as primeiras, como ocorre atualmente com mosaicos floresta-campo no sul do Brasil. A partir de meados do século XX, têm-se evidenciado um fenômeno mundial de avanço de elementos lenhosos sobre áreas abertas. Neste sentido, a modelagem dos processos ecológicos envolvidos na manutenção de ambas as formações numa escala de paisagem permite o esclarecimento dos mecanismos que atuam na manutenção dessa coexistência até o presente e permite prever estados futuros diante dos prognósticos de drásticas alterações climáticas globais já nas próximas décadas. Para tanto, desenvolveu-se um modelo espacialmente explícito (2D-aDGVM) que agrega um Modelo Adaptativo Global de Dinâmica de Vegetação (aDGVM) e ainda inclui heterogeneidades topográficas, propagação do fogo e dispersão de sementes. Este modelo busca satisfazer a necessidade de modelagem mais realista de processos biofísicos, fisiológicos e demográficos na escala de indivíduos e relacionados de forma adaptativa às variações ambientais e aos regimes de distúrbios, ao mesmo tempo que agrega importantes processos ecológicos espaciais, até então pouco ou nada abordados por esse grupo de modelos numa escala de paisagem. Com este modelo, avaliaram-se os efeitos das variações topográficas da radiação solar incidente e destas nos mecanismos de interação (*feedbacks*) positiva e negativa que surgem daqueles processos na escala de indivíduos e que definem localmente os limites da coexistência entre elementos arbóreos e herbáceos. Ainda, foram analisados os efeitos do aumento da temperatura, precipitação e CO₂ atmosférico, desde o período pré-industrial até projeções futuras para as próximas décadas, na performance das diferentes fisiologias envolvidas, bem como no balanço daquelas interações entre as mesmas e, finalmente, na sensibilidade da dinâmica dos mosaicos floresta-campo. Os resultados evidenciaram que, sob o regime climático vigente, uma coexistência relativamente estável entre floresta e campo numa mesma paisagem é mantida por uma alta frequência de distúrbios, que por sua vez, resulta do forte *feedback* positivo do acúmulo de biomassa inflamável da vegetação campestre na intensidade do fogo, proporcionado pela condição altamente produtiva do atual clima mesotérmico. Por outro lado, intensificadas pela declividade do terreno, as heterogeneidades espaciais afetaram o balanço dessas interações, interferindo nos padrões espaço-temporais relacionados ao comportamento do fogo e dependentes da densidade de elementos arbóreos. Ainda, tanto esses efeitos observados na escala das manchas de vegetação, como o arranjo espacial inicial das mesmas na paisagem, afetaram as taxas de expansão florestal. Em outras palavras, a manutenção da coexistência de duas formações vegetais constituídas por elementos de inerente assimetria competitiva é possível pela manutenção de uma maior conectividade daquela que propicia o distúrbio, superando a vantagem da outra, que por sua vez é dependente da densidade dos indivíduos. Numa escala de paisagem, isto causa a manutenção de uma baixa conectividade entre as manchas florestais, propiciando sua relativa estabilidade num contexto de dispersão predominante a curtas distâncias. Contudo, embora ambos os sistemas tenham apresentado incremento no crescimento, produtividade e fecundidade, observou-se uma sensibilidade maior no sentido de aumento das taxas de avanço florestal em resposta às projeções climáticas futuras, principalmente nos próximos 90 anos, mesmo na presença do fogo. Isto seria proporcionado pela vantagem fotossintética das árvores-C₃ sobre gramíneas-C₄ na presença do fogo sob altas concentrações de CO₂ atmosférico. Por fim, uma abordagem mais sistêmica dos mosaicos como estados alternativos mostrou ser adequada para o entendimento dos mecanismos que propiciam essa coexistência dinâmica na paisagem.

Palavras-chave: autômatos celulares, DGVM, topografia, fogo, dispersão, campos sulinos.

ABSTRACT

A longstanding problem in ecology is how to explain the coexistence over thousands of years of forests and natural grasslands under the same climatic regime, which favors the first, such as in forest-grasslands mosaics in South Brazil. Since the middle of the 20th century, a worldwide *bush encroachment* phenomenon of woody invasion in open vegetation has been threatening this relatively stable coexistence. In this sense, modelling ecological processes that arbitrate the maintenance of both vegetation formations at the landscape scale allows a better understanding of the mechanisms behind the maintenance of this coexistence, as well as predictions of future states under projections of drastic climate change over the next decades. For this, we developed a bidimensional spatial explicit model (2D-aDGVM) that aggregates an adaptive Global Vegetation Model (aDGVM), which includes topographic heterogeneity, fire spread and seed dispersal. The model aims at fulfilling the need for a more realistic representation of biophysical, physiological and demographical processes using an individual-based approach as it adapts these processes to environmental variations and disturbance regimes. In addition, the model includes important spatial ecological processes that have gained less attention by such models adopting a landscape-scale approach. Therefore, we evaluated the effect of topographic variations in incoming solar radiation on positive and on negative feedbacks that rise from those individual-based processes, and which in turns define the limiting thresholds upon which woody and grassy forms coexist. Additionally, the effects of increasing temperature, rainfall and atmospheric CO₂ levels on the performance of distinct physiologies (C₃-tree and C₄-grass) were analyzed, as well as the sensitivity of forest-grassland mosaics to changes in climate from the preindustrial period to the next decades. Results showed that a relatively stable coexistence of forests and grasslands in the same landscape was observed with more frequent fires under the present climatic conditions. This was due to strong positive feedbacks of the huge accumulation of flammable grass biomass on fire intensity promoted by the high productivity of the present mesic conditions. On the other hand, spatio-temporal density dependent processes linked to fire and enhanced by slope at the patch scale, as well as the initial spatial arrangement of vegetation patches affected the rate of forest expansion at the landscape scale. The persistence of coexisting vegetation formations with an inherent asymmetry of competitive interactions was possible when the higher connectivity of the fire-prone patches (grassland) affected negatively the performance of the entire fire-sensitive system (forest). This was possible by overcoming its local density-dependent advantage, or by maintaining it with a low connectivity, which is expected to reduce the rate of coalescence of forest patches in a scenario of predominantly short distance dispersal. Despite the increments in biomass production, stem growth and fecundity that were observed in both grassland and forest, climate change increased the rates of forest expansion over grasslands even in presence of fire, and mainly over the next 90 years. This was attributed to a high photosynthetic advantage of C₃-trees over C₄-grasses in presence of fire under higher atmospheric CO₂ levels. Finally, in the face of the general observed tendency of forest expansion over grasslands, the ancient grasslands have persisted as alternative ecosystem states in forest-grassland mosaics. In this sense, exploring this dynamic coexistence under the concept of alternative stable states have showed to be the most appropriate approach, and the outcomes of this novel perspective may highlight the understanding of the mechanisms behind the long-term coexistence.

Key words: Climate change, grass-feedbacks on fire, seed dispersal, forest expansion, demographic model, process-based model, adaptive DGVM, cellular automata model, subtropical grasslands.

SUMÁRIO

Lista de Figuras	9
Lista de Tabelas	12
Introdução Geral	13
Capítulo 1: 2D-aDGVM: An adaptive Global Vegetation Model in a spatially explicit approach	20
Introduction	21
aDGVM parameterization and verification of vegetation growth and biomass	23
Parameterization and testing of stand-scale vegetation growth and biomass	23
Implementations for aDGVM spatialization.....	30
Solar radiation for inclined surfaces	30
<i>Results from predicted solar radiation</i>	32
Solar radiation and fuel moisture.....	35
<i>Results from simulated fuel moisture and fire intensity</i>	38
Fire spread in the 2D-aDGVM	42
Seed dispersal in the 2D-aDGVM.....	46
Model flow	47
2D-aDGVM parameterization and testing of spatio-temporal dynamics of forest-grassland mosaics	51
Input maps.....	51
Parameterization and validation of the 2D-aDGVM	52
<i>Seed dispersal</i>	53
<i>Fire frequency</i>	54
Validation of the 2D-aDGVM.....	54
References	59
Capítulo 2 (Artigo 1): Spatial heterogeneity and feedback mechanisms in forest-grassland mosaics	62
ABSTRACT	63
INTRODUCTION	65
METHODS.....	69
Model Description.....	69
Study site	71
Simulation experiments.....	72
Topography, fire frequency and vegetation dynamics	72

Spatial heterogeneity, patch aggregation and dynamics of forest-grassland mosaics	73
RESULTS	75
Spatio-temporal density-dependent mechanisms at the forest-fire fronts	75
Effects of spatial heterogeneity and patch aggregation on dynamics of forest-grassland mosaics	77
DISCUSSION	79
ACKNOWLEDGEMENTS	83
REFERENCES	83
Capítulo 3 (artigo 2): Sensitivity of forest-grassland mosaics to changes in climate and atmospheric CO₂	90
Abstract	91
Introduction	92
Materials and methods	95
<i>Model Description</i>	95
<i>Vegetation growth</i>	95
<i>Fire</i>	95
<i>Seed dispersal</i>	96
<i>Study site</i>	97
<i>Simulations</i>	98
<i>Sensitivity of forest expansion under changing climate and fire regimes</i>	98
<i>Potential vegetation growth under different climatic conditions</i>	101
<i>Data analysis</i>	101
Results	102
Discussion	106
Acknowledgements	109
References	110
Considerações finais	114
Referências bibliográficas	117
Apêndice 1: aDGVM: An adaptive dynamic global vegetation model for tropical ecosystems. Version 1.0	123

LISTA DE FIGURAS

CAPÍTULO 1: 2D-aDGVM: an adaptive Global Vegetation Model in a spatially explicit approach

- Figure 1. (A) Simulated and observed aboveground biomass on grassland sites. Observed data are from natural grasslands in Morro Santana, Porto Alegre, Brazil (Fidelis 2008), with different fire regimes. These simulations were conducted in scenarios with no trees and fire return interval of two-years, six-years or without fire. (B) Simulated and observed distribution of tree individuals (bars) and mean basal area (lines) per size class. Observed data are from semi-deciduous forest in Morro Santana, Porto Alegre, Brazil (Müller 2005). These simulations were conducted for 250 years starting with one young tree. Simulated results in A and B are the final means of ten repetitions of each simulation case (random seed varying from one to ten) 29
- Figure 2. Simulated and observed daily global solar radiation for horizontal surfaces (R_s). Observed data are from a climatic station of the Fundação Estadual de Pesquisa Agropecuária (FEPAGRO) in Cachoeirinha (a site 17 km away from Porto Alegre, Brazil. Means and standard deviations were obtained from periods of ten days, (Cargnelutti-Filho et al. 2007)). Simulated results used percentage of sunshine per day for Porto Alegre (New et al. 2002) to calculate R_s . Simulated results from the modified aDGVM include additional implementations proposed by Allen et al. (2006) to calculate radiation for inclined surfaces and were generated considering zero degrees of slope inclination 33
- Figure 3. Simulated ratio, R_d , of direct radiation for inclined surface to direct radiation on a horizontal surface showing seasonal variations as a function of slope aspect (A) and slope inclination. Simulations in (A) were conducted for 15 degrees of slope inclination and in (B) for north and south facing surfaces 34
- Figure 4. Moisture content of live and dead fuel biomass in north and south facing, forested and non-forested (A) cells (B). The graphs show mean monthly results of the new implementations for humidity at the fuel level, which accounts for solar heating (with the new implementations for solar radiation on inclined surfaces in open and shaded conditions) and wind cooling effects. These new implementations include improvements of the Canadian Fine Fuel Moisture Code (FFMC) for sunny (non-forested sites) conditions, as well as shaded (forested sites) conditions (Rothermel et al. 1986). Simulations in (A) and (B) were conducted with 50 degrees of slope inclination. Observed relative air humidity is from 1961–90 mean monthly data from a climatic station of the Instituto Nacional de Meteorologia (INMET) in Porto Alegre, Brazil. H_f = moisture content of open live fuel biomass; $H_f(\text{shaded})$ = moisture content of shaded live fuel biomass; $FFMC_{\text{open}}$ = moisture content of open dead fuel biomass; $FFMC_{\text{shaded}}$ = moisture content of shaded dead fuel biomass 39
- Figure 5. Simulated fire intensity and fuel moisture in non-forested (A) and forested cells (B), considering the new implementations for radiation on inclined surfaces (Allen et al. 2006), as well as the improvements of the Canadian Fine Fuel Moisture Code (FFMC) for moisture content at the fuel level for sunny (non-forested sites) conditions and shaded (forested sites) conditions (Rothermel et al. 1986). The graphs show mean monthly values for north and south facing cells with 50 degrees of slope inclination 41
- Figure 6. Probability of fire spread in forest and non-forest cells. The graph shows mean monthly values for horizontal (0° slope inclination), north and south facing cells with 50° of slope inclination. 45
- Figure 7. Schematic drawing showing the bias values attributed to a target cell and each of its eight neighbors in each fire spread iteration rule as a function of the prevailing northeast

wind direction (gray arrow). The hachured cell is the first ignited cell or any new ignited one.45

Figure 8. General scheme of model flow. Routines in bold are the new implementations in 2D-aDGVM. The other routines are original aDGVM routines.48

Figure 9. Observed and simulated forest expansion over grasslands in Morro Santana, Porto Alegre, Brazil (30°04'32"S; 51°06'05"W) considering vegetation and topographic sampled maps from a predominantly south face of the hill (72 ha). The graphic shows simulation results from different combinations of parameter values for seed dispersal distances (λ_1 = mean distance of short distance dispersal; λ_2 = mean distance of long distance dispersal, represented by colors of columns and squares) and probability of fire spread ($p_{fire} = 2.2\theta_{F(grass)} + 1.489$ for strong feedback of grass biomass on fire frequency, or a fixed value of $p_{fire} = 10\%$), searching for the best spatio-temporal fit between observed and simulated dynamics through simple matching (columns) and final proportion of landscape covered by forest (squares). Due to different observed dynamics from 1941 to 1985 and from 1985 to 2002 (see *Parameterization and validation of 2D-aDGVM*), parameters were tested considering different initial observed vegetation maps (1941 or 1985). Simulations considering the initial vegetation map of 1941 (black columns and squares) were conducted only with lower values of dispersal distance parameters, searching for the best fit with observed map from 1985 and 2002. Results for year 2002 were obtained from simulations considering the initial vegetation map from 1985. Simulations considered a spin-up phase of 100 years before starting seed dispersal and fire spread rule, to assure the aDGVM stabilization inside each 25m² cell. The lower panel shows snapshots from observed and simulated maps (black = forest; grey = grassland)..... 58

CAPÍTULO 2 (ARTIGO 1): Spatial heterogeneity and feedback mechanisms in forest-grassland mosaics

Figure 1. Simulation results of increasing tree density and cover using different values of slope inclination and orientation, in the absence of fire and considering frequent fires (fire return interval of 1-5 years) generated by strong feedback of grass biomass on fire frequency (Eq. 1). Vegetation growth is a function of input climatic and edaphic data from Morro Santana Hill, Porto Alegre, Brazil (30°04'32"S; 51°06'05"W). Simulations were conducted starting with one adult tree in one individual cell of size. Results from simulations are mean values from ten replicates of each simulation case 76

Figure 2. Simulation results from an artificial small grid with 20 x 20 cells of 25 m² each showing fire intensity and fuel biomass as a function of tree density in N facing (A) and S facing (S) cells, with different slope inclination. Vegetation growth is a function of input climatic and edaphic data from Morro Santana Hill, Porto Alegre, Brazil (30°04'32"S; 51°06'05"W). The grid was initialized with forest cover only in the central zone (the horizontal zone), and grasslands in the other surrounding zones (which had 15° of slope inclination in the first run and 30° of slope inclination in the second run). 77

Figure 3. Simulation results from observed and artificial landscapes (25-m² cells) showing forest expansion over grasslands in Morro Santana Hill, Porto Alegre, Brazil (30°04'32"S; 51°06'05"W) considering different initial proportion of landscape cover (A) and patch aggregation (lines in panel B), and in different topographic scenarios (observed predominantly south, observed predominantly north and artificial horizontal). Starting vegetation maps were the observed mosaic from year 1941 in the predominantly south face and an artificial map created by random allocation of forest patches (C). Results in panel A are mean values from ten replicates of each simulation case.

Expansion rates (bars in panel B) were obtained from these mean cover values of 50-year intervals (A)..... 79

CAPÍTULO 3 (ARTIGO 2): Sensitivity of forest-grassland mosaics to changes in climate and atmospheric CO₂

Figure 1. Predicted changes in temperature, rainfall and atmospheric CO₂ in Morro Santana (30°04'32"S; 51°06'05"W, Porto Alegre, Southern Brazil) from projected climate forcing data from IPCC (2007) SRES A1B scenario. Predictions for changes in temperature show only data from annual mean temperature (i.e., annual minimum and maximum temperatures are not shown). Predictions for rainfall show total annual rainfall (mm). 100

Figure 2. Dynamics of a forest-grassland ecotone under changing climate (IPCC (2007) SRES A1B projected climate scenario) from Morro Santana (30°04'32"S; 51°06'05"W, Porto Alegre, Southern Brazil). The graph shows simulated rates of forest expansion in 50 year-intervals in terms of increments in the proportion of cells with tree cover $\geq 50\%$, considering fire on (grey line) and fire off (dark line). Simulations were conducted in an artificial map with 9 km² (grain size 30 m). Starting landscape cover was a treeline covering 10% of the map with forest and the remaining adjacent 90% with grassland. The graph shows only results after the 100-years spin-up phase. Topographical variations were ignored (i.e., all cells had horizontal surface). Parameters for seed dispersal were: $p_{seed} = 0.80$ (proportion of seeds dispersed short distances from the sources); $\lambda_1 = 30$ m (mean distance for short distance dispersal of seeds); $\lambda_2 = 500$ m (mean distance for long distance dispersal of seeds) 103

Figure 3. Effects of increasing fine fuel biomass (aboveground live and dead grass biomass) on fire intensity (a) and on the proportion of trees killed by fire (b) from simulations in a forest-grassland ecotone under changing climate (IPCC (2007) SRES A1B projected climate scenario) from Morro Santana (30°04'32"S; 51°06'05"W, Porto Alegre, Southern Brazil). The graphs shows mean and error values from all cells with different fire-exclusion period (Last fire: 1 year, 2 years, 3 years, >3 years) burned during the periods 1900-1950 (303 ppm), 1950-2000 (333 ppm), 2000-2050 (434 ppm) and 2050-2100 (616 ppm), which are indicated by the corresponding increasing CO₂ levels (ppm). Simulations were conducted in an artificial map with 9 km² (grain size 30 m). Starting landscape cover was a treeline covering 10% of the map with forest and the remaining adjacent 90% with grassland. Topographical variations were ignored (i.e., all cells had horizontal surface). Parameters for seed dispersal were: $p_{seed} = 0.80$ (proportion of seeds dispersed short distances from the sources); $\lambda_1 = 30$ m (mean distance for short distance dispersal of seeds); $\lambda_2 = 500$ m (mean distance for long distance dispersal of seeds) ... 104

Figure 4. Potential values (no grass-tree interactions) of total grass production (aboveground and belowground biomass) for different fire return intervals (A), seed production (B) and tree height increment (C) under changing climatic conditions in the Morro Santana site (30°04'32"S; 51°06'05"W, Porto Alegre, Southern Brazil) from IPCC SRES A1B projected climate data. Simulations were conducted in a single cell with 900 m² (i.e., seed dispersal and fire spread in two dimensions were ignored). Simulations for evaluation of grass biomass production were conducted with no trees, and with fire on. Simulations for evaluation of seed production and tree growth were conducted with no grasses and no fire. For seed production, simulations started with one seedling (initial mass = 10 g) and for tree growth single seeds were allowed to germinate in specified years, as shown in C. Depicted values are the mean and the standard deviations after 10 replicates of each simulation case (random initializing seed varying from one to ten). In C, standard deviations are not show because the values were < 0.001 105

LISTA DE TABELAS

CAPÍTULO 1: 2D-aDGVM: an adaptive Global Vegetation Model in a spatially explicit approach

Table 1. Input data of general site characteristics required by the aDGVM (Scheiter and Higgins 2009). Data are from Morro Santana, Porto Alegre, Brazil (30°04'32"S; 51°06'05"W).....	25
Table 2. General overview of model input and output data.	49
Table 3. Model parameters used for validation of vegetation growth and spatio-temporal dynamics at Morro Santana, Porto Alegre, Brazil (30°04'32"S; 51°06'05"W). Table shows parameters from new implementations in 2D-aDGVM and only aDGVM parameters with changed values for model fitting. For a complete overview of all aDGVM parameters see Tables 1-15 in Appendix 1.	57

INTRODUÇÃO GERAL

No sul do Brasil, a co-ocorrência de florestas e campos persiste por milênios, mesmo sob um regime climático que favoreceria um domínio florestal, e continua instigando discussões acerca dos fatores e mecanismos envolvidos na coexistência dinâmica desses dois tipos vegetacionais de exigências ecológicas tão distintas (Lindman, 1906; Rambo, 1956; Klein, 1975; Pillar e Quadros, 1997; Pillar, 2003; Müller, 2005; Duarte, Santos *et al.*, 2006; Pinillos, Sarmiento *et al.*, 2009; Silva e Anand, 2011). Atualmente, no sul do Brasil as formações campestres naturais misturam-se na paisagem com diferentes formações florestais formando mosaicos (Teixeira, Coura-Neto *et al.*, 1986; Leite e Klein, 1990). Estudos de registros paleopolínicos, partículas de carvão (Behling, 2002) e isótopos de carbono (Duemig, Schad *et al.*, 2008; Silva e Anand, 2011) mostram que esses campos naturais são relictos de climas passados mais frios e mais secos do final do Pleistoceno e início do Holoceno (~12.000 anos antes do presente) e que uma expansão mais evidente das florestas sobre os campos foi estimulada por condições climáticas gradativamente mais quentes e úmidas após a última glaciação ocorrida nesse período. Por outro lado, análises dos registros de partículas de carvão em perfis de solo também evidenciaram um aumento na ocorrência de fogo no mesmo período, provavelmente relacionado à ocupação humana, o que deve ter favorecido a manutenção dos dois tipos vegetacionais na paisagem sob tais condições climáticas ao longo desses milhares de anos antes do presente (Behling, 2002).

Assim como as formações florestais (Oliveira-Filho e Fontes, 2000), atualmente esses campos antigos possuem uma alta diversidade de espécies e constituem uma fonte histórica de importantes serviços ambientais, culturais e sócio-econômicos locais (Overbeck, Müller *et al.*, 2007; Boldrini, Eggers *et al.*, 2009; Boldrini, 2009). Contudo, sob o atual clima subtropical úmido e diante das mais acentuadas modificações climáticas ocorridas nos últimos séculos devido ao aumento descontrolado de emissões de gases atmosféricos que causam o efeito

estufa (IPCC, 2007), na maioria dos casos, atualmente a persistência de grandes áreas de campo só é possível pela manutenção de algum regime de distúrbios (Boldrini e Eggers, 1997; Overbeck, Müller *et al.*, 2007). Contudo, a ocorrência de distúrbios como o fogo está na contramão da atual proposta nacional de redução de emissões (Lei nº12.187/2009 e Decreto nº7.390/2010) e dos procedimentos previstos na legislação ambiental para unidades de conservação que contemplam esse ecossistema (Lei nº 9.985/2000; Vélez, Chomenko *et al.*, 2009; Pillar e Vélez, 2010).

Neste sentido, a modelagem dos processos ecológicos envolvidos na co-ocorrência de florestas úmidas (sensíveis ao fogo) e formações abertas (campos e savanas) pirofíticas numa mesma unidade de paisagem permite o esclarecimento dos mecanismos que atuam na manutenção dessa coexistência de campos e florestas no Sul do Brasil até o presente e permite prever cenários futuros diante dos prognósticos de alterações climáticas globais, com efeitos diferentes (por vezes, drásticos) para cada regime climático regional predominante (principalmente em zonas de ecótonos vegetacionais), já nas próximas décadas (IPCC, 2007). Por exemplo, modelos globais de distribuição da vegetação prevêm a ocorrência de um domínio florestal na região sul do Brasil para as próximas décadas (na ausência de distúrbios), ao passo que para as regiões centro-norte e nordeste do Brasil é prevista a ocorrência de um rápido avanço das formações abertas pirofíticas, como o Cerrado, e de vegetação semi-desértica, como a Caatinga, sobre as florestas tropicais (Oyama e Nobre, 2004; Salazar, Nobre *et al.*, 2007; Hirota, Nobre *et al.*, 2010).

Diversos Modelos Globais de Dinâmica de Vegetação (*Dynamic Global Vegetation Models - DGVMs*) têm sido desenvolvidos para suprir uma carência geral dos modelos anteriores de tornar as previsões até então “estáticas” de modelos biogeográficos de distribuição potencial final da vegetação com base num clima predominante (Whittaker, 1971; 1978), em previsões que incluem processos biogeoquímicos em interação com distúrbios, sob um clima em constante alteração (Peng, 2000; Bachelet, Lenihan *et al.*, 2001; Cramer,

Bondeau *et al.*, 2001; Fisher, Mcdowell *et al.*, 2010). Mais recentemente, esse grupo de modelos tem refinado a representação dos sistemas ecológicos para a escala de indivíduos, permitindo um tratamento mais explícito e realista dos efeitos locais dos distúrbios nos processos demográficos (Sato, Itoh *et al.*, 2007; Scheiter e Higgins, 2009). Contudo, possivelmente devido à sua natureza voltada à modelagem em escala global, não só a espacialização dos mesmos para aplicação numa escala de paisagem, mas também importantes processos espaciais ecológicos que por conseguinte atuam nessa escala, como os efeitos das heterogeneidades espaciais na propagação dos distúrbios e a dispersão de propágulos em duas dimensões (i.e. considerando a interação entre as unidades operacionais de modelagem no espaço – células), até então tinham sido pouco ou nada abordados por esse tipo de modelo (Fisher, Mcdowell *et al.*, 2010).

Modelos são uma simplificação da realidade. Para tanto, torna-se necessária a representação da estrutura do sistema ecológico em questão com base em tipos funcionais representativos que exigem, por conseguinte, o conhecimento dos principais processos biofísicos, fisiológicos e demográficos envolvidos no desenvolvimento dos mesmos e que afetam localmente suas interações. A grande maioria dos estudos buscando compreender os mecanismos envolvidos na manutenção da coexistência entre elementos arbóreos e herbáceos num mesmo ambiente são referentes às savanas africanas. Por que essas duas formas tão distintas coexistem de maneira relativamente estável nesses ecossistemas, ao passo que em outras regiões um exclui o outro, tem sido o principal questionamento acerca do “problema das savanas” (Sarmiento, 1984). Várias explicações determinísticas (baseadas apenas em processos físicos) têm sido propostas, assim como várias tentativas de unificação das duas grandes categorias de modelos conceituais que se desenvolveram – os modelos baseados nos recursos (*botton-up controls*, como clima e disponibilidade de água e nutrientes no solo) e aqueles baseados nos distúrbios (*top-down controls*, como herbivoria e fogo) como controladores da estabilidade do sistema na escala de interação dos indivíduos (i.e. do

ecossistema savana) (Walter, 1971; Walker e Noy-Meir, 1982; Sarmiento, 1992; Pivello e Noton, 1996; Scholes e Archer, 1997; Higgins, Bond *et al.*, 2000; Langevelde, Van De Vijver *et al.*, 2003; Sankaran, Ratnam *et al.*, 2004; Bond, 2008). Contudo, tentativas recentes de previsão da distribuição dos ecossistemas numa escala continental com base em interações entre clima e distúrbios não chegaram a um consenso entre os tipos de vegetação esperados com aqueles observados, principalmente em regiões de clima mesotérmico, onde as condições hídricas e térmicas não são limitantes (Sankaran, Hanan *et al.*, 2005; Staver, Archibald *et al.*, 2010). Isto sugere que o entendimento dos mecanismos envolvidos na manutenção da coexistência de ecossistemas estáveis, porém de exigências ecológicas distintas, numa paisagem sob a influência de um mesmo limite restrito de condições climáticas necessita de uma abordagem mais sistêmica, ou seja, envolvendo as interações (*feedbacks*) positivas e negativas que surgem da atuação daqueles mecanismos controladores da dinâmica na escala dos indivíduos (Scheffer, Carpenter *et al.*, 2001; Beisner, Haydon *et al.*, 2003; Beckage e Ellingwood, 2008; Beckage, Platt *et al.*, 2009; Beckage, Gross *et al.*, 2011). Ou seja, num ambiente de coexistência entre tipos vegetacionais com exigências ecológicas distintas, interações positivas intra-específicas que favorecem a persistência de um determinado tipo vegetacional (*positive feedbacks*) constituem interações negativas inter-específicas (*negative feedbacks*), como a eliminação de elementos arbóreos pelo fogo ou a eliminação de elementos herbáceos pelo efeito de sombreamento proporcionado pelo adensamento dos primeiros (Warman e Moles, 2009; Staver, Archibald *et al.*, 2010).

Em outras palavras, embora indiscutível o papel determinante do clima na definição dos limites de ocorrência das formações vegetais (Woodward, Lomas *et al.*, 2004), os modelos existentes conseguem prever apenas transições graduais entre diferentes tipos vegetacionais, com base no clima predominante, mas falham ao tentar reproduzir as transições rápidas e abruptas que se observam naturalmente, por exemplo, entre savanas e florestas e entre florestas e vegetações campestres abertas nas zonas de clima mesotérmico (Sankaran, Hanan

et al., 2005; Beckage, Platt *et al.*, 2009; Higgins, Scheiter *et al.*, 2010; Staver, Archibald *et al.*, 2010). Assim, salvos os aspectos ecológicos particulares das espécies que constituem os sistemas em questão, surge o questionamento se essas interações positivas e negativas que definem os padrões espaço-temporais de organização e coexistência dentro de um determinado ecossistema (ex. árvores e gramíneas em savanas) são aplicáveis para o entendimento da coexistência de distintas formações vegetacionais que se estabelecem quando um elemento exclui o outro em zonas de tensão ecológica (Warman e Moles, 2009; Staver, Archibald *et al.*, 2010). Ainda, o quanto e como o balanço dessas interações será afetado pelas alterações climáticas futuras, assim como os possíveis impactos na estabilidade das coexistências, são questões que necessitam ser exploradas (Walther, Post *et al.*, 2002; Parmesan, 2006).

Um dos fenômenos que tem sido observado em escala global e que pode ser atribuído diretamente ao “efeito fertilizante” da contínua elevação dos níveis de dióxido de carbono atmosférico (CO₂) desde o início do período industrial é o aumento da invasão de elementos lenhosos nas formações abertas de um modo geral (*bush encroachment*) (Bowman, 2000; Van Auken, 2000; Roques, O'Connor *et al.*, 2001; Cabral, De Miguel *et al.*, 2003; Oliveira e Pillar, 2004; Goetze, Hörsch *et al.*, 2006; Silva, Sternberg *et al.*, 2008; Bai, Boutton *et al.*, 2009). Uma das hipóteses para explicar esse favorecimento das formações lenhosas é o efeito desse aumento de CO₂ (efeito fertilizante) no incremento das taxas de recrutamento e sobrevivência dos elementos lenhosos em ambientes propícios à queima, como as formações abertas, devido à vantagem fotossintética dos elementos florestais C₃ em relação aos elementos graminóides C₄ sob altos níveis de CO₂ (Bond e Midgley, 2000). No entanto, essa hipótese tem sido mais frequentemente explorada na mesma escala de tratamento teórico, empírico e preditivo daqueles descritos anteriormente para as interações entre os mecanismos controladores da dinâmica dos sistemas, necessitando, contudo, da exploração da possibilidade de sua aplicação para o entendimento da coexistência de distintas formações vegetacionais numa

mesma paisagem (Drake, Gonzàlez-Meler *et al.*, 1997; Bond, Midgley *et al.*, 2003; Silva, Anand *et al.*, 2009).

Finalmente, surge a necessidade de ferramentas adequadas para modelagem dos padrões observados de coexistência entre formações vegetacionais distintas numa mesma paisagem para o entendimento dos processos que desencadeiam esses fenômenos e para a previsão de comportamentos e cenários futuros frente às alterações climáticas globais, assim como para a sua utilização em estratégias de conservação. Neste sentido, o objetivo geral desta tese foi o desenvolvimento de um modelo para a simulação da dinâmica de vegetação de mosaicos floresta-campo numa escala de paisagem (i.e., um cenário de coexistência entre as duas formações vegetacionais numa área geográfica definida). Para tanto, desenvolveu-se um modelo espacialmente explícito (2D-aDGVM), que agrega um Modelo Adaptativo Global de Dinâmica de Vegetação (aDGVM, Scheiter e Higgins, 2009) e ainda inclui heterogeneidades topográficas, propagação do fogo e dispersão de sementes. O modelo simula uma formação vegetacional (campo, floresta ou coexistência árvores-gramíneas) com base nas condições climáticas e edáficas locais. Esse modelo é dito adaptativo porque adapta fenologia e alocação de carbono às variações climáticas e ainda simula outros processos biofísicos, fisiológicos e demográficos na escala de indivíduo. Interações competitivas entre tipos funcionais representativos dos sistemas (um tipo C_3 -arbóreo e um tipo C_4 -graminóide) são determinadas por luz e disponibilidade hídrica do solo, e o fogo atua nas interações inter-específicas e na dinâmica das populações arbóreas. Neste trabalho, esse modelo foi adaptado para simular independentemente a dinâmica de vegetação em cada unidade da paisagem (pixel = célula), ajustando as condições microclimáticas de cada célula às variações topográficas da radiação solar incidente, ao mesmo tempo em que permite a interação entre várias dessas unidades através da propagação do fogo e da dispersão de sementes ao longo da paisagem. Esse modelo foi utilizado para simular a dinâmica espaço-temporal dos mosaicos floresta-campo que se encontram no Morro Santana, Porto Alegre, RS, permitindo elucidar algumas questões acerca

dos mecanismos controladores dessa coexistência dinâmica e que constituem os objetivos específicos desta tese, a saber: elucidar os efeitos das heterogeneidades espaciais nas interações (*feedbacks*) positivas e negativas entre os tipos vegetacionais, bem como os efeitos das variações climáticas no balanço dessas interações e na dinâmica dos mosaicos.

Assim, a presente tese está estruturada em três capítulos, sendo os dois últimos apresentados na forma de artigo científico. O primeiro capítulo apresenta uma abordagem técnica para a descrição, parametrização e validação do modelo proposto para o local de estudo e constitui um material complementar na forma de apêndice do segundo capítulo. O segundo capítulo constitui o primeiro artigo científico da tese. Neste capítulo são explorados os efeitos das heterogeneidades espaciais nos mecanismos de interação (*feedbacks*) positiva e negativa que surgem de processos biofísicos, fisiológicos e demográficos e que definem localmente os limites da coexistência entre elementos arbóreos e herbáceos. Ainda, são explorados como esses mecanismos determinam a dinâmica dos mosaicos de vegetação na escala de paisagem considerando as condições climáticas atuais. O terceiro capítulo constitui o segundo artigo científico da tese. Neste capítulo são avaliados os efeitos de mudanças climáticas futuras na dinâmica de vegetação dos mosaicos floresta-campo. Numa abordagem temporal, são analisados os efeitos de projeções futuras (IPCC, 2007) de mudanças na temperatura, precipitação e níveis de dióxido de carbono atmosférico (CO₂) na produção primária e crescimento dos indivíduos e consequentemente na performance das diferentes fisiologias envolvidas (árvores C₃ e gramíneas C₄), bem como no balanço daquelas interações positivas e negativas entre as mesmas e, finalmente, na sensibilidade da dinâmica dos mosaicos floresta-campo às variações climáticas ocorridas desde o período pré-industrial até projeções futuras para as próximas décadas.

CAPÍTULO 1

2D-aDGVM

An adaptive Global Vegetation Model in a spatially explicit approach¹

¹ Este capítulo é o material complementar do capítulo 2 da tese, que constitui o manuscrito de Blanco, C.C., Scheiter, S., Sosinski, E. Fidelis, A., Anand, M. e Pillar, V.D., intitulado “Spatial heterogeneity and feedback mechanisms in forest-grassland mosaics, que será submetido para publicação na revista Ecology.

Introduction

Dynamic Global Vegetation Models are models capable to capture the effect of changing climate on biosphere dynamics, considering the effect of natural disturbances and human activities in shaping vegetation dynamics and distribution (Peng 2000). In these models, vegetation is represented by pre-defined plant types, which grow according to mechanistic physiological processes (e.g. Woodward et al. 1995). Therefore, climatic, ecological (e.g., ontogeny and phenology) and disturbance-based processes define structure and dynamics of the operational “communities”.

The primarily purpose for the development of the first DGVMs was to simulate terrestrial ecosystem responses to CO₂ and climate change going a step further from static to a dynamic biogeographical global vegetation modelling (for reviews about progress in modeling vegetation dynamics and a general overview of DGVMs structure and functioning see Cramer et al., 2001 and Peng, 2000). Therefore, the first generation of DGVMs two decades ago had focused on climate as the predominant factor shaping vegetation structure and dynamics, attempting to fulfill the need for modelling vegetation dynamics through population processes at a larger scale than the existing gap (or patch) models. This was achieved by coupling large-scale static biogeographic models (which simulate climatic-based distribution of potential vegetation) with dynamic biogeochemical models (which simulate processes such as carbon and nitrogen cycling) (Peng 2000). During the last decade, the second generation of DGVMs has treated more explicitly the effects of disturbance in individual-based representations of demographic processes within their discrete units of modelling (e.g. cell, pixel) (e.g., Bond et al., 2003; Woodward and Lomas, 2004; Sato et al., 2007; Scheiter and Higgins, 2009). However, important spatio-temporal processes operating at the landscape scale, such as variations in microclimatic conditions (e.g. topography), fire-

spread behavior and the movement of propagules in two dimensions, have gained little attention by such models (Cramer et al. 2001, Fisher et al. 2010).

This supplemental material presents the description, parameterization and testing of the 2D-aDGVM, a spatially explicit model implemented in C++ programming language, which incorporates an adaptive Global Vegetation Model (aDGVM) (Scheiter and Higgins 2009) to simulate dynamics of forest-grassland mosaics in Southern Brazil. The model includes topographic variation (slope declination and orientation) and simulates fire spread behavior and seed dispersal in two dimensions. Data from Morro Santana, Porto Alegre, Southern Brazil (30°04'32"S; 51°06'05"W) were used for modelling dynamics of forest-grassland mosaics with the 2D-aDGVM. Therefore, first we present the parameterization of the aDGVM (Scheiter and Higgins 2009) to this site, as well as further verification of predicted vegetation growth, structure and biomass in the presence and absence of fire. For the spatialization of the aDGVM, additional algorithms for scaling-down from climatic to microclimatic predictions (i.e. adjusted to topographic variations) were included in the aDGVM, such as those for calculating solar radiation on inclined surfaces, as well as heating and drying of dead fuel moisture accordingly. To simulate vegetation processes in discrete space, additional algorithms were implemented to adjust probability of fire spread and to define the distribution of seeds dispersed across the landscape. A general overview of the 2D-aDGVM model flow provides a synthesis of all aDGVM modifications and new implementations, as well as how the 2D-aDGVM simulates vegetation processes in a two-dimensional context. Finally, parameterization and testing of the 2D-aDGVM were conducted by using vegetation maps of the same study site and from different time steps to evaluate the predictive power of the model in simulating observed spatio-temporal vegetation dynamics.

aDGVM parameterization and verification of vegetation growth and biomass

Data from Morro Santana, Porto Alegre, Southern Brazil (30°04'32"S; 51°06'05"W) were used for aDGVM parameterization and testing. Morro Santana is a granitic hill (altitude max. 311 m a.s.l.) with approximately 1,000 ha. The climate is subtropical humid, with mean annual precipitation of 1348 mm, well distributed in the year, and average annual temperature of 19.5°C (Nimer 1990). Soils are developed from granite (acrisols, alisols and umbrisols) and there's apparently no restriction for forest development on grassland areas (Garcia Martinez 2005). Vegetation is a mosaic of forest (with species from Semideciduous Seasonal Forest and Atlantic Rain Forest) and "Campos" grasslands (with a dominance of C₄ grasses). The dominant forest tree species is *Guapira opposita* (Vell.) Reitz (Nyctaginaceae), and the most frequent forest tree species colonizing adjacent grassland areas are *Myrciaria cuspidata* O.Berg (Myrtaceae), *Lithrea brasiliensis* March. (Anacardiaceae) and *Symplocos uniflora* (Pohl) Benth. (Symplocaceae) (Müller 2005). Local evaluations in forest-grassland boundaries in burned and unburned grasslands areas in Morro Santana found that from all woody species colonizing grasslands, 65.8% were resprouters. However, more than 90% of individuals were shrub species. Forest trees were represented by low number of individual (average of 1.09/m² in border plots – 0 to 4.5 m from forest edge – and 0.13/m² in grassland plots unburned in the last four years) (Müller 2005).

Parameterization and testing of stand-scale vegetation growth and biomass

Stand-scale vegetation dynamics (grassland, forest, grass-tree coexistence) are simulated by the aDGVM (Scheiter and Higgins 2009) as a function of climatic and soil conditions, as well as competitive inter and intra-specific interactions between C₃-trees and C₄-grasses mediated by light (shading effects), water (in different soil layers) and fire (frequency is defined by a fixed probability p_{fire} , and intensity is calculated by a semi-

empirical model based on fuel biomass, moisture and wind speed). Trees and grasses are morphologically represented as ‘typical’ ones. Trees are simulated individually but grasses are considered to be of two kinds of superindividuals (grass biomass between and grass biomass below tree canopies). For a more detailed description of the aDGVM, see Appendix 1.

Some input data of monthly climatic and general edaphic site characteristics are required by the aDGVM (Scheiter and Higgins 2009) (Table 1). Climatic data for maximum, mean and minimum temperatures, as well as relative air humidity were obtained from 1961–1990 mean monthly data from a climatic station of the Instituto Nacional de Meteorologia (INMET) in Porto Alegre, Brazil. Wind speed, sunshine, probability of wet days and frost, as well as the two parameters for the rain generator were obtained from New et al. (2000, 2002). Elevation and soil input variables such as bulk density, soil nitrogen and soil carbon content were obtained from a local study (Garcia Martinez 2005) of soil profiles in grassland and forest patches in Morro Santana, Porto Alegre. Field capacity and wilt point were obtained from Solano Peraza (2003) for unidade Gravataí (PVAd9) following the local soil classification of Streck et al. (2008).

Table 1. Input data of general site characteristics required by the aDGVM (Scheiter and Higgins 2009). Data are from Morro Santana, Porto Alegre, Brazil (30°04'32"S; 51°06'05"W).

Parameter	Description	Value												Units
		Jan	Feb	Mar	Apr	Mai	Jun	Jul	Ago	Sep	Oct	Dec		
T_{\min}	Minimum temperature ¹	20.5	20.8	19.3	16.3	13	10.7	10.7	11.5	13.1	15	17	17	°C
T_{\max}	Maximum temperature ¹	30.2	30.1	28.3	25.2	22.1	19.4	19.7	20.4	21.8	24.4	26.7	26.7	°C
\bar{T}	Mean temperature ¹	24.6	24.7	23.1	20.1	16.8	14.3	14.5	15.3	16.8	19.2	21.3	21.3	°C
r_{α}	Parameter for rain generator ²	3.23E-06	4.06E-06	3.92E-06	2.50E-06	2.08E-06	3.14E-06	3.31E-06	3.13E-06	4.38E-06	3.44E-06	2.66E-06	2.66E-06	unitless
r_{β}	Parameter for rain generator ²	3.52E-04	4.60E-04	4.28E-04	2.44E-04	2.02E-04	4.27E-04	4.14E-04	4.29E-04	6.29E-04	4.12E-04	2.67E-04	2.67E-04	unitless
h_s	Relative humidity ¹	71	74	75	77	81	82	81	79	78	74	71	71	%
w_f	Wet day frequency ²	0.625	0.569	0.585	0.385	0.450	0.549	0.529	0.532	0.598	0.539	0.516	0.516	frequency
p_s	Percentage of sunshine per day ²	0.549	0.55	0.521	0.528	0.508	0.448	0.464	0.44	0.42	0.498	0.526	0.526	%
u_{ref}	Reference wind speed ²	2.7	2.5	2.1	1.9	1.7	1.8	1.8	2.1	2.7	3	3	3	m/s
d_f	Frost ²	0	0	0	0	0	0.4	0.5	0.1	0	0	0	0	days/month
Z	Elevation ³	291												m
θ_{wp}	Wilting point ⁴	0.13												mm
θ_{fc}	Field capacity ⁴	0.23												mm
p_b	Bulk density ⁴	1.37												g/cm ³
S_N	Soil nitrogen content ³	150												g/m ²
S_C	Soil carbon content ³	880												g/m ²

¹Mean monthly data (1961-1990) from Instituto Nacional de Meteorologia (INMET) in Porto Alegre, Brazil.

²New et al. (2000, 2002).

³Garcia Martinez (2005).

⁴Solano Peraza (2003).

Besides the input of soil and climate variables, some of the most sensitive parameters of the aDGVM are allometric parameters such as the coefficients used to translate the calculated aboveground plant biomass into plant height (H_1 and H_2) (Scheiter and Higgins 2009). Local data from Morro Santana for tree height (m) and stem diameter (cm) were used to calculate the allometric parameters H_1 and H_2 . To estimate aboveground biomass (Kg), tree volume (m^3) and wood density ($Kg.m^{-3}$) are needed. Tree volume (V) was obtained by the product $V = h \times d^2 \times 0.4$, where h is tree height (m), d is stem diameter (m) and 0.4 is a general correction factor for trees (Tilki and Fisher 1998). Volume was calculated for species for which wood density is known from local literature (36 species) (Reitz et al. 1988, Lorenzi 2000) or local floristic surveys. A total of 1684 individuals were used to calculate V from mean values of individual h and d measurements for each of the 36 species. Following the procedures described by Higgins et al. (2007) (Appendix B of the related online support material in that paper) to estimate tree biomass from height, the obtained empirical relationship between height (h , m) and stem diameter (d , cm) $d = 1.5893h$ ($R^2 = 0.65$) was applied to the general equation that estimates biomass (M , Kg) from stem diameter (d , cm) for Morro Santana $M = 0.0312d^{2.7824}$ ($R^2 = 0.97$) to yield the equation for tree height (h , m) as function of aboveground tree biomass (M , kg) $h = 2.1877M^{0.3594}$, where $H_1 = 2.1877$ and $H_2 = 0.3594$.

For verification of vegetation growth and grass biomass, simulated aboveground live and dead biomass grass ($Kg.m^{-2}$), tree basal area (m^2) and tree height (m) were compared to observed values in Morro Santana, Porto Alegre (Müller 2005, Fidelis 2008). In the aDGVM, grassland is the default state; otherwise, an initial input number of trees is required (Scheiter and Higgins 2009). In addition, fire frequency can be parameterized by changing p_{fire} . Therefore, simulations for verification of grass biomass were conducted in scenarios with no trees and mean fire return intervals of two-years ($p_{fire} = 50\%$) and six-years ($p_{fire} = 10\%$)

(calibrated values of p_{fire} to generate these observed fire-return intervals). Simulations for verification of tree growth in grassland cells were conducted by starting with one seedling (initial weight of 10 g) after a spin-up phase of 100 years and in the absence of fire. Mean basal area and mean tree height were used to compare the observed and the simulated vegetation structure. The set of observed data used for verification of basal area was different from the set of data used in model parameterization as described earlier. All simulations were conducted for 250 years (considering a spin-up phase of 100 years) in a one-hectare cell. All the comparisons are qualitative and the simulated results were obtained by averaging ten repetitions of each simulation case (random seed varying from one to ten).

Simulation results showed that aboveground grass biomass (live and standing dead leaves) was more similar to the observed mean (considering only grasses, live and dead biomass) for a fire interval of two years than for a six-year fire interval (Figure 1A). Considering the fire interval of six years, simulated grass biomass was higher than the observed mean grass biomass. In addition, the latter was lower for six-year fire interval than for a two-year interval. This was attributed to the observed increase of herbs and tall shrubs (max. height of 1 m) as fire frequency decreases (from two to six years) in the experimental area, causing a pronounced reduction in total grass biomass (Fidelis 2008). In fact, even without considering trees these simulations have showed an accumulation of dead biomass of grasses in the absence of fire (Figure 1A). Simulations conducted by starting with one young tree and in the absence of fire predicted the local observed general tendency of a woodland cover (proportional tree cover > 60%, following the classification adopted by Scheiter and Higgins (2009)).

In general, after 40 ± 0.52 years in the absence of fire, the simulated space was completely covered by trees (proportional tree cover reached 100%), and tree cover remained stabilized until the end of simulations (not shown). In the simulated forested cell, the average maximum tree height was 11.6 m and mean basal area was $0.007618 \text{ m}^2 (\pm 0.0004693)$ (not

shown). Local studies in forested areas of Morro Santana (Müller 2005) recorded a maximum tree height of 12 m and mean basal area of 0.003710 m^2 (± 0.01643) between all tree individuals (not shown). The higher value of simulated mean basal area can be explained by the different patterns between observed and simulated distribution of tree individuals in size classes (bars in Figure 1B). Simulated results showed higher proportions of individuals in the higher size classes (47.7% of simulated individuals with more than 9 m) (light grey bars in Figure 1B) than the observed data (3.11% with more than 9 m) (dark grey bars in figure 1B). Alternatively, 64.2% of observed tree individuals had a maximum of 2 m (dark grey bars in Figure 1B). These observed higher numbers of mid-sized individuals might be an evidence of recent forest regeneration after logging during the 19th century in the region. Simulated results are from the end of simulations, i.e., after stabilization of tree cover and number. Mid-sized trees were more abundant in intermediate (non-stable) periods during simulations (not shown). Despite the difference between simulated and observed mean basal area when considering all individuals, the values showed better agreement when compared by size class, except for individuals higher than 10 m (lines in Figure 1B).

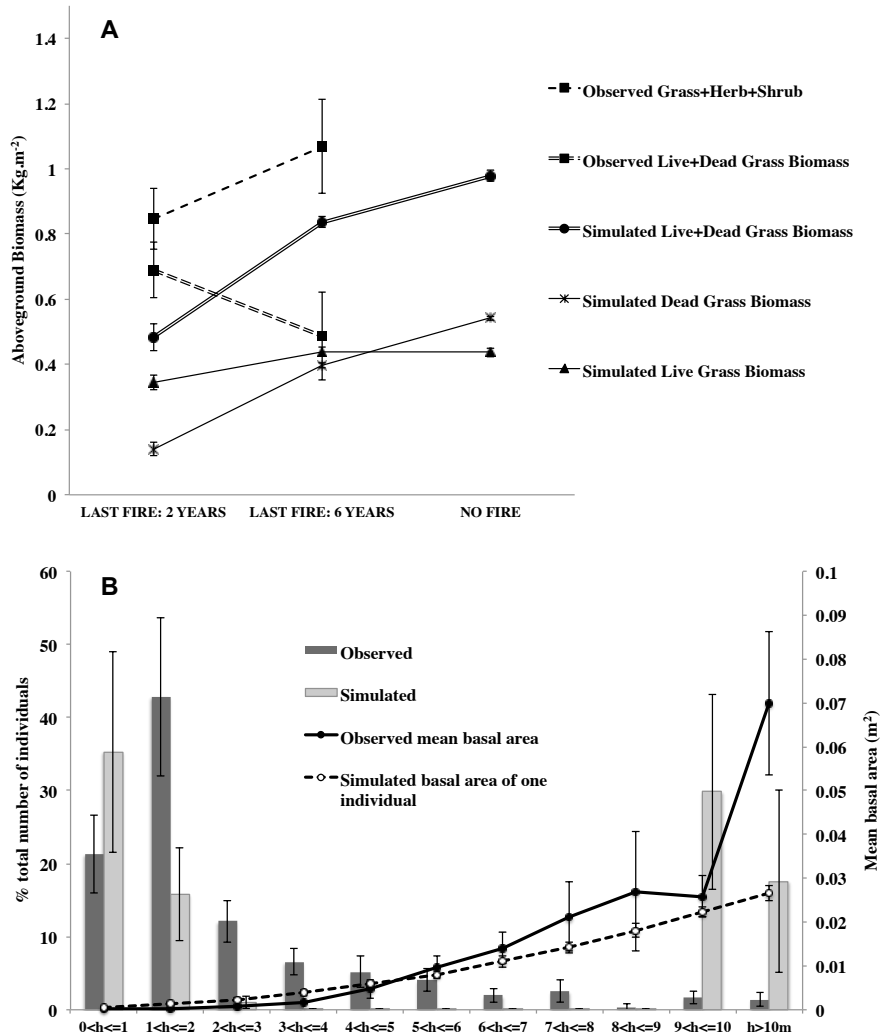


Figure 1. (A) Simulated and observed aboveground biomass on grassland sites. Observed data are from natural grasslands in Morro Santana, Porto Alegre, Brazil (Fidelis 2008), with different fire regimes. These simulations were conducted in scenarios with no trees and fire return interval of two-years, six-years or without fire. (B) Simulated and observed distribution of tree individuals (bars) and mean basal area (lines) per size class. Observed data are from semi-deciduous forest in Morro Santana, Porto Alegre, Brazil (Müller 2005). These simulations were conducted for 250 years starting with one young tree. Simulated results in A and B are the final means of ten repetitions of each simulation case (random seed varying from one to ten).

Implementations for aDGVM spatialization

Solar radiation for inclined surfaces

In the aDGVM (Scheiter and Higgins 2009), photosynthetic active radiation and net radiation are computed for daily periods and horizontal surfaces using guidelines from Allen et al. (1998). In the 2D-aDGVM, the procedures described in Allen et al. (2006) for estimating solar radiation for inclined surfaces for all combinations of slope, aspect and latitude were included.

In the aDGVM, the net radiation (Rn) (difference between incoming net shortwave radiation, Rns , and outgoing net longwave radiation, Rnl) is used to compute soil and plant's evapotranspiration. For the calculations of Rns and Rnl (Allen et al., 1998; Equations (38) and (39), respectively), extraterrestrial radiation (Ra) (the solar radiation received at the top of the earth's atmosphere on a horizontal surface), global radiation (Rs) (the sum of direct shortwave radiation from the sun and diffuse sky radiation from all upward angles) and clear-sky solar radiation (Rso) (the same global radiation that would actually reaches the surface but under cloudless conditions) are needed.

To calculate Ra , the aDGVM follows the procedures for daily periods (Allen et al., 1998; Equation (21)) and further calculates Rs and Rso from Ra (Allen et al., 1998; Equations (35) and (36), respectively). Additional input data of monthly percentage of sunshine per day is needed to calculate Rs , an alternative procedure suggested by the authors when there is no local measurements of Rs . Rso calculations also need two empirical constants (a_s and b_s) defining the proportion of extraterrestrial radiation reaching Earth on overcast days.

In the 2D-aDGVM, the modifications to calculate net radiation for inclined surfaces followed the procedures described by Allen et al. (2006) to calculate total extraterrestrial radiation for 24-h periods (Ra_{24}) (Allen et al., 2006; Equation (6)) on sloping surfaces with refinement for two sets of integration limits (the beginning and ending sun-hour angles, $\omega_{1,24}$

and ω_{24} , when the sun's beam first and last strikes the particular surface). $R_{s_{24}}$ was used to calculate clear-sky solar radiation for inclined surfaces ($R_{s_{o(24)}}$) (Allen et al., 2006; Equation (29)) with a procedure that does not require the empirical constants a_s and b_s . The calculations of the global radiation for inclined surfaces $R_{s(slope)}$ (Allen et al., 2006; Equation (38)) used the guidelines for the translation of the calculated R_s from a horizontal surface ($R_{s_{hor}}$) to slopes. The aDGVM calculated R_s from a horizontal surface used input data of monthly percentage of sunshine per day as described earlier. Incoming net shortwave radiation for inclined surfaces, $R_{ns(slope)}$ and the outgoing net longwave radiation for inclined surfaces, $R_{nl(slope)}$, followed Allen *et al.* (1998), but using the new global radiation ($R_{s(slope)}$) and clear-sky solar radiation ($R_{s_{o(24)}}$) for inclined surfaces. The net radiation for inclined surfaces $R_n(slope)$ was then obtained from the difference between $R_{ns(slope)}$ and $R_{nl(slope)}$.

All the radiation calculations described by Allen et al. (2006) did not include impacts of terrain shading (i.e., shading during long periods or even all of the year by surrounding obstacles in very rough terrains). In addition, the corrections suggested for cases where periods of sun occur twice per day (the slope may be shaded during all or portions of the day), when slopes are steep and northerly facing in northern latitudes or southerly facing in southern latitudes, were not considered in the 2D-aDGVM.

Usually, direct solar radiation is the larger proportion of global radiation compared to diffuse radiation. Therefore, the ratio, R_d , of direct radiation on the slope to direct radiation on a horizontal surface (Tian et al. 2001) was used to show simulated seasonal variations on incoming solar radiation. Simulations were performed with 10 to 80 degrees of slope inclination (15 degrees intervals) for north and south facing cells, as well as with 0 to 360 degrees of slope aspect for cells with 15 degrees of slope inclination (mean value of slope inclination in Morro Santana). Global solar radiation from 1975-2002 daily measurements from a climatic station of the Fundação Estadual de Pesquisa Agropecuária (FEPAGRO) (Cargnelutti-Filho et al. 2007) in Cachoeirinha (a site 17 km away from Porto Alegre) was

used for model verification of simulated global radiation for horizontal surfaces (R_s from the aDGVM and $R_{s(slope)}$, with slope inclination set to zero, after the implementations described earlier for radiation on inclined surfaces).

Results from predicted solar radiation

Simulations of global solar radiation for horizontal surfaces were very similar to local measurements (Figure 2). Deviations from observed mean were more pronounced in summer and late spring using both models. The deviations yielded by including slope follow the deviations yielded by the original aDGVM. This is because the same global radiation (R_s) estimated by the original aDGVM is used to calculate global radiation for inclined surfaces ($R_{s(slope)}$), therefore it was not well adjusted to the observed when slope is set to zero. Two factors may be causing such deviations. The first could be the use of empirical constants (a_s and b_s) in the estimation of R_s and the other could be the differences in data source, since the empirical sunshine data used to estimate R_s is an estimation from New et al. (2000) to Porto Alegre and the observed global radiation used in the comparisons with simulated values is from a climatic station in Cachoeirinha, near Porto Alegre (Cargnelutti-Filho et al. 2007). Nevertheless, the great majority of simulated results were within observed deviations limits (Figure 2).

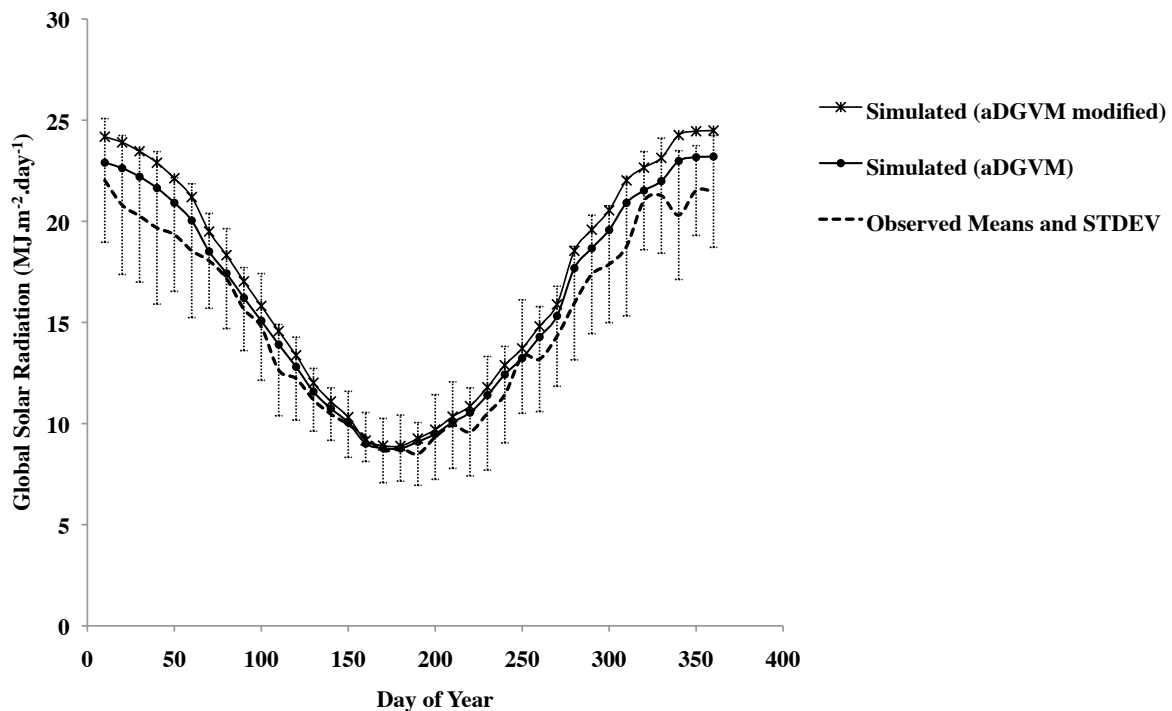


Figure 2. Simulated and observed daily global solar radiation for horizontal surfaces (R_s). Observed data are from a climatic station of the Fundação Estadual de Pesquisa Agropecuária (FEPAGRO) in Cachoeirinha (a site 17 km away from Porto Alegre, Brazil. Means and standard deviations were obtained from periods of ten days, (Cargnelutti-Filho et al. 2007)). Simulated results used percentage of sunshine per day for Porto Alegre (New et al. 2002) to calculate R_s . Simulated results from the modified aDGVM include additional implementations proposed by Allen et al. (2006) to calculate radiation for inclined surfaces and were generated considering zero degrees of slope inclination.

The effects of slope inclination and aspect on incoming direct solar radiation can be seen in Figure 3A and 3B. The greatest differences occurred in winter between north and south facing slopes (Figure 3A) and this difference reached a maximum at 50 degrees of inclination (Figure 3B). Similar trends were found by Tian et al. (2001) at latitude 35°S in New Zealand using a different model for estimating topographical solar radiation based on measured global solar radiation (the figures showed here were intentionally designed in a similar way to facilitate comparison). The higher sensitivities of solar radiation to inclined slopes during winter are attributed to the lower elevation of the sun and consequently the decrease in the angle between the sun and the normal of slope (Tian et al. 2001).

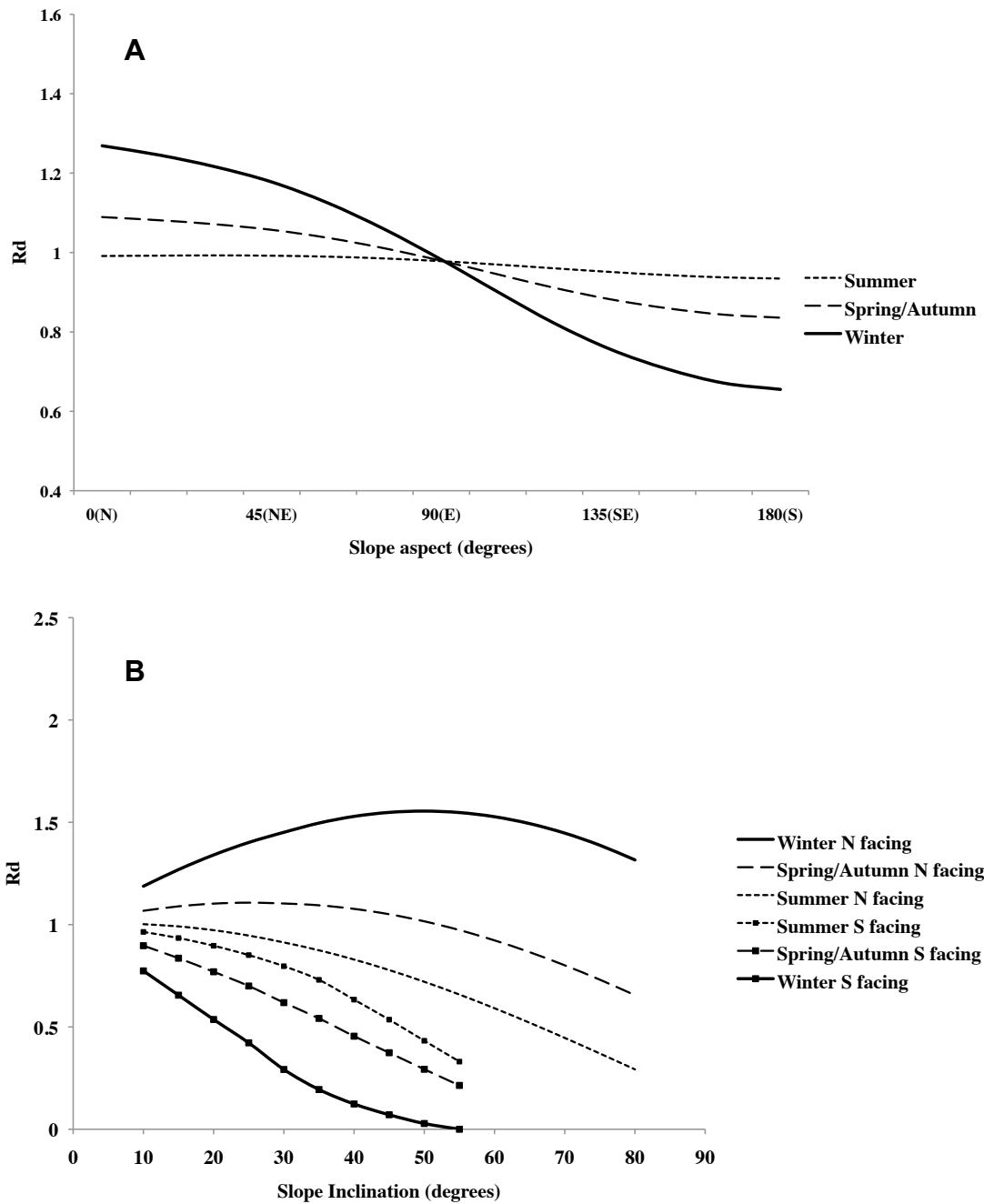


Figure 3. Simulated ratio, R_d , of direct radiation for inclined surface to direct radiation on a horizontal surface showing seasonal variations as a function of slope aspect (A) and slope inclination. Simulations in (A) were conducted for 15 degrees of slope inclination and in (B) for north and south facing surfaces.

Solar radiation and fuel moisture

In the aDGVM, fuel moisture (θ_f) is assumed to equal air humidity and dead fuel biomass (B_{dead}) dries out quickly as a function of the number of days since litter fall, i.e., fuel moisture does not account directly for spatial variations in the amount of solar radiation. Therefore, to account for spatial variability on heating and drying of dead fuel moisture (through the evaluation of solar heating and wind cooling effects) the improvements of the Canadian Fine Fuel Moisture Code (FFMC) for sunny conditions (open sites) as described by Rothermel et al. (1986) were implemented in the 2D-aDGVM. Solar radiation for inclined surfaces ($Rs_{(slope)}$) and wind speed at the fuel level ($U_{h'}$) are used to calculate the difference in temperature between the air (T_a) and the fuel (T_f) and further, a correction for relative air humidity at the fuel level (H_f). For the calculation of wind speed at the fuel level ($U_{h'}$), where h' is vegetation height, the aDGVM monthly local input variable *reference wind speed* (u_{ref}) ($m.s^{-1}$) (measured at the international standard height of 10 meters in the open, $U_{10+h'}$) is used. Vegetation height h' is calculated each day for each cell as the mean vegetation height between grass and tree populations. Mean tree height was adjusted to the proportional tree cover of the cell. Therefore, when the cell has no trees, h' is equal to mean height of grasses and when the cell is totally covered by trees, h' is equal to mean height of trees. The calculated wind speed at the fuel level ($U_{h'}$) and solar radiation for inclined surfaces ($Rs_{(slope)}$) are then used to calculate air temperature at the fuel level (T_f). Daily air temperature (T_a) is calculated by the aDGVM, following the guidelines from Allen et al. (1998). When a cell has trees, the calculated solar radiation for inclined surfaces ($Rs_{(slope)}$) is adjusted for shade by an alternative procedure to that proposed by Rothermel al. (1986), which considers cloud and timber canopy cover in the attenuation of solar radiation. As a simplification, in the present model, the adjustments for cloud cover were ignored and solar radiation reaching the understorey vegetation is given by $Rs_u = Rs_{(slope)}\tau_d$ or $Rs_u = Rs_{(slope)}\tau_e$, where $\tau_d = 0.082$ and

$\tau_e = 0.033$ are local empirical values of canopy transmittance in deciduous or semi-deciduous forests during autumn and winter, and in evergreen forests or in deciduous or semi-deciduous forests during spring and summer, respectively (a simplification of the values from Hernandez et al. (2004)). Relative air humidity at the fuel level (H_f) is finally calculated based on monthly aDGVM input local data for relative air humidity ($h_s = H_a$) and the difference between the calculated daily air temperature (T_a) and temperature at the fuel level (T_f), also accounting for shaded conditions ($H_{f(shaded)}, T_{f(shaded)}$).

Once the aDGVM distinguishes between open and sub canopy fuel biomass, both of the following procedures occur when trees colonize a grassland cell: calculations of daily dead fine fuel moisture for open ($FFMC_{open}$) and shaded conditions ($FFMC_{shaded}$). In the aDGVM, the moisture content of aboveground live biomass of grasses (live fuel moisture of both open and sub canopy grasses, θ_{live}) is assumed to equal air humidity h_s and this value decreases quickly by an exponential function to simulate the drying out of the dead biomass (dead fuel moisture, θ_{dead} , where B_{dead} includes grass lying and standing dead biomass for both open and sub canopy conditions, as well as leaf litter of all trees), accounting for the number of days since litter fall (last transition from the active to the dormant state of trees). After the new implementation, the 2D-aDGVM assumes the live fuel moisture of open grasses to be equal to relative air humidity at the fuel level (H_f) and the live fuel moisture of sub canopy grasses to be equal to $H_{f(shaded)}$. Dead fuel moisture is similarly distinguished between open and shaded conditions and, therefore, dead fuel moisture for open dead grass biomass is $FFMC_{open}$ and dead fuel moisture for sub canopy dead grass biomass and leaf litter of trees is $FFMC_{shaded}$. Finally, fuel moisture, adapted from Scheiter and Higgins (2009), is calculated by

$$\theta_F = \frac{B_{live(open)}H_f + B_{dead(open)}FFMC_{open} + B_{live(shaded)}H_{f(shaded)} + B_{dead(shaded)}FFMC_{shaded}}{B_F} \quad (\text{Eq.1})$$

where,

$B_{live(open)}$ = open live fuel biomass, which is leaf biomass and one half of standing dead biomass of open grasses;

$B_{live(shaded)}$ = shaded live fuel biomass, which is leaf biomass and one half of standing dead biomass of sub canopy grasses;

$B_{dead(open)}$ = open dead fuel biomass, which is leaf litter of all tree as well as lying dead biomass and one half of the standing dead biomass of open grasses;

$B_{dead(shaded)}$ = shaded dead fuel biomass, which is leaf litter of all tree as well as lying dead biomass and one half of the standing dead biomass of sub canopy grasses;

B_F = fuel biomass, which is $B_{live(open)} + B_{live(shaded)} + B_{dead(open)} + B_{dead(shaded)}$;

H_f = moisture of open live fuel biomass, which is the relative air humidity adjusted to the fuel level;

$H_{f(shaded)}$ = moisture of shaded live fuel biomass, which is H_f adjusted for understorey radiation (shaded conditions);

$FFMC_{open}$ = moisture of open dead fuel biomass;

$FFMC_{shaded}$ = moisture of shaded dead fuel biomass;

According to Rothermel et al. (1986), the obtained daily values of fuel moisture are equivalent to the early afternoon fine fuel moisture (values between 12:00 and 16:00) needed for predictions of fire behavior. In addition, considering the scale and the sites to which the present model will be applied, the corrections for elevation differences between cells were ignored, once they are less than 300 m (Rothermel et al. 1986).

A simplified sensitivity analysis was performed to test the effects of slope inclination and aspect on fuel moisture and potential fire intensity considering forested and non-forested

cells. Variations on these outputs were evaluated for north and south facing cells with 50 degrees of slope inclination (which yield the greater difference between incoming direct radiation on inclined surfaces relative to horizontal surface for north and south orientations in winter). The effects of trees on grass biomass production and moisture were evaluated by adding one young tree (with initial weight equal 10 g) after a spin-up phase of 20 years. Ten repetitions of each simulation case (random seed varying from one to ten) were performed for 150 years (considering a spin-up phase of 20 years) considering one cell of 1 hectare and the absence of fire.

Results from simulated fuel moisture and fire intensity

In the aDGVM, fuel biomass is composed mainly of grass biomass. Therefore, by increasing tree cover, fuel biomass decreased from around 0.55 Kg.m^{-2} , when the cell had no trees, to less than 0.1 Kg.m^{-2} when the cell was totally forested (not shown). Additionally, moisture contents of live (H_f , $H_{f(\text{shaded})}$) and dead ($FFMC_{\text{open}}$, $FFMC_{\text{shaded}}$) fuel biomass were 19.43% and 27.57% higher (annual average of monthly differences) in forested (Figure 4A) than in non-forested cells (Figure 4B), respectively. However, differences in moisture between north and south facing cells were more pronounced in non-forested cells, where in the south facing cells moisture was higher than in north facing cells for both live (11.67%) and dead (12.03%) fuel biomass (annual average of monthly differences) (Figure 4B).

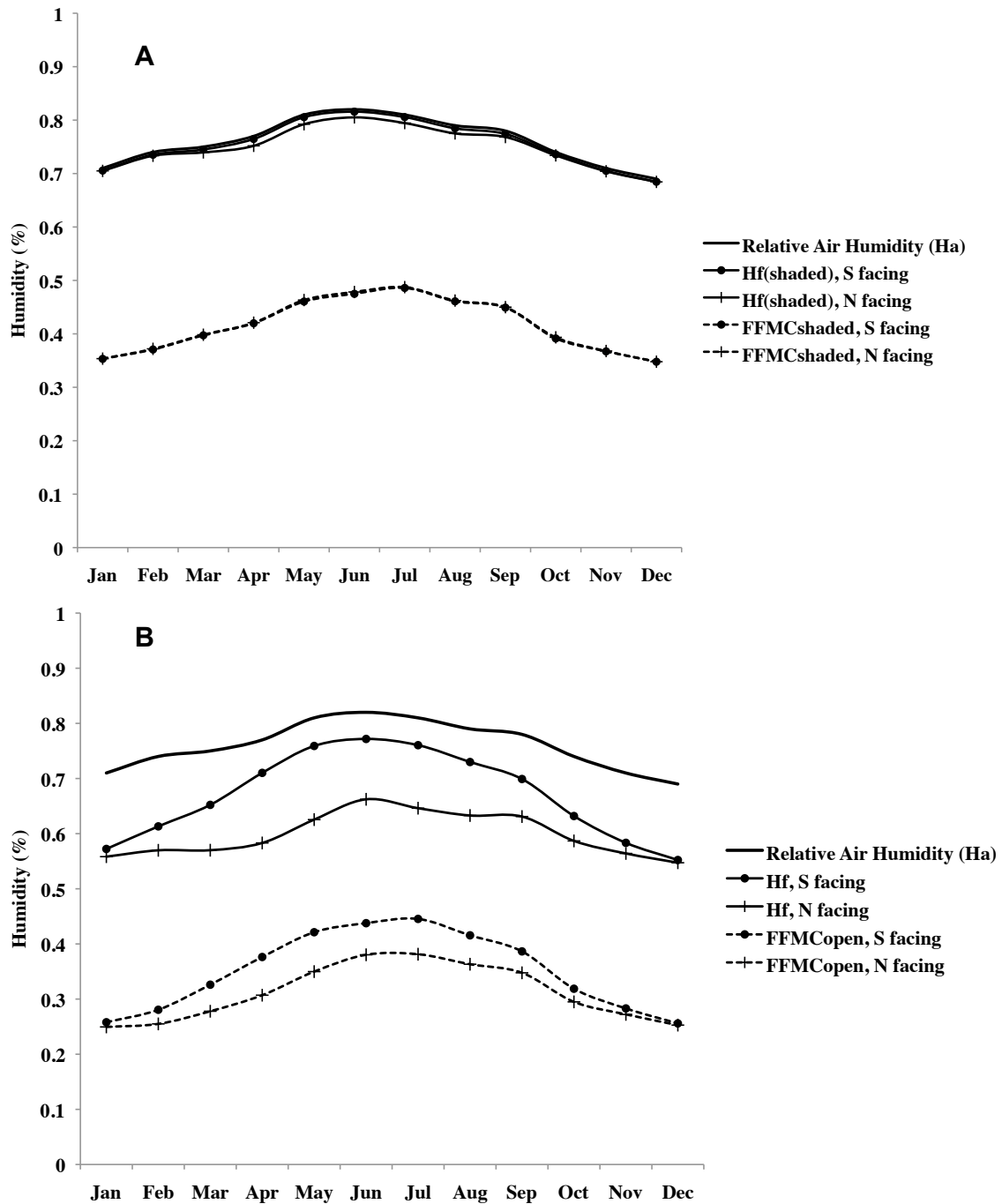


Figure 4. Moisture content of live and dead fuel biomass in north and south facing, forested and non-forested (A) cells (B). The graphs show mean monthly results of the new implementations for humidity at the fuel level, which accounts for solar heating (with the new implementations for solar radiation on inclined surfaces in open and shaded conditions) and wind cooling effects. These new implementations include improvements of the Canadian Fine Fuel Moisture Code (FFMC) for sunny (non-forested sites) conditions, as well as shaded (forested sites) conditions (Rothermel et al. 1986). Simulations in (A) and (B) were conducted with 50 degrees of slope inclination. Observed relative air humidity is from 1961–90 mean monthly data from a climatic station of the Instituto Nacional de Meteorologia (INMET) in Porto Alegre, Brazil. Hf = moisture content of open live fuel biomass; Hf(shaded) = moisture content of shaded live fuel biomass; FFMCopen = moisture content of open dead fuel biomass; FFMCshaded = moisture content of shaded dead fuel biomass.

As a result, simulated final fuel moisture and potential fire intensity also showed similar trends (Figure 5A and 5B). Differences in fire intensity and fuel moisture between north and south facing surfaces were evident only in non-forested cells (Figure 5A). Fuel moisture was 11.72% higher (annual average of monthly differences) in south facing cells, with higher differences in autumn and winter (17.15%, average difference from April to September) in relation to spring and summer (6.28%, average difference from January to March and from October to December). Thus, since fuel moisture contributes inversely to fire intensity (see equation 6 in Scheiter and Higgins, 2009), fire intensity was 5.61% lower in south facing cells during autumn-winter but 2.71% higher than in north facing cells during summer and late spring (Figure 5A). When compared to forested cells (Figure 5B), fuel moisture was 27.98% higher (annual average of monthly differences between north and south values) in non-forested cells (Figure 5A). Considering the higher moisture content of live and dead fuel biomass in forested cells (Figure 4B) compared to non-forested cells (Figure 4A), one should expect an inverse relationship (final fuel moisture to be higher in forested cells). However, as mentioned before, fuel biomass, which is composed mainly by grass biomass, is sharply reduced due to the shading effect of trees. Nevertheless, fire intensity was 94.78% lower in forested cells than in non-forested cells and remained below the minimum threshold value of $300 \text{ KJ.s}^{-1}.\text{m}^{-1}$ for a fire to spread. In conclusion we found that fire will rarely spread to an already totally forested cell, as locally observed during fire events in grassland-forest mosaics.

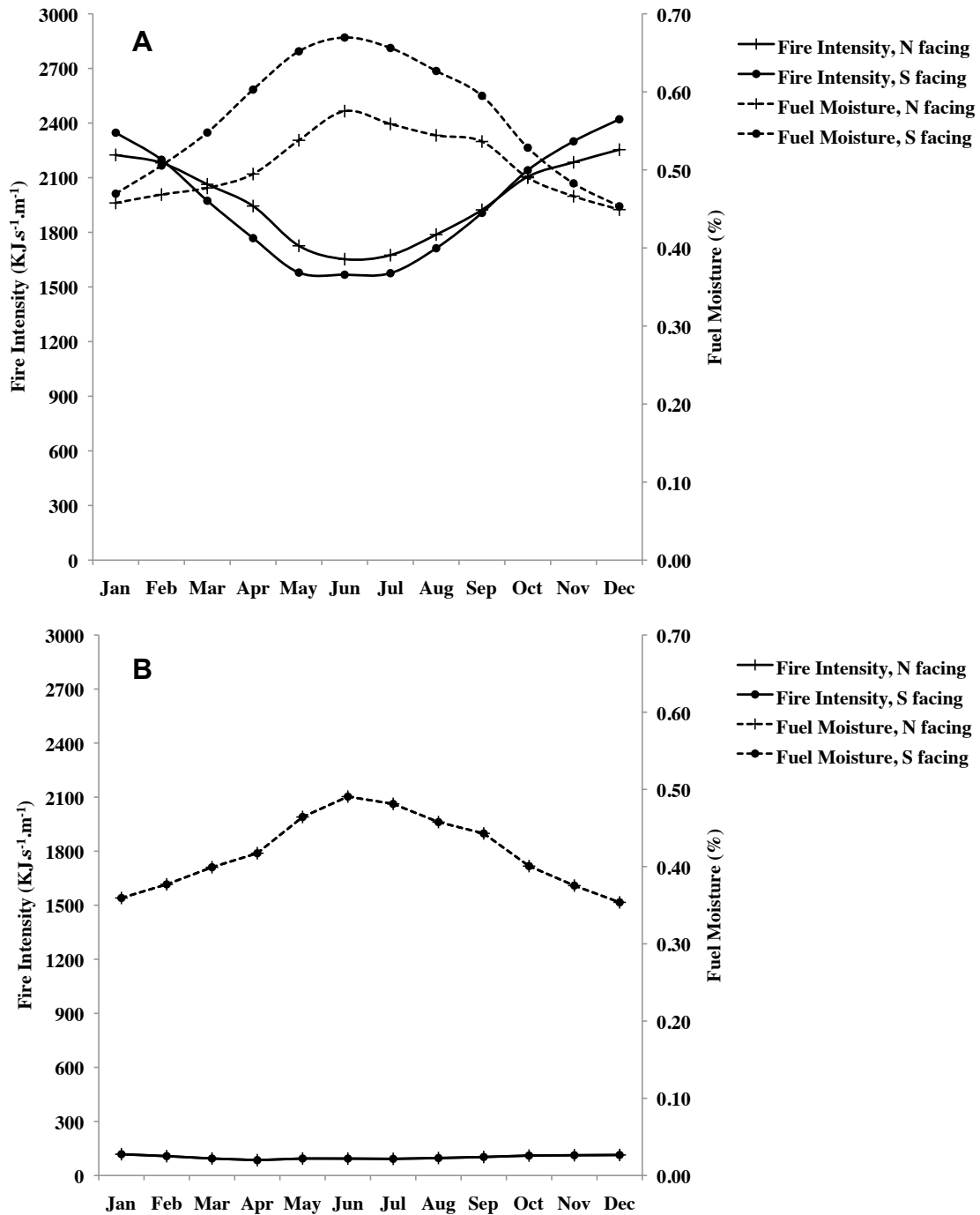


Figure 5. Simulated fire intensity and fuel moisture in non-forested (A) and forested cells (B), considering the new implementations for radiation on inclined surfaces (Allen et al. 2006), as well as the improvements of the Canadian Fine Fuel Moisture Code (FFMC) for moisture content at the fuel level for sunny (non-forested sites) conditions and shaded (forested sites) conditions (Rothermel et al. 1986). The graphs show mean monthly values for north and south facing cells with 50 degrees of slope inclination.

Fire spread in the 2D-aDGVM

In the aDGVM, fire ignition is determined by an annual stochastic ignition sequence to determine days when ignition occurs and is based on a probability, which is calculated from mean relative air humidity (mean of monthly values) of the site (not shown). On an ignition day, fire spreads based on a fixed probability (p_{fire}). For Porto Alegre, mean annual relative air humidity is 76% and the calculated probability of daily ignition is 1.12%, yielding a mean of four ignitions per year (results not shown). A global evaluation of total lightning flashes per month (fls/mon) in this region has shown a much higher frequency of 10^5 fls/mon as potential sources of natural ignition (Cardoso et al. 2008). Although lightning has been considered the major source of natural fires in the tropical regions, and hence defining patterns of potential occurrence of savanas, it is expected that the frequency of successful ignitions caused by lightning in subtropical humid areas (such as in the present study site) is much lower. In the aDGVM, fire intensity is a function of fuel biomass, fuel moisture, and wind speed (an arctan transformation of wind speed, since slope does not influence the predicted spread rates), and the probability of an individual tree be killed by fire (topkill) is a function of fire intensity and tree height (Scheiter and Higgins 2009).

The 2D-aDGVM modelling space is a regular grid of square cells with specified sizes. On an ignition day, the model randomly selects which cell will be tested to be the first ignited one among all cells with tree cover <50% (to avoid bias on fire frequency due to recurrent failed ignitions eventually occurring in forested cells, because the test for a fire to spread is applied once to every ignition event). In the aDGVM, the first selected cell will be ignited if the calculated potential fire intensity exceeds a pre-defined threshold ($300 \text{ KJ.s}^{-1}.\text{m}^{-1}$) and fire spreads inside this cell with a fixed probability p_{fire} (Scheiter and Higgins 2009). In the 2D-aDGVM, this probability applied to the first ignited cell can be adjusted to fuel moisture of grass biomass, described as follows.

In the 2D-aDGVM, for a fire to spread to adjacent cells, p_{fire} is adjusted to fuel moisture of grass biomass ($\theta_{F(grass)}$). The adjusted probability ($p_{fire(t)}$) ranges from 1.5% (Scheiter and Higgins 2009) to 60% and is calculated locally (to each target cell). The equation to calculate $\theta_{F(grass)}$ is the same as Equation 1, but without considering the leaf biomass of trees in the component $B_{dead(shaded)}$, and hence in B_F . The maximum ($\theta_{F(open)max.} = 67\%$) and minimum ($\theta_{F(open)min.} = 45\%$) values obtained from simulated fuel moisture in non-forested cells (Figure 5A) were used in equation $a\left(\frac{\theta_{F(open)max.}}{100}\right) + b = 0.015$ and equation $a\left(\frac{\theta_{F(open)min.}}{100}\right) + b = 0.6$, respectively, to solve for parameters a and b , yielding the final equation of fire spread probability to each cell $p_{fire(t)} = -2.2\theta_{F(grass)} + 1.489$ (Eq. 2)

When the first cell is ignited, the model starts a test searching for cells with potential fire intensity among the eight adjacent neighboring cells. Fire will spread (cells will be burned) from the first ignited cell to the surrounding ignited ones based on a pre-defined bias value that is used to calculate the wind-corrected directional probabilities of fire spread to each neighboring cell $i_{wj} = 0.6 - (0.6 - p_{fire})^{b_j}$, where 0.5 is the maximum value settled for $p_{fire(t)}$ (Figure 6). A similar method using bias values relative to wind direction to correct the probability of fire spread was used by Hargrove *et al.*, (2000). Fire spread is evaluated in the neighborhood of each new ignited cell until there are no more cells to burn. The 2D-aDGVM considers only moderate winds ranging from 1 – 6 m.s⁻¹ and a prevailing northeast wind direction in the definition of the bias values b_j (Figure 7).

It is well known that topographic variations have a direct effect on fire spread rates (Rothermel 1972, Trollope et al. 2004) and the majority of fire behavior models aim at evaluating fire spread by the elapsed time required to reach the opposite edge of a grid map or to burn a pre-defined elliptically shaped area (Finney 1998, Hargrove et al. 2000, Berjak and Hearne 2002). However, in the 2D-aDGVM only the location, size and shape of the final

burned area are required. Therefore, the effects of topography are not incorporated to fire spread rate into the aDGVM fire intensity calculations (Scheiter and Higgins, 2009), but are considered to affect fuel moisture due to the resulting variations on incoming solar radiation and hence on drying and heating of biomass, and finally on evapotranspiration, soil moisture content, fuel biomass content and fire intensity inside each cell.

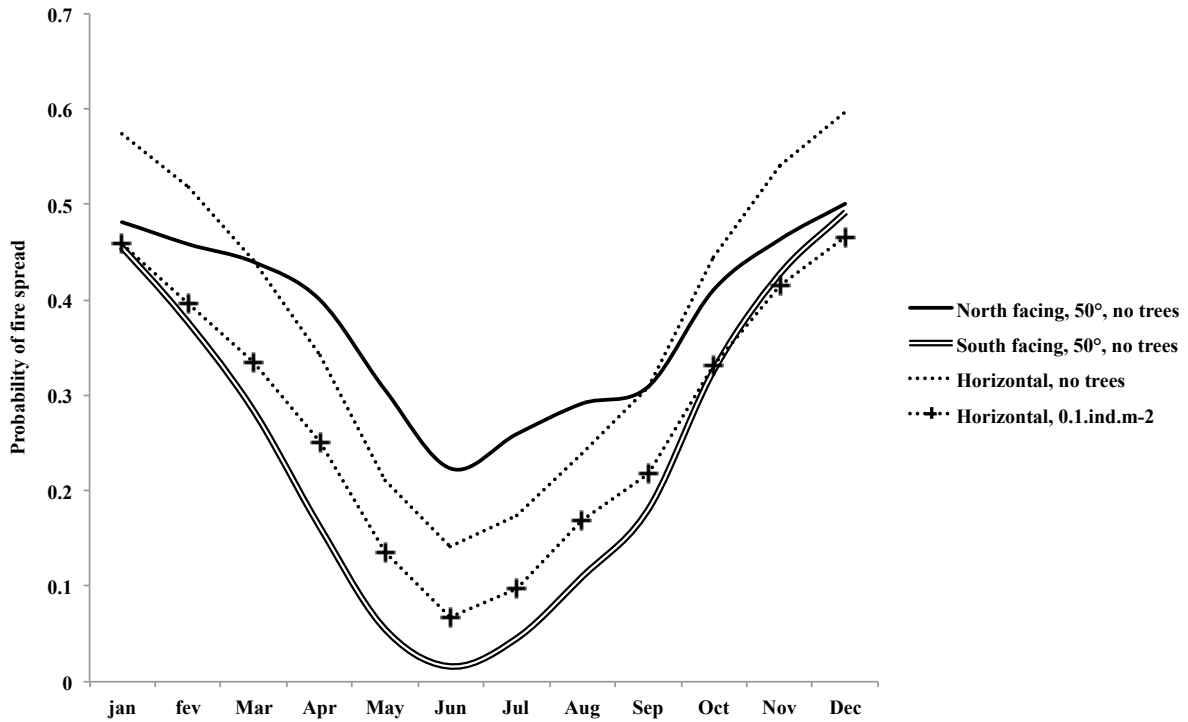


Figure 6. Probability of fire spread in forest and non-forest cells. The graph shows mean monthly values for horizontal (0° slope inclination), north and south facing cells with 50° of slope inclination.

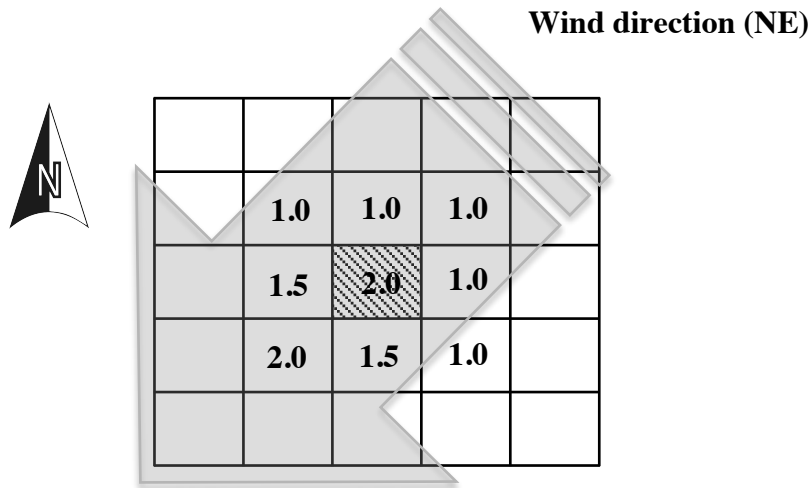


Figure 7. Schematic drawing showing the bias values attributed to a target cell and each of its eight neighbors in each fire spread iteration rule as a function of the prevailing northeast wind direction (gray arrow). The hatched cell is the first ignited cell or any new ignited one.

Seed dispersal in the 2D-aDGVM

The aDGVM considers only seed dispersal of individual trees. In the 2D-aDGVM, seed dispersal is a function of seed production and distance from seed sources. The seed dispersal rule is applied once a year, when the produced seeds (Φ_{ij}) are collected in each cell by the aDGVM (Scheiter and Higgins, 2009). The expected number of seeds landing in each cell is calculated by $N_S = \sum g_{(d_{ij})} \Phi_{ij}$, where Φ_{ij} is the number of produced seeds in each possible donor cell and $g_{(d_{ij})}$ is the probability density function of each seed to land in a target cell a certain distance d_{ij} from seed source (or, alternatively, the probability of a target cell to receive a seed a certain distance from a donor cell). The sum of expected proportion of seeds dispersed from a donor cell to each possible target cell was adjusted to one. The following equation was used to calculate $g_{(d_{ij})}$:

$$g_{(d_{ij})} = P_{seed} \frac{1}{\lambda_1} \exp\left(-\frac{d_{ij}}{\lambda_1}\right) + (1 - P_{seed}) \frac{1}{\lambda_2} \exp\left(-\frac{d_{ij}}{\lambda_2}\right) \quad (\text{Eq. 3})$$

In Equation 3, d_{ij} is the distance between cell's midpoints, P_{seed} is the proportion of seeds dispersed short distances and λ_1 (m) and λ_2 (m) are mean distance of short and long distance dispersal, respectively. Similar equations were used to simulate seed dispersal in other spatial explicit models (Higgins and Cain 2002, Caplat et al. 2008) and they were referred to as stratified (mixed) kernels, allowing a more flexible way to model short (first component of Eq. 3) and long (second component of Eq. 3) distance dispersal.

In this way, each expected seed (from calculated N_S) will land in a target cell when a uniformly distributed random number between zero and one is less than $g_{(d_{ij})}$. Finally, seeds dispersed to other cells are subtracted from the cell's resident pool of collected seeds. Seeds

arriving from other cells are added to the seed bank, as well as seeds that ‘fail’ to disperse to other cells. Following seed decay rate and probability of seed germination are applied daily by the aDGVM (Appendix 1).

Model flow

Figure 8 shows the general model flow of the bidimensional spatially explicit model (2D-aDGVM) that incorporates the adaptive Dynamic Global Vegetation Model (aDGVM) (Scheiter and Higgins, 2009), and Table 2 shows an outline of all required input data, as well as the generated model outputs. The 2D-aDGVM modelling space is a regular grid of square cells with specified sizes. To set an starting vegetation map, input information about the presence of trees, slope inclination angle and slope orientation angle for each cell is required. If it is a real map, these inputs can be obtained using any software for GIS analysis by extracting matrices containing the referenced information from each image pixel to output files in ASCII format (the files must be converted to a text file without the heading information). The matrix containing information about the presence of trees in each cell is used to initialize the ‘initial number of trees’ in the aDGVM (Scheiter and Higgins 2009) (Table 2). In this way, the values in the matrix can be zero, one or higher than one. Value ‘zero’ initializes a cell without trees (only grasses), value ‘one’ initializes a cell with one young tree (initial mass = 10g; Scheiter and Higgins, 2009), value higher than one (n) initializes a cell with n trees with random sizes and ages.

```

Read initial input arguments (text file): number of lines, columns, simulation years, longitude, latitude, random seed, fire
Create a grid with N lines and N columns (N x N cells)
Read input data matrices (text files): initial number of trees, slope inclination, slope orientation
Read aDGVM input climatic and soil data from database (text file)
For each cell
{
  Initialize aDGVM:
    Calculate secondary atmospheric data
    Calculate leaf photosynthesis
    Initialize tree and grass populations
}
For each year
{
  Generate rainfall sequence and fire ignition sequence to the entire grid
  Random selection of the first cell to ignite

  For each day
  {
    For each cell
    {
      Calculate net radiation for inclined surface
      Run death process for trees
      Calculate soil, grass and tree evapotranspiration
      Update soil moisture content
      Run tree and grass physiology
      Collect seeds
      If there are seeds produced
      {
        Calculate expected number of seeds landing in each cell
        Update seed bank in each cell
      }
      Check if fire spreads inside the first ignited cell
      if yes
      {
        While there is a new ignited cell
        {
          Check if there is available biomass to burn in the eight surrounding neighbors (if yes, ignition is on)
          Calculate wind-corrected directional probabilities to spread to the eight surrounding neighbors
          Check if fire spreads from each new ignited cell to the eight surrounding neighbors
        }
        Burn all cells where fire is able to spread
        Update biomass in all burned cells
      }
    }
  }
}
For each cell
{
  Print outputs
}
}

Finish simulation

```

Figure 8. General scheme of model flow. Routines in bold are the new implementations in 2D-aDGVM. The other routines are original aDGVM routines.

Table 2. General overview of model input and output data.

File names: <i>InputData</i> folder	Data	Value	Resolution
<i>InputArguments.txt</i>			
	Number of lines (n_{lines})	variable	grid
	Number of columns (n_{cols})	variable	grid
	Number of simulation years (yr)	variable	Grid
	Longitude (Lon)	-51	grid
	Latitude (Lat)	-30	grid
	Seed for random number generator	1-10	grid
	Fire (on/off)	1/0	grid
	Print aDGVm outputs (yes/no)	1/0	cell (daily and yearly)
<i>InputTrees.txt</i>	Presence of trees (yes/no)	1/0	cell: matrix ($n_{lines} \times n_{cols}$)
<i>InputSlope.txt</i>	Slope inclination angle (degrees)	variable	cell: matrix ($n_{lines} \times n_{cols}$)
<i>InputAspect.txt</i>	Slope orientation angle (degrees)	variable	cell: matrix ($n_{lines} \times n_{cols}$)
<i>shortlist_Lat.0000000_Lon.0000000_0.0000000.dat</i>	Climate/Elevation and Soil	variable/constant (described in Table 1)	grid (monthly/constant)
File names: <i>OutputData</i> folder			
<i>YearData.txt</i>	aDGVm outputs (Appendix 1)	variable	cell (yearly: day 365)
<i>SysData.txt</i>	aDGVm outputs (Appendix 1)	variable	cell (daily)
<i>FireData.txt</i>	aDGVm fire outputs (Appendix 1)	variable	cell (only burned cells)
<i>Year_yr_SizeData.txt</i>	aDGVm output: population structure of trees*	variable	cell (yearly: day 365)
<i>Year_yr_FireGrid.txt</i>	Burned/unburned cells	1/0	cell (only fire years)
<i>Year_yr_VegGrid.txt</i>	Tree cover	variable	cell (yearly: day 365)
<i>Year_yr_VegGrid_round.txt</i>	Forest/nonforest ($\geq 50\%$ tree cover/ $< 50\%$ tree cover)	1/0	cell (yearly: day 365)

Since reproduction inside each cell is also related to tree size and age in the aDGVM, the higher the initial number of trees, the higher will be the total number of trees (and probably the number of reproductive ones) and hence tree cover in the beginning of simulations. This has implications when translating information about forested pixels from a starting real vegetation map to the corresponding initialized cells in the grid. Input parameters of climatic and edaphic site characteristics are also required by the aDGVM (Tables 1 and 2) and can be obtained from global or local databases (as described before, in *Parameterization and testing of stand-scale vegetation growth and biomass*). These database parameters are stored in another input file (Table 1). Since the spatially explicit model is designed to run at a regional scale, these parameters are set to be the same for all grid cells. Similar to the original aDGVM, other input options can be defined by the user in the 2D-aDGVM, such as number of cells (inputs ‘number of lines’ and ‘number of columns’), number of years to simulate, site longitude (negative for Southern Hemisphere), site latitude (negative for Southern Hemisphere), seed for random number initialization and fire (on = 1; off = 0) and if simulations consider the presence of fire or not (fire on = 1; fire off = 0) (Scheiter and Higgins 2009). These options are stored in another input text file (Table 1).

After setting model inputs, initialization of the aDGVM in each cell is then started by calculating some secondary parameters and by initializing grass and tree populations (Table 1 in Appendix 1). At the beginning of each year, new rainfall sequence and fire ignition sequence are generated in the aDGVM (Figure 8). Demographic, physiological and reproductive processes are simulated by the aDGVM in daily time steps. Seed dispersal rule is applied once a year, only on the day when seeds are collected by the aDGVM. Fire-spread rule across the landscape is applied only when ignition in the first randomly selected cell is successful. If yes, the model stops the day loop and starts a recursive evaluation of potential new ignited cells among the surrounding eight adjacent ones. Fire stops when there are no

more new ignited cells. All ignited cells are then burned and have their biomass updated by the aDGVM before continuing the day loop (Figure 8).

Finally, model outputs include yearly proportional tree cover in each cell, and optionally, fire growth (each step of model check of fire spread in the loop of fire spread rule). Demographic (e.g. total number of trees in each size class) and productivity results (e.g., grass and tree biomass), as well as fire outputs (e.g., fire intensity, fuel moisture) in each cell are also some of the daily and annual possible outputs (Table 2 and Appendix 1).

2D-aDGVM parameterization and testing of spatio-temporal dynamics of forest-grassland mosaics

Input maps

Vegetation maps from Morro Santana were obtained from local studies that generated categorical maps of land use cover with grain size of 5 m (25 m² pixel size) from years 1941 and 1985 (Adelmann and Zellhuber 2004) and 2002 (Matte 2006) through supervised digitalization of aerial photographs and Quickbird satellite images. However, only one sampled window was considered (722,275 m²), taking into account areas in which dynamics of forest-grassland borders were evident from a previous analysis of those three time steps. This sample was located in the predominantly south face of the hill (40% S, 16% SW, 9.4% SE, 12.6% N, 7.2% NW, 5.3% NE, 6.8% W, 2.7% E), with average slope inclination of 15.24°±7.89. Therefore, the 2D-aDGVM input grid size was 167 lines x 173 columns (i.e., the total number of pixels in the maps) containing a binary code for the aDGVM ‘initial number of trees’ input in each cell (i.e., 1 for forested pixels and 0 for grassland pixels). Therefore, since there was no detailed information about the exact tree cover values in each forested pixel informed in the input vegetation map, a spin-up phase of 100 years was considered,

before starting seed dispersal and fire spread rule across the landscape, to assure the aDGVM stabilization inside each cell.

Parameterization and validation of the 2D-aDGVM

Model parameterization and validation were conducted by searching for the best fit between simulated and observed spatio-temporal dynamics of forest-grassland mosaics. For this, yearly simulated output maps with tree cover values of each cell (cover values converted to zero when $< 50\%$ and converted to one when $\geq 50\%$, for grassland and forest, respectively) were compared to the observed maps (years 1985 and 2002) by simple matching. Each map (observed and simulated ones) was considered a “variable” and each pixel of the map was considered a “sampling unit”. In this way, in the equation $S_{iK} = (a+d)/q$, $a+d$ were the total number of pixels where forest (value 1) and grasslands (value 0) coincided (a and d , respectively) in observed and simulated compared maps and q were the total number of pixels in each comparison. Therefore, for each combination of parameters tested (see *Seed dispersal* and *Fire frequency*), observed maps (1985 and 2002) could be compared to all yearly output maps using the generated similarity matrix (simple matching). Therefore, the fitting procedure searched for the combination of parameters that generated the highest values of simple matching between the observed (1985, 2002) and the simulated maps after the corresponding time interval; i.e. 44 years from 1941 to 1985, 17 years from 1985 to 2002, and 61 years from 1941 to 2002. In addition to this fitting of spatio-temporal dynamics at the patch scale (pixel comparisons through simple matching), we also compared observed and simulated total forest cover (% of landscape map covered by forest pixels) between observed and simulated time intervals. These analyses were done with the software MULTIV v. 2.4.2. (Pillar 2006).

In the observed dynamics of forest-grassland mosaics, tree cover increment (new forested area) over grasslands during the first analyzed period (1941-1985) was lower than during the second period (1985-2002) (not shown). There was an increment of 1.92 ha in forests from

1941 to 1985, whereas from 1985 to 2002, the observed increment in forest area was 4.95 ha, with a higher number of isolated forest patches on grasslands in 2002 than 1985. Analysis of land use cover during these periods showed a more intensive use of grassland areas for agriculture in 1941 and 1985 (Adelmann and Zellhuber 2004), whereas in 2002 these areas were already abandoned and recovered by grasslands (Matte 2006). Therefore, model parameterization and validation were conducted for both initial maps from 1941 and 1985, searching for the best fit to maps from 1985 and 2002 as described in the previous paragraph.

Seed dispersal

In Santana hill, most of the forest tree species colonizing grasslands are zoochoric (Müller and Forneck 2004). Local studies suggest that the main dispersal vectors are small-sized birds (28% of bird species are frugivorous and with mean body weight of $22\text{g} \pm 17.73$) (Forneck 2001) and small rodents, such as *Akodon montensis* (Thomas 1913) and *Oligoryzomys flavescens* (Waterhouse, 1837) (Penter et al. 2008). It is well known that animal body size is strongly correlated to space use (Jetz et al. 2004, Spiegel and Nathan 2007). Despite the absence of local studies relating the space use of dispersal vectors with plant dispersion patterns, other studies reporting movement behavior of such small sized animals showed that small passerines (weight <110g) and small rodents (mean weight ranging from 35g to 68g) dispersed mostly <51m from seed sources (Vieira et al. 2005, Jordano et al. 2007). Therefore, model parameterization for the best fitting of simulated and observed vegetation maps was conducted considering a higher proportion of seeds dispersed short distances ($p_{seed} = 0.95$, Eq. 3) and a fixed value of mean distance for short distance dispersal ($\lambda_1 = 5$ m) to account for the cell size considered (5 m x 5 m), yielding the following combination of parameters for mean dispersal distances λ_1 and λ_2 : $\lambda_1 = 5$ m, $\lambda_2 = 10$ m; $\lambda_1 = 5$ m, $\lambda_2 = 50$ m; $\lambda_1 = 5$ m, $\lambda_2 = 100$ m. These values for long distance dispersal were chosen to

account for the range of distance values found for seeds dispersed by small-sized frugivorous birds (Jordano et al. 2007).

Fire frequency

Model parameterization of fire frequency was conducted by changing the way the probability of fire spread (p_{fire}) was considered in the test for a fire to spread in the first ignited cell. In a first simulation case, p_{fire} was calculated locally in the first ignited cell (Eq. 2), i.e., based on local values of fuel moisture and grass biomass, as described before (see *Fire spread in the 2D-aDGVM*). In a second simulation case, a pre-defined constant value ($p_{fire} = 10\%$) was considered. For both cases, the tests for a fire to spread to other surrounding cells remained as described before (see *Fire spread in the 2D-aDGVM*).

Validation of the 2D-aDGVM

Table 3 shows an outline of parameter values used for validation of local vegetation growth and biomass at the cell scale (only changed aDGVM parameter values), as well as spatio-temporal vegetation dynamics at the landscape scale (parameters from the new implementations in 2D-aDGVM). To an overview of all other aDGVM parameters' descriptions and values see Tables 1-15. Simulations conducted with probability of fire spread (p_{fire}) calculated as a function of grass biomass (see *Fire spread in the 2D-aDGVM*) generated more frequent fires (fire return interval varied from 1 to 5 years) than those considering a fixed value of $p_{fire} = 10\%$ (fire return intervals varied from 1-10 years) (not shown). The best fit between observed and simulated spatio-temporal dynamics of forest-grassland mosaics (i.e., highest values of simple matching and more similar values of final total landscape forest cover) were obtained with parameters $\lambda_1 = 5$ m and $\lambda_2 = 10$ m (mean distances for short and long distance dispersal, respectively) (black and striped columns and squares in Fig. 9) for both fire regimes and initial starting vegetation map (black for starting in

1941 and striped for starting in 1985) (Fig. 9). Simulations starting with observed map of 1941 reproduced well the observed landscape of 1985 (simple matching = 0.9572) when considering more frequent fires, and the observed landscape of 2002 (simple matching = 0.9362) when considering less frequent fires (Fig. 9). On the other hand, simulations starting with observed map from 1985 showed good agreement (simple matching = 0.9283) with observed vegetation in 2002 only with less frequent fires (Fig. 9). However, they underestimated the number of isolated forest patches on grassland (lower panel in Fig. 9).

The highest matching between observed and simulated vegetation maps was obtained with the lowest value of parameter λ_2 (mean distance of long distance dispersal; Eq. 3). In addition, the failure in predicting the number of isolated forest patches in grasslands suggests that the good agreement between simulated and observed forest increment in time (Fig. 1) could mainly be attributed to dynamics throughout the edges. Together with the possible failures in model parameterization, we did not consider other sources of local environmental heterogeneity, such as rocky outcrops in grasslands, which could enhance the chances of tree establishment on open sites more distant from the main seed sources by increasing the attractiveness for long distance dispersal (Carlucci et al. 2011), or affecting local site humidity and/or primary production and, finally, the range of conditions necessary for a fire to spread locally (Pillar 2003), irrespective of the slope orientation. Indeed, spatially explicit models showed that increased seed availability in localized clumps had the strongest impact on the long-term tree-grass coexistence in savannas (Jeltsch et al. 1998) and improved water conditions generated by spatial heterogeneity should play a significant effect on tree establishment in arid and semiarid regions (water limited sites) and when it constitutes an advantage to trees (fire breaks) in the presence of fire in mesic regions (Favier et al. 2004).

Further, the model used here did not consider the effect of topography on surface water runoff. However, despite the observed and expected relationship between the occurrence of forests in sites with higher convergence of groundwater flow or nearby

thalwegs, this was not so evident to predict the probability of forest patch occurrences beyond thalwegs as a function of topographic features in areas with smooth relief and under frequent fires and intensive grazing in the southern Brazilian Plateau (Matte 2009). In addition, a recent study in the same southern Brazilian Plateau and using soil organic matter carbon isotopes to quantify shifts across a vegetation gradient showed no topographic-related nutrient inputs from water surface runoff associated to forest expansion, which have been occurring continuously during the past millennia and simultaneously from continuous-forest borders and patches formation/expansion in outposts ahead, i.e., in adjacent grasslands (Silva and Anand 2011).

Table 3. Model parameters used for validation of vegetation growth and spatio-temporal dynamics at Morro Santana, Porto Alegre, Brazil (30°04'32"S; 51°06'05"W). Table shows parameters from new implementations in 2D-aDGVM and only aDGVM parameters with changed values for model fitting. For a complete overview of all aDGVM parameters see Tables 1-15 in Appendix 1.

Scope	Parameter	Description	Value	Units	
Grid resolution	x	Cell size	25	m ²	
	H_1	Linear factor for height calculation	2.1877 (C_3)	unitless	
Allometric constants	H_2	Exponent for height calculation	0.3594 (C_3)	unitless	
	d_{st}	Parameter to calculate stem diameter	1.5893 (C_3)	unitless	
Fire sub-model	P_{fire}	Fire spread probability	variable		
	a	Parameter to calculate P_{fire}	-2.2	unitless	
	b	Parameter to calculate P_{fire}	1.489	unitless	
	$\theta_{f(grass)}$	Fuel moisture of grass biomass	variable	%	
	U_{hr}	Wind speed at the fuel level	variable	m/s	
	T_a	Daily air temperature	variable	°C	
	T_f	Air temperature at the fuel level	variable	°C	
	H_f	Relative humidity at the fuel level	variable	%	
	R_{sr}	Solar radiation at the understory vegetation	variable	MJ/m ² /day	
	τ_d	Canopy transmittance in deciduous and semi-deciduous forests	8.2	%	
	τ_e	Canopy transmittance in evergreen forests	3.3	%	
	Seed dispersal sub-model	b_j	Bias value for wind-corrected directional probabilities of fire spread	2.0: target cell [i,j] 2.0: cell [(i+1), (j-1)] 1.5: cell [(i), (j-1)] 1.5: cell [(i+1), (j)] 1.0: cell [(i+1), (j+1)] 1.0: cell [(i), (j+1)] 1.0: cell [(i-1), (j+1)] 1.0: cell [(i-1), (j)] 1.0: cell [(i-1), (j-1)]	unitless
		P_{seed}	Probability of short distance dispersal	0.95	prop
λ_1		Mean distance for short distance dispersal	5	m	
λ_2		Mean distance for long distance dispersal	10	m	

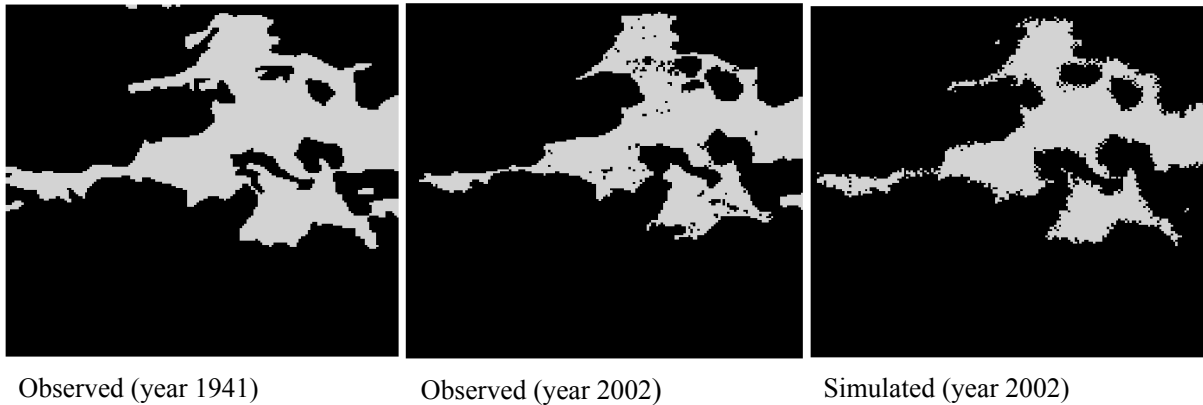
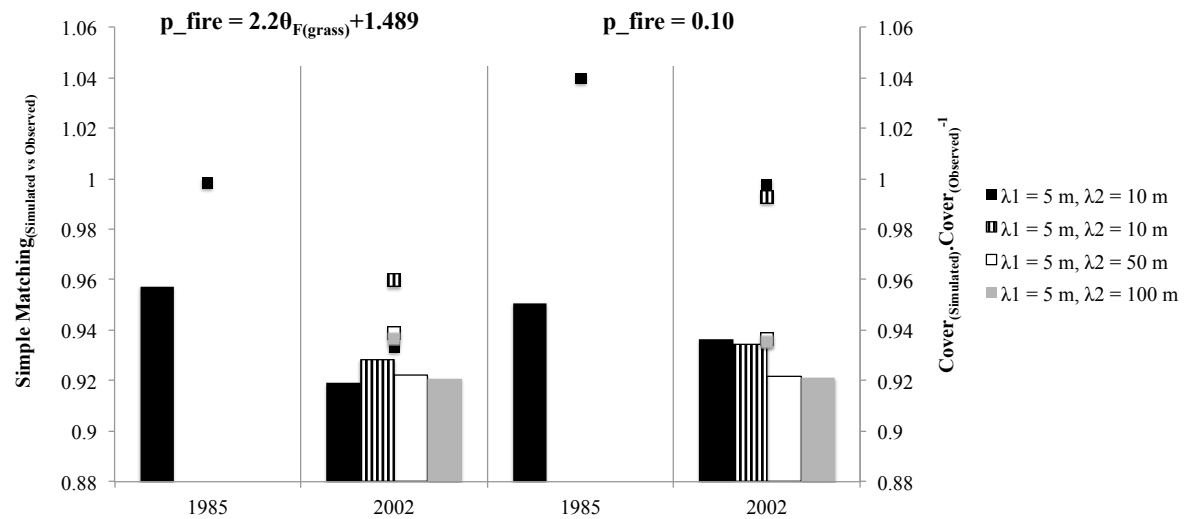


Figure 9. Observed and simulated forest expansion over grasslands in Morro Santana, Porto Alegre, Brazil ($30^{\circ}04'32''S$; $51^{\circ}06'05''W$) considering vegetation and topographic sampled maps from a predominantly south face of the hill (72 ha). The graphic shows simulation results from different combinations of parameter values for seed dispersal distances (λ_1 = mean distance of short distance dispersal; λ_2 = mean distance of long distance dispersal, represented by colors of columns and squares) and probability of fire spread ($p_{fire} = 2.2\theta_{F(grass)} + 1.489$ for strong feedback of grass biomass on fire frequency, or a fixed value of $p_{fire} = 10\%$), searching for the best spatio-temporal fit between observed and simulated dynamics through simple matching (columns) and final proportion of landscape covered by forest (squares). Due to different observed dynamics from 1941 to 1985 and from 1985 to 2002 (see *Parameterization and validation of 2D-aDGVM*), parameters were tested considering different initial observed vegetation maps (1941 or 1985). Simulations considering the initial vegetation map of 1941 (black columns and squares) were conducted only with lower values of dispersal distance parameters, searching for the best fit with observed map from 1985 and 2002. Results for year 2002 were obtained from simulations considering the initial vegetation map from 1985. Simulations considered a spin-up phase of 100 years before starting seed dispersal and fire spread rule, to assure the aDGVM stabilization inside each $25m^2$ cell. The lower panel shows snapshots from observed and simulated maps (black = forest; grey = grassland).

References

- Adelmann, W. and A. Zellhuber. 2004. Analysis of environmental conflicts in areas of urban expansion using scenario methods (com versão em português). Pages 60-64 *in* Workshop "Proteção e manejo da vegetação natural da região de Porto Alegre com base em pesquisas de padrões e dinâmica da vegetação". PPG-Ecologia, UFRGS, Porto Alegre.
- Allen, R. G., L. S. Pereira, D. Raes, and M. Smith. 1998. Crop evapotranspiration - Guidelines for computing crop water requirements. FAO - Food and Agriculture Organization of the United Nations, Rome.
- Allen, R. G., R. Trezza, and M. Tasumi. 2006. Analytical integrated functions for daily solar radiation on slopes. *Agricultural and Forest Meteorology* **139**:55-73.
- Berjak, S. G. and J. W. Hearne. 2002. An improved cellular automaton model for simulating fire in a spatially heterogeneous Savanna system. *Ecological Modelling* **148**:133-151.
- Caplat, P., M. Anand, and C. Bauch. 2008. Interactions between climate change, competition, dispersal, and disturbances in a tree migration model. *Theoretical Ecology* **1**:209-220.
- Cardoso, M. F., C. A. Nobre, D. M. Lapola, M. D. Oyama, and G. Sampaio. 2008. Long-term potential for fires in estimates of the occurrence of savannas in the tropics. *Global Ecology and Biogeography* **17**:222-235.
- Cargnelutti-Filho, A., R. Matzenauer, J. R. T. Maluf, I. A. Didoné, A. C. m. Bueno, J. I. K. d. Trindade, and J. T. Sawasato. 2007. Radiação Solar Global Decendial no Estado do Rio Grande do Sul: Tabelas de Probabilidades. FEPAGRO, Porto Alegre.
- Carlucci, M. B., L. d. S. Duarte, and V. D. Pillar. 2011. Nurse rocks influence forest expansion over native grassland in southern Brazil. *Journal of Vegetation Science* **22**:111-119.
- Cramer, W., A. Bondeau, F. I. Woodward, I. C. Prentice, R. A. Betts, V. Brovkin, P. M. Cox, V. Fisher, J. A. Foley, A. D. Friend, C. Kucharik, M. R. Lomas, N. Ramankutty, S. Sitch, B. Smith, A. White, and C. Young-Molling. 2001. Global response of terrestrial ecosystem structure and function to CO₂ and climate change: results from six dynamic global vegetation models. *Global Change Biology* **7**:357-373.
- Favier, C., J. Chave, A. Fabing, D. Schwartz, and M. A. Dubois. 2004. Modelling forest-savanna mosaic dynamics in man-influenced environments: effects of fire, climate and soil heterogeneity. *Ecological Modelling* **171**:85-102.
- Fidelis, A. 2008. Fire in subtropical grassland in southern Brazil: effects on plant strategies and vegetation dynamics. Doutorado. Technische Universität München, Freising.
- Finney, M. A. 1998. FARSITE: Fire Area Simulator—model development and evaluation. Page 47. Res. Pap. RMRS-RP-4. U.S. Department of Agriculture, Forest Service, Rocky Mountain Research Station, Fort Collins, CO.
- Fisher, R., N. McDowell, D. Purves, P. Moorcroft, S. Sitch, P. Cox, C. Huntingford, P. Meir, and F. Ian Woodward. 2010. Assessing uncertainties in a second-generation dynamic vegetation model caused by ecological scale limitations. *New Phytologist* **187**:666-681.
- Forneck, E. D. 2001. Biótopos naturais florestais nas nascentes do Arroio Dilúvio (Porto Alegre e Viamão, RS) caracterizados por vegetação e avifauna. Master. UFRGS, Porto Alegre.
- Garcia Martinez, P. 2005. Caracterización química y física de los suelos del Morro Santana (Porto Alegre, Rio Grande do Sul, Brasil). Master. Technische Universität München, Freising.
- Hargrove, W. W., R. H. Gardner, M. G. Turner, W. H. Romme, and D. G. Despain. 2000. Simulating fire patterns in heterogeneous landscapes. *Ecological Modelling* **135**:243-263.

- Hernandes, J. L., M. J. Pedro Júnior, and L. Bardin. 2004. Variação estacional da radiação solar em ambiente externo e no interior de floresta semidecídua. *Revista Árvore* **28**:167-172.
- Higgins, S. I., W. J. Bond, E. C. February, A. Bronn, D. I. W. Euston-Brown, B. Enslin, N. Govender, L. Rademan, S. O'Regan, A. L. F. Potgieter, S. Scheiter, R. Sowry, L. Trollope, and W. S. W. Trollope. 2007. Effects of four decades of fire manipulation on woody vegetation structure in savanna. *Ecology* **88**:1119-1125.
- Higgins, S. I. and M. L. Cain. 2002. Spatially realistic plant metapopulation models and the colonization–competition trade-off. *Journal of Ecology* **90**:616-626.
- Jeltsch, F., S. J. Milton, W. R. J. Dean, N. van Rooyen, and K. A. Moloney. 1998. Modelling the impact of small-scale heterogeneities on tree–grass coexistence in semi-arid savannas. *Journal of Ecology* **86**:780-793.
- Jetz, W., C. Carbone, J. Fulford, and J. H. Brown. 2004. The Scaling of Animal Space Use. *Science* **306**:266-268.
- Jordano, P., C. García, J. A. Godoy, and J. L. García-Castaño. 2007. Differential contribution of frugivores to complex seed dispersal patterns. *Proceedings of the National Academy of Sciences* **104**:3278-3282.
- Lorenzi, H. 2000. Árvores Brasileiras: manual de identificação e cultivo de plantas arbóreas nativas do Brasil. 3 edition. Instituto Plantarum, Nova Odessa, São Paulo.
- Matte, A. L. 2006. Padrões espaciais de manchas florestais em mosaicos de floresta-campo nos morros de Porto Alegre, RS. Page 461 *in* Salão de Iniciação Científica UFRGS/PROPESQ, Porto Alegre, Brazil.
- Matte, A. L. 2009. Padrões de distribuição, estrutura e contexto de manchas florestais em um mosaico de campo e floresta no planalto sul brasileiro. Universidade Federal do Rio Grande do Sul, Porto Alegre.
- Müller, S. C. 2005. Padrões de espécies e tipos funcionais de Plantas lenhosas em bordas de floresta e Campo sob influência do fogo. Universidade Federal do Rio Grande do Sul, Porto Alegre.
- Müller, S. C. and E. D. Forneck. 2004. Forest-grassland mosaics in the hills of Porto Alegre city: a study case of forest expansion patterns in Santana hill, Rio Grande do Sul, Brazil. Pages 29-37 *in* Workshop - Proteção e manejo da vegetação natural da região de Porto Alegre, com base em pesquisas de padrões e dinâmica da vegetação. Programa de Pós-Graduação em Ecologia/UFRGS, Porto Alegre.
- New, M., M. Hulme, and P. Jones. 2000. Representing Twentieth-Century Space-Time Climate Variability. Part I: Development of a 1961-1990 Mean Monthly Terrestrial Climatology. *Journal of Climate* **12**:829-856.
- New, M., D. Lister, M. hulme, and I. Makin. 2002. A high-resolution data set of surface climate over global land areas. *Climate Research* **21**:1-25.
- Nimer, E. 1990. Clima. Pages 151-187 *in* IBGE, editor. Geografia do Brasil: Região Sul. IBGE, Rio de Janeiro.
- Peng, C. 2000. From static biogeographical model to dynamic global vegetation model: a global perspective on modelling vegetation dynamics. *Ecological Modelling* **135**:33-54.
- Penter, C., E. Pedó, M. E. Fabián, and S. M. Hartz. 2008. Inventário Rápido da Fauna de Mamíferos do Morro Santana, Porto Alegre, RS. *Revista Brasileira de Biociências* **6**:117-125.
- Pillar, V. D. 2003. Dinâmica de expansão florestal em mosaicos de floresta e campos no sul do Brasil. Pages 209-216 *in* V. Claudino-Sales, editor. Ecossistemas brasileiros: manejo e conservação. Expressão Gráfica e Editora, Fortaleza.
- Pillar, V. D. 2006. MULTIV, software for multivariate exploratory analysis, randomization testing and bootstrap resampling (for Macintosh and Windows OS). Porto Alegre.

- Reitz, R., R. M. Klein, and A. Reis. 1988. Projeto Madeira do Rio Grande do Sul. Corag, Porto Alegre.
- Rothermel, R. C. 1972. A mathematical model for predicting fire spread in wildland fuels. USDA Forest Service Research Paper **INT-115**.
- Rothermel, R. C., R. A. Wilson, G. A. Morris, and S. S. Sackett. 1986. Modeling moisture content of fine dead wildland fuels: Input to the BEHAVE fire prediction system. U.S. Department of Agriculture, Forest Service, Intermountain Research Station, Ogden, UT.
- Sato, H., A. Itoh, and T. Kohyama. 2007. SEIB-DGVM: A new Dynamic Global Vegetation Model using a spatially explicit individual-based approach. *Ecological Modelling* **200**:279-307.
- Scheiter, S. and S. I. Higgins. 2009. Impacts of climate change on the vegetation of Africa: an adaptive dynamic vegetation modelling approach. *Global Change Biology* **15**:2224-2246.
- Silva, L. C. R. and M. Anand. 2011. Mechanisms of Araucaria (Atlantic) forest expansion in southern Brazil, *Ecosystems* (accepted).
- Solano-Peraza, J. E. 2003. Retenção de água e pedofunções para solos do Rio Grande do Sul. Universidade Federal de Santa Maria, Santa Maria.
- Spiegel, O. and R. Nathan. 2007. Incorporating dispersal distance into the disperser effectiveness framework: frugivorous birds provide complementary dispersal to plants in a patchy environment. *Ecology Letters* **10**:718-728.
- Streck, E. V., N. Kämpf, R. S. D. Dalmolin, E. Klamt, P. C. Nascimento, P. Schneider, E. Giasson, and L. F. S. Pinto. 2008. Solos do Rio Grande do Sul. 2 edition. EMATER/RS - ASCAR, Porto Alegre.
- Tian, Y. Q., R. J. Davies-Colley, P. Gong, and B. W. Thorrold. 2001. Estimating solar radiation on slopes of arbitrary aspect. *Agricultural and Forest Meteorology* **109**:67-74.
- Tilki, F. and R. F. Fisher. 1998. Tropical leguminous species for acid soils: studies on plant form and growth in Costa Rica. *Forest Ecology and Management* **108**:175-192.
- Trollope, W. S. W., C. de Ronde, and C. J. GELDENHUYS. 2004. Fire Behavior. Pages 27-59 in J. G. Goldammer and C. de Ronde, editors. *Wildland Fire Management Handbook for Sub-Saharan Africa*. Global Fire Monitoring Center (GFMC).
- Vieira, E. M., G. Iob, D. C. Briani, and A. R. T. Palma. 2005. Microhabitat selection and daily movements of two rodents (*Necromys lasiurus* and *Oryzomys scotti*) in Brazilian Cerrado, as revealed by a spool-and-line device. *Mammalian Biology - Zeitschrift für Säugetierkunde* **70**:359-365.
- Woodward, F. I., T. M. Smith, and W. R. Emanuel. 1995. A global land primary productivity and phytogeography model. *Global Biogeochem. Cycles* **9**:471-490.

CAPÍTULO 2 (ARTIGO 1)

Spatial heterogeneity and feedback mechanisms in forest-grassland mosaics²

² Este manuscrito, com Simon Scheiter³, Enio Sosinski⁴, Alessandra Fidelis⁵, Madhur Anand⁶ e Valério D. Pillar¹ como co-autores, será submetido para publicação na revista Ecology.

¹Laboratory of Quantitative Ecology, Department of Ecology, Universidade Federal do Rio Grande do Sul, Porto Alegre, Brazil

³Biodiversity and Climate Research Centre (LOEWE BiK-F), Frankfurt, Germany

⁴Embrapa Temperate Agriculture, Pelotas, Brazil

⁵Department of Ecology, Universidade de São Paulo, São Paulo, Brazil

⁶ Global Ecological Change Laboratory, School of Environmental Sciences, University of Guelph, Canadá

ABSTRACT

A longstanding question in ecology is how mosaics of forests and open-canopy ecosystems persist over millennia in sites where climatic conditions favor forests. We evaluate the effect of spatial heterogeneity on density-dependent feedback mechanisms linked to fire that arbitrate dynamics of forest-grassland mosaics in South Brazil. We therefore incorporated a Dynamic Global Vegetation Model (the aDGVM) into a spatially explicit model (2D-aDGVM) that simulates topographic heterogeneity, fire spread behavior and seed dispersal. Our results showed that coexistence of forests and grasslands as alternative stable states was possible over long periods at the same mesic conditions only in response to frequent fires promoted by a strong feedback between grass biomass and fire frequency. However, spatio-temporal density dependent processes linked to fire and topographic properties at the patch scale affected the rate of forest expansion at the landscape scale. In addition, dynamics of forest-grassland mosaics were sensitive to the spatial arrangement of vegetation patches, showing the strong effect of size and distribution of fire-prone (grassland) and fire-sensitive (forest) patches on defining the availability of conditions under which coexistence is possible. At the landscape scale, the persistence of two coexisting vegetation types with an inherent asymmetry of competitive interactions was possible when fire-prone patches (grassland) were highly aggregated and negatively affected the connectivity of the fire-sensitive patches (forest). Therefore, the impact of the spatial component of fire behavior on the stability of these contrasting systems is dependent on the relative cover and spatial arrangement of fire-prone and fire-sensitive vegetation patches. These vegetation patches interacted with seed dispersal to arbitrate the persistence of grasslands when they coexist with forests. The present model is the first to consider the impacts of both biotic (dispersal) and abiotic (topographic heterogeneity) spatial processes on alternative stable states in terrestrial ecosystems, and the good agreements on predicting spatio-temporal forest-grassland

dynamics in South Brazil suggests that this approach is appropriate for understanding this complex mosaic system.

KEY WORDS: Adaptive DGVM, cellular automata model, spatial heterogeneity, topography, dispersal, forest expansion, subtropical grasslands.

INTRODUCTION

A longstanding problem in ecology is how mosaics of forests and open-canopy ecosystems (natural grasslands and savannas) persist over millennia at sites where climatic conditions favor forests. When climate alone does not explain or predict such a long-term coexistence, these co-occurring and contrasting vegetation types have been treated as alternative stable states (Grimm 1984, Beckage and Ellingwood 2008, Warman and Moles 2009, Staver et al. 2010). In the context of vegetation mosaics, positive feedbacks from components of a particular vegetation state in promoting its own required conditions (e.g. open-canopy conditions promoted by frequent burnings of fire-prone grasses; facilitation effect of trees on newly establishing ones) may imply negative feedbacks for the persistence of the other vegetation state (e.g. mortality of fire-sensitive forest trees by grass fires and mortality of grasses by shade effect of closed-canopy trees). Models are essential tools for understanding which and how biotic and abiotic interactions control system behavior and for exploring long-term vegetation dynamics. However, predictions for explaining any situation where grasses and trees closely interact (grass-tree coexistence in savannas, forest-grassland or forest-savanna mosaics) has shown to be a challenging task.

Climatic factors control the thresholds of system stability and the variability of disturbance-return intervals (Sternberg 2001, Bond et al. 2003, Sankaran et al. 2005, Higgins et al. 2010). However, different non-spatial models have shown that the way disturbances are considered to affect or to be affected by vegetation have implications on predictions of grass-tree coexistence at the patch scale and the biogeographical distribution of any situation where grasses and trees closely interact, as well as analytical evidences of alternative stable states. Continental and global scale analysis that explore how patterns of woody cover distribution are mediated by rainfall-disturbances interactions found high uncertainties in transitional zones (Cramer et al. 2001), where woody cover in mesic sites (mean annual precipitation ranging from 850 mm to 2000 mm) was overestimated (Bond et al. 2005, Sankaran et al.

2005, Hickler et al. 2006, Staver et al. 2010, Lehmann et al. 2011). In these transition zones, climatic ranges overlap and primary production of both grasses and trees are high, giving rise to the observed similar frequency of occurrence of forests and open-canopy systems (grasslands and savannas), sometimes forming mosaics, in these regions (Sankaran et al. 2005, Staver et al. 2010).

Fire is one of the main evolutionary forces shaping ecosystems distribution worldwide (Bird and Cali 1998, Bond and Keeley 2005), and has been pointed as a key factor determining tree cover and grass persistence under mesic conditions (Sankaran et al. 2005, Higgins et al. 2010). In fact, in the absence of fire, woody vegetation is expected to dominate in humid regions (Bond et al. 2005, Scheiter and Higgins 2009), suggesting a strong feedback of vegetation on fire, which can establish coexistence of grasses and trees in transition zones. Numerous modelling approaches explored the feedbacks between vegetation and fire and the mechanisms driving the observed long-term stability of grass-tree coexistence in savannas. These studies aim to explain vegetation patterns where climate does not seem to be the limiting factor for closed forests (e.g. Sarmiento 1992, Higgins et al. 2000, D'Odorico et al. 2006, Beckage et al. 2009, Higgins et al. 2010). Nevertheless, due to the presence of a continuous dominant grass layer, regardless of having fire-resistant trees with higher resprouting ability than forest trees (Hoffmann et al. 2003) that promotes an advantage to survive over a pyrophytic ground cover, savannas and grasslands may share similar biophysical explanations related to fire for their persistence when co-occurring with forests in more mesic conditions.

Therefore, when fire frequency is defined by climate alone and causes only fixed rates of fuel loss in time, prevailing climate can only predict gradual transitions between dominant vegetation types as fire frequency changes, but does not explain the observed abrupt shifts between co-occurring ecosystems (grassland, savannas and forests) at the regional scale (Sankaran et al. 2005, Beckage et al. 2009, Higgins et al. 2010, Staver et al. 2010). However,

by considering positive feedbacks of grass abundance on fire frequency, negative feedbacks of fire on survival of forest trees, and by modeling fire as discrete and stochastic events in time (Beckage et al. 2011), rapid shifts between alternative vegetation states (D'Odorico et al. 2006, Beckage et al. 2009) can be predicted, and stable solutions for grass-tree coexistence in savannas were achieved. Therefore, stability at the patch scale is attained by preventing grasses to be excluded by trees when aboveground competition is intense, even in the absence of separate rooting niches (Scheiter and Higgins 2007). In addition, by including mechanistic and empirically well-supported assumptions of fire effects on different life stages of trees, continental-scale analysis have successfully improved predictions of vegetation distribution in Africa (Scheiter and Higgins 2009) as well as alternative stable solutions (savanna and forest) for mesic sites (1000 - 2000 mm) (Staver et al. 2010).

At the regional scale, complex interactions may arise by the effect of spatial heterogeneity on fire due to variations on vegetation controls across space and spatial scales (Danz et al. 2011). Spatial heterogeneity of factors such as topography, soil texture and drainage and density of woody vegetation influence the distribution of suitable habitats and the spread of disturbances across the landscape (Pickett and White 1985, Turner 1989), as well as how disturbance will affect the system locally (Watt 1947, Chesson and Huntly 1989, Turner 1989, Skarpe 1992, Scholes and Archer 1997), by changing the balance between positive and negative feedbacks (e.g. the asymmetry of competitive interactions among grasses and trees). For instance, among the sources of spatial heterogeneity, topography is probably the most important variable controlling fire regimes and providing the mechanisms for grass-tree coexistence at the fine-intermediate scale of prairie-forest boundary in Minnesota, USA (Danz et al. 2011). Though the role of topography as the major determinant of the microclimate of a site (Geiger 1965, Oke 1987) through variations on incoming solar radiation is well known, to what extent radiation is related to fire behavior through feedback interactions with vegetation structure and fuel moisture has been less explored by models. In

addition, the outcomes of considering space, as well as interactions between spatial processes driven by abiotic (e.g. topographic heterogeneity) and biotic factors (e.g. dispersal) were less explored when dealing with alternative stable states in terrestrial ecosystems (Scheffer and Carpenter 2003, van Nes and Scheffer 2005).

In Southern Brazil, fire-prone ancient grasslands intermingle with mostly nonflammable humid forests, composed of fire-sensitive species, and have coexisted over millennia in presence of fire (Behling 2002), forming mosaics with sharp boundaries, which have persisted even under the modern wet climatic conditions that favor forests (1250 mm - 2000 mm; Quadro et al. 2010). Therefore, these mosaics are a great case to investigate the scaling of interactions among positive and negative feedbacks that arise between vegetation structure and disturbance behavior at the patch scale to the complex patterns of co-occurring alternative vegetation states at the landscape scale (grassland and forest patches). For this, the adaptive Dynamic Global Vegetation Model (aDGVM; Scheiter and Higgins 2009) was incorporated in a spatially explicit modeling framework (2D-aDGVM) for capturing microclimatic variations at the patch scale in relation to topography (topographic variations in incoming solar radiation) and for exploring interactions between vegetation and fire spread behavior at the boundaries of a forest-grassland mosaic. The importance of the emerging spatial component of stochastic fire behavior, promoted by such local density-dependent mechanisms on the stability of grass-tree coexistence is not well known (Higgins et al. 2000). In addition, at the landscape scale, this is expected to govern the rate of canopy closure and hence the persistence of any system with a continuous grass layer, irrespective of the presence of trees (Lehmann et al. 2011). We hypothesize that this is dependent on the relative cover and spatial arrangement of fire-prone and fire-sensitive vegetation patches, which interact with seed dispersal on arbitrating persistence of open-canopy ecosystems (in this case, grasslands) when they coexist with forests.

METHODS

Model Description

The model (2D-aDGVM) we develop is a spatially explicit model that incorporates the adaptive Dynamic Global Vegetation Model (aDGVM) (Scheiter and Higgins 2009) to simulate forest-grassland dynamics at a regional landscape scale, including several new spatial components, such as topographic variation (slope declination and orientation), fire spread behavior and seed dispersal. A detailed motivation and description of the 2D-aDGVM, as well as model parameterization and validation is presented in the Supplementary material. The following paragraphs provide a brief overview.

In 2D-aDGVM, a regular grid of square cells with specified size represents the landscape. Inside each cell, the aDGVM simulates the dynamics of a stand (grassland, forest or grass-tree coexistence) as a function of climatic and edaphic conditions. In daily time steps, the aDGVM simulates biophysical, physiological and demographic processes at the leaf, canopy, plant, population and ecosystem level in an individual based framework. Trees (C_3 -photosynthesis) are simulated individually and are represented by a “typical” tree type (e.g. forest is constituted by this representative plant type) i.e., aDGVM do not consider species. Grasses (C_4 -photosynthesis) are simulated by grass biomass below and grass biomass between tree canopies, i.e. population structure and demography of grasses are ignored. Inter-specific (grass-tree) and intra-specific (grass-grass; tree-tree) competitive interactions are mediated by light (shading effects) and water (in different soil layers). Fire is simulated by a semi-empirical model, in which fire intensity is a function of fuel biomass, moisture and wind speed (Higgins et al. 2008), and stem mortality is a function of fire intensity and tree size, affecting tree population and inter-specific interactions. For a more detailed description of the aDGVM, see Supplementary material S1 of the online additional supporting information from Scheiter and Higgins (2009).

In addition to the spatially explicit structure where the aDGVM simulates vegetation in each grid cell, 2D-aDGVM includes algorithms to adjust the incoming solar radiation for inclined surfaces (Allen et al. 2006) and the corrections to heating and drying of dead fuel moisture (Rothermel et al. 1986) from aDGVM accordingly, as well as the spread of fire and the dispersal of produced seeds across the landscape. Fire ignition is determined by an annual stochastic ignition sequence to determine days when ignition occurs, based on mean annual relative air humidity of the site (Scheiter and Higgins 2009). On an ignition day, the first ignited cell is chosen at random by 2D-aDGVM and is ignited if fire intensity exceeds a pre-defined threshold (i.e., if the amount of fuel biomass is sufficient to burn) (Scheiter and Higgins 2009). If this ignition is successful, fire spreads based on an empirical probability p_{fire} , which is calculated locally from fuel moisture of grass biomass ($\theta_{F(grass)}$) by

$$p_{fire} = -2.2\theta_{F(grass)} + 1.489 \text{ (Eq. 1)}$$

Finally, for a fire to spread to the adjacent eight neighboring grid cells, wind-corrected directional probabilities are calculated using p_{fire} and a bias value applied for each of the eight adjacent cells in relation to their orientation towards a prevailing northeast wind. Tree mortality is a function of fire intensity and tree height (Scheiter and Higgins, 2009)

Seed dispersal is a function of seed production and distance from seed sources in 2D-aDGVM. The distribution of seeds is defined by the probability density function

$$g_{(d_{ij})} = p_{seed} \frac{1}{\lambda_1} \exp\left(-\frac{d_{ij}}{\lambda_1}\right) + (1 - p_{seed}) \frac{1}{\lambda_2} \exp\left(-\frac{d_{ij}}{\lambda_2}\right) \text{ (Eq. 2)}$$

In Equation 2, d_{ij} is the distance between cell's midpoints, p_{seed} is the proportion of seeds dispersed short distances and λ_1 (m) and λ_2 (m) are mean distance of short and long distance dispersal, respectively. Similar equations were used to simulate seed dispersal in other spatial explicit models (Higgins et al. 2000, Higgins and Cain 2002, Caplat et al. 2008) and they were referred to as stratified (mixed) kernels, by considering short (first component of Eq. 2) and long (second component of Eq. 2) distance dispersal. Dispersed seeds are stored in the seed bank of each cell. Seed decay rate and probability of seed germination are applied daily by the aDGVM (see Supplement material S1 of the online additional supporting information from Scheiter and Higgins, 2009).

Study site

Data from Morro Santana, Porto Alegre, Southern Brazil (30°04'32"S; 51°06'05"W) were used for simulating forest-grassland mosaics. Morro Santana is a granitic hill (altitude max. 311 m a.s.l.) with approximately 1,000 ha. At this mesic site, mean annual precipitation is 1348 mm, with no marked dry season, and the average annual temperature is 19.5°C (Nimer 1990). Vegetation is a mosaic of forest (with species from Semideciduous Seasonal Forest and Atlantic Rain Forest) (Müller et al. 2007) and ancient “Campos” grasslands (Overbeck et al. 2007), with forest dominating on southern, eastern and western slopes, as well as in isolated patches frequently related to rock outcrops in grassland areas (Brack et al. 1998, Overbeck et al. 2006). Soils are developed from granite (acrisols, alisols and umbrisols) and those upon which grasslands occur today have apparently no restriction for the establishment of forest species (Garcia Martinez 2005). This forest-grassland mosaic system has occurred under the influence of fire since the late Holocene (Behling et al. 2007). At present, fire is still a frequent anthropogenic disturbance in Morro Santana, with return intervals of 2–6 years (Fidelis et al. 2010). Fire does not burn mature forest and forest expansion over grasslands is also evident (Overbeck et al. 2007). More detailed descriptions

of the study site, parameterization of aDGVM for testing vegetation growth, structure and biomass in presence and absence of fire, as well as parameterization of 2D-aDGVM for testing observed spatio-temporal vegetation dynamics in Morro Santana are provided in the Supplementary material.

Simulation experiments

Topography, fire frequency and vegetation dynamics

In a first experiment we evaluate spatio-temporal effects of topographic variation of incoming solar radiation on feedbacks between density-dependent fire spread behavior and vegetation dynamics. We therefore conducted simulations with one unique cell of size 1 ha; i.e., for these simulations, seed dispersal and fire spread in two dimensions (i.e., at the landscape scale) were not considered, and no assumptions concerning the spatial arrangement of trees and grasses inside the cell was made. These simulations were conducted in the presence and absence of fire, at different values of slope inclination (15° and 30°), which are representative of the average local value (see supplemental material), and two contrasting slope orientations (0° = North; 180° = South). These simulations were initialized with one adult reproductive tree.

To evaluate the effect of topographic variations on feedbacks between density-dependent fire spread behavior and vegetation dynamics in a two-dimensional context (i.e., at the landscape scale), simulations with the 2D-aDGVM were conducted on artificial landscapes. These artificial landscapes had 20×20 cells of 25m^2 each, and the cells were initialized with a central forest cell surrounded by nine grassland cells. A buffer of one cell width was considered surrounding the grid to avoid edge effects. The grid was subdivided in nine topographically different zones to account for the main eight slope orientations (0° = north, 45° = northeast, 90° = east, 135° = southeast, 180° = south, 225° = southwest, 270° = west and 315° = northwest) and a central zone with horizontal surfaces. Each topographic

zone was composed of 36 adjacent cells each (total of 900 m² in each zone). Therefore, simulations started with forest cover only in the central zone of the grid (the horizontal zone) and considered 15° of slope inclination (first simulation run) and 30° of slope inclination (second simulation run) in the surrounding eight grassland zones. All simulations considered a strong feedback of grass biomass on fire frequency (Eq. 1) and a predominant short-distance dispersal (in Eq. 2: proportion of seeds dispersed at short distances $p_{seed} = 0.95$; mean distance for short and long distance dispersal $\lambda_1 = 5$ m and $\lambda_2 = 10$ m, respectively), based on 2D-aDGVM parameterization to the study site (Supplement material).

Spatial heterogeneity, patch aggregation and dynamics of forest-grassland mosaics

We conducted 2D-aDGVM simulations to evaluate the sensitivity of forest-grassland dynamics to terrain heterogeneity and to different initial spatial arrangement of forest and grassland patches. In 2D-aDGVM, each cell can represent each pixel of an observed map with equal grain size. Therefore, observed and artificial maps were used to initialize the model. An observed vegetation map of Morro Santana from year 1941 was obtained from a categorical map of land use cover with grain size of 5 m (25 m² pixel size) (Adelmann and Zellhuber 2004). Two sampled windows were considered looking for predominantly south (sample 1: 722,275 m²) and predominantly north (sample 2: 675,325 m²) faces of the hill. Slope inclination (degrees) and orientation (degrees) maps from sample 1 and sample 2 were obtained from a Digital Elevation Model (CENECO/FAURGS 2004). Both sampled windows have relatively smooth terrain. Average slope inclination in sample 1 is 15.24°±7.89 and in sample 2 is 14.3°±10.16. Finally, the vegetation map from the predominantly south face was obtained according to topographical map sample 1. For operational reasons, the observed vegetation map from the predominantly north-facing terrain (sample 2) could not be used.

In one simulation case, the spatial arrangement of vegetation patches was the observed forest-grassland mosaic with well-aggregated patches and a predominant forest cover (76%). The second pattern was created artificially by random allocation of forest patches (cells with mature forest) covering a maximum of 10% of total landscape. With the observed vegetation pattern, simulations were conducted for the predominantly south-facing terrain (observed topographical map from sample 1). With the artificial vegetation pattern, simulations were conducted for the predominantly north-facing terrain (observed topographical map from sample 2), the predominantly south-facing terrain (observed topographical map from sample 1) and a horizontal terrain (artificial map with equal size of sample 1, but all cells with horizontal surfaces, i.e., 0° of slope inclination).

All simulations considered a strong feedback of grass biomass on fire frequency (Eq. 1) and a predominant short-distance dispersal (in Eq. 2: proportion of seeds dispersed at short distances $p_{seed} = 0.95$; mean distance for short and long distance dispersal $\lambda_1 = 5$ m and $\lambda_2 = 10$ m, respectively), based on 2D-aDGVM parameterization to the study site (Supplement material). Since there was no detailed information about the exact tree cover values in each forested pixel in the input observed vegetation map, a spin-up phase of 100 years was considered, before starting seed dispersal and fire spread rule across the landscape, to assure the aDGVM stabilization inside each cell. For each simulation case, coalescence of forest patches in time was evaluated through the Landscape Shape Index (LSI), which is a measure of aggregation or clumpiness (the LSI increases when patches become more disaggregated) (McGarigal and Marks 1995).

RESULTS

Spatio-temporal density-dependent mechanisms at the forest-fire fronts

Simulations conducted in the single 1ha-cell predicted a complete cover of forest even under frequent fires (Fig. 1). However, dynamics of vegetation stands was sensitive to topography in time (Fig. 1) and space (Fig. 2), showing strong feedbacks of grass biomass, tree density and topography on fire spread behavior. Simulations conducted in the single 1-ha cell (i.e., no seed dispersal and fire spread in two dimensions, no spatial arrangement of trees and grasses inside the cell) showed that the delay of at least 20 years in the time needed to a complete forest cover under frequent fires (fire return interval ranging from 1 to 5 years) was enhanced by tree density and slope orientation and inclination (Fig. 1). Tree density increased faster and fire occurrence stopped earlier when the cell was oriented to south and had a higher slope inclination (30°S), as opposed to the north-facing situation at lower inclination (15°N) (Fig. 1). Both situations occurred for a similar threshold value of tree density (around 0.12 ind.m⁻²), suggesting a strong effect of topography on fire control of the rate of increasing tree density in time. This threshold value was lower (<0.1 ind.m⁻²) for the other situations (30°N and 15°S) but also approximately the same when compared to each other (Fig. 1).

In a two-dimensional context, simulations of the artificial small grid (see *Simulation experiments: Topography, fire frequency and vegetation dynamics*) showed that under lower terrain inclination (15°) fire could spread even to sites with higher tree density, but this was more frequent in north facing sites (Fig. 2A). With higher inclination (30°, black dots and lines), fire spread only to sites with lower tree density, irrespective of their slope orientation (Fig. 2A and 2B).

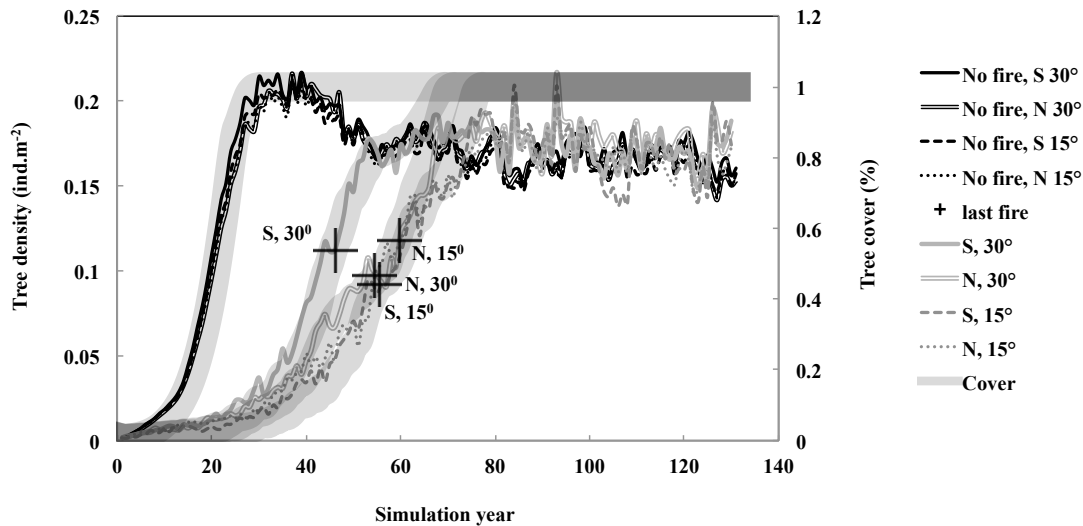


Figure 1. Simulation results of increasing tree density and cover using different values of slope inclination and orientation, in the absence of fire and considering frequent fires (fire return interval of 1-5 years) generated by strong feedback of grass biomass on fire frequency (Eq. 1). Vegetation growth is a function of input climatic and edaphic data from Morro Santana Hill, Porto Alegre, Brazil (30°04'32"S; 51°06'05"W). Simulations were conducted starting with one adult tree in one individual cell of size. Results from simulations are mean values from ten replicates of each simulation case.

The simulated total number of trees was sensitive to cell size, when comparing results from the single 1-ha cell (Fig. 1) with those from 25-m² cells considered in simulations with the artificial small grid (Fig. 2). In the 1-ha cell, fire was able to spread until a tree density value of 0.13 ind.m⁻² (1,300 individuals) (Fig. 1) whereas in the 25-m² cells, fire fronts stopped in cells with more than 2.5 ind.m⁻² (60 individuals) (Fig. 2). The higher the tree density, the lower the fuel biomass (Fig. 2) and also the probability of fire spread (Supplement material; see Eq. 1 and results from horizontal surfaces in Fig. 6). In addition with the expected more rapid increase of tree density in 30°S facing cells of 25 m² as shown in those of 1-ha size (Fig. 1), fuel biomass is also expected to decrease slower in the 1-ha cells (not shown) compared to the 25-m² cells (Fig. 2) and that is the probable explanation for the absence of fire in 30°S facing cells of 25-m² with higher values of tree density (Fig. 2B).

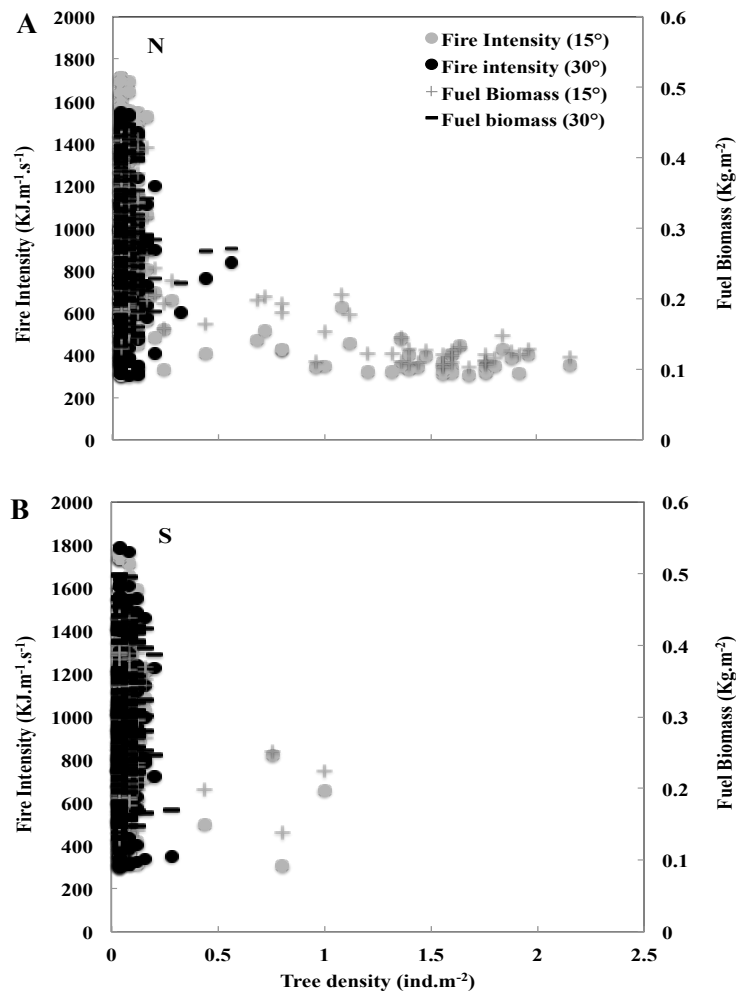


Figure 2. Simulation results from an artificial small grid with 20 x 20 cells of 25 m² each showing fire intensity and fuel biomass as a function of tree density in N facing (A) and S facing (S) cells, with different slope inclination. Vegetation growth is a function of input climatic and edaphic data from Morro Santana Hill, Porto Alegre, Brazil (30°04'32"S; 51°06'05"W). The grid was initialized with forest cover only in the central zone (the horizontal zone), and grasslands in the other surrounding zones (which had 15° of slope inclination in the first run and 30° of slope inclination in the second run).

Effects of spatial heterogeneity and patch aggregation on dynamics of forest-grassland mosaics

Dynamics of forest grassland mosaics were sensitive to the initial cover and spatial arrangement of vegetation patches at the landscape scale (Fig. 3). Under the same fire regime (fire return interval ranging from 1 to 5 years) results from simulations conducted for artificial vegetation maps (10% of initial forest cover, located randomly in cells of 25 m² each) and

topographically homogeneous landscapes (only horizontal cells of 25 m² each) showed slow changes over time (Fig. 3A). On the other hand, simulations considering topographically heterogeneous landscapes showed that forest expansion was faster in the predominantly south facing landscapes than in the predominantly north facing landscapes (Fig. 3A and 3B). However, the observed more aggregated forest-grassland mosaic was more stable, despite its predominantly south facing topography and higher initial proportion of forest cover (76%) (Fig. 3A and 3B). In other words, simulations conducted with 2D-aDGVM for the same predominantly south facing landscape, showed that forest expansion was faster through coalescence of initially disaggregated small forest patches than through advancing as large fronts (Fig. 3B and 3C). The rate of expansion varied between topographical scenarios, initial patch aggregation and along simulation years (Fig. 3B). Simulations initialized with the observed vegetation mosaic with more aggregated patches showed the lowest values of forest expansion considering all the simulation period (average of 20±4.4 m.year⁻¹) (Fig. 3B). Simulations initialized with a random vegetation map in the predominantly south and north topographic maps showed initial increasing values of forest expansion before a decrease or invariance as forest patch aggregation increases (Fig. 3B). The threshold at which expansion starts slowing down occurred earlier in the predominantly south (after 300 years) than in the predominant north topography (after 450 years) (Fig. 3B). Average forest expansion rates of random vegetation maps considering all the simulation period were 33±4.5 m.year⁻¹ in the predominantly south facing landscape, 32±5.8 m.year⁻¹ in the predominantly north facing landscape, and 24±3.2 m.year⁻¹ in the horizontal landscape.

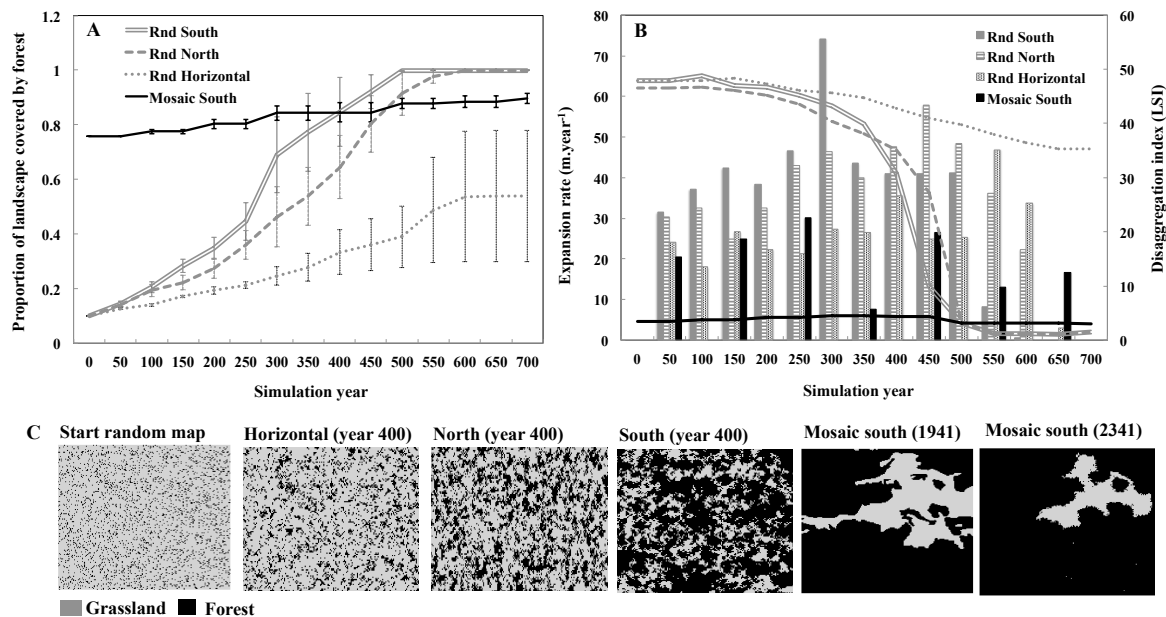


Figure 3. Simulation results from observed and artificial landscapes (25-m² cells) showing forest expansion over grasslands in Morro Santana Hill, Porto Alegre, Brazil (30°04'32"S; 51°06'05"W) considering different initial proportion of landscape cover (A) and patch aggregation (lines in panel B), and in different topographic scenarios (observed predominantly south, observed predominantly north and artificial horizontal). Starting vegetation maps were the observed mosaic from year 1941 in the predominantly south face and an artificial map created by random allocation of forest patches (C). Results in panel A are mean values from ten replicates of each simulation case. Expansion rates (bars in panel B) were obtained from these mean cover values of 50-year intervals (A).

DISCUSSION

In the presented work we used a spatially explicit modeling approach to evaluate the effects of spatial heterogeneity on feedbacks between vegetation and fire, which influence the rates of forest expansion over grasslands and the stability of forest-grassland mosaics in a landscape scale. Recent results from non-spatial models predicted stability of savannas (i.e., grass-tree coexistence at the patch scale) (Beckage et al. 2009, Higgins et al. 2010, Beckage et al. 2011), and alternative stable states (savannas and forests patches) under the same mesic conditions in a continental scale analysis (Staver et al. 2010), when considering a strong feedback of grass biomass on fire. In addition, in a spatially explicit model of pine savannas of southeastern United States, two alternative stable states were possible (grassland or forest patches) when vegetation had positive feedbacks with disturbances, but the rapid shift to the

final state was dependent on a vegetation-fire threshold, which was sensitive to the initial landscape configuration (Beckage and Ellingwood 2008). Similarly, our results showed that coexistence of forest and grasslands patches in the same mesic site was possible over longer periods only under the frequent fires (fire return interval ranging from 1-5 years) promoted by high productive grasslands (Eq. 1; Fig. 3A, simulation case with ‘Mosaic south’).

In addition, the sensitivity of vegetation dynamics to the initial arrangement of patches showed that the observed more aggregated patches play an important role in the maintenance of forest-grassland coexistence in a scenario of predominantly short distance dispersal. With a starting random distribution of disaggregated forest patches in the landscape, a complete forest cover was observed even in presence of fire, irrespective of the predominant topography (Fig. 3A). However, spatio-temporal density dependent processes linked to fire and slope at the patch scale (Fig. 1 and 2) affected the rate of forest expansion at the landscape scale, mainly during the first initial stages of tree establishment on grasslands (i.e. at low tree density in the cells). This was evidenced by the more rapid coalescence of patches in south facing sites compared with the north facing sites when forest patches were initially disaggregated (Fig. 3).

On the other hand, forest-grassland mosaics with higher patch aggregation (as in the observed vegetation mosaic) were more stable than initially disaggregated patches (Fig. 3). This was the case even with a higher proportion of forest cover and in a predominantly south facing landscape, which was expected to have more advantageous humid microclimatic conditions for forests. In fact, a recent study conducted in the highlands in South Brazil (mean annual precipitation of 2252 mm) showed that the large and highly connected forest patches have been expanding at a relatively slow rate (<100 m over the past few millennia; Silva and Anand 2011).

These results show the strong effect of size and distribution of fire-prone and fire-sensitive patches on defining the conditions under which coexistence is possible in the

presence of fire. This is further supported by more stable vegetation patterns at topographically homogeneous landscapes (all horizontal cells), initialized with a higher proportion of grassland cells (90%), which formed a completely aggregated fire-prone background matrix surrounding disaggregated forest patches (Figure 3C). In this case, the persistence of grassland even in a landscape “sown” with trees could be attributed to the higher probability of fire spread at the patch scale in open horizontal cells (and similarly in north-facing cells) than in open south-facing cells (Supplement material, Figure 6), which is expected to yield higher fire frequencies in the first case. Therefore, comparing both situations (Mosaic south, random homogeneous; Figure 3), the persistence of coexisting vegetation types with inherent asymmetry of competitive interactions was possible at the landscape scale when the higher connectivity of the fire-prone system negatively affected the connectivity of the fire-sensitive patches (forest) in a scenario of predominantly short distance dispersal (Figure 3B and 3C) by overcoming its local density-dependent advantage at the patch scale (Figure 2).

The effect of tree density on constraining fire spread was one of the main positive feedbacks to forest expansion over grasslands (Fig. 1 and 2), due to higher local site humidity (Supplement material, Figs 4 and 5) and lower fuel content beneath the trees (Fig. 2). In addition, our simulation results showed that this constraint was sensitive to slope orientation and inclination at the patch scale, mainly during the earlier stages of tree establishment in grasslands (i.e. lower tree density in the cell; Figs. 1 and 2). Indeed, differences in fuel moisture and fire intensity between north and south facing sites are more evident at non-forested and more inclined sites. At south facing sites, higher fuel moisture and lower fire intensity were found, compared to north facing sites (Supplement material, Fig. 5A). With increasing tree density and slope inclination, the differences in fuel moisture and fire intensity between north and south facing sites were enhanced, decreasing the probability of fire spread (Fig. 2 and Supplement material, Fig. 6), and this occurs earlier in south facing sites than in

north facing ones (Fig. 1). Finally, at higher inclinations and tree cover, differences in fuel moisture and fire intensity between south and north facing sites vanish, until conditions are inappropriate for fire (Supplement material, Fig. 5B). This asymmetry in fire behavior at the patch scale creates patches at different stages of transition between grassland and forest. Hence, coexistence at the landscape scale is possible due to temporal (Higgins et al. 2000) and spatial (Jeltsch et al. 1998) variations in opportunities for tree recruitment (Warner and Chesson 1985) here generated by spatial heterogeneity and variations on fire frequencies (Gardner 2006). In addition, a recent study evaluating patterns of forest expansion in the highlands in South Brazil has found that once established, forest trees colonizing grassland sites may enhance nutrient uptake due to symbiotic interactions (Silva and Anand 2011). This corroborates the nurse effect of isolated trees (Duarte et al. 2006) on grasslands favoring further local wood encroachment, and constitutes evidence of positive feedback to forest expansion (Silva and Anand 2011) and another source of spatial heterogeneity raised by growing isolated forest patches on grasslands sites.

Our model results showed that the stable coexistence of forests and grasslands observed in Southern Brazil is, even under the current mesic climate, supported by strong vegetation feedbacks on fire, suggesting that grasslands have persisted as an alternative stable state. Although shifts in dominance between forests and grasslands have been occurring since at least the Late Quaternary (Behling et al. 2004, Behling et al. 2007), transitions from forest to grassland are unlikely to occur without anthropogenic deforestation under the current regional wetter climate (with absence of seasonal droughts). Therefore, under the current regional climate in Southern Brazil, only two scenarios are conceivable: forest-grassland coexistence or forest dominance.

Disturbance frequency and system feedback play a key role for exploring alternative stable states and the limiting thresholds of bistability at the landscape scale (Warman and Moles 2009, Staver et al. 2010). Our results showed that fine-scale site heterogeneity altered

this tenuous limiting threshold between flammable and nonflammable states, especially under lower local values of tree density at the spatio-temporal forest-fire boundaries. In addition, at the landscape scale, this threshold was sensitive to initial conditions of size and spatial arrangement of fire-prone and fire-sensitive patches, showing that interactions (feedbacks) between and within vegetation types become more important when the spatial dimension is added. Our results shed new light on the role of spatial processes in controlling the mechanisms under which coexistence of forests and open-canopy ecosystems is possible in mesic sites. However, future work should look more closely at the role of biotic processes, such as seed dispersal, in the dynamics of these complex systems.

ACKNOWLEDGEMENTS

This research was supported by grants from the Interamerican Institute for Global Change Research (IAI) and from CAPES, Brazil. Simon Scheiter acknowledges support by the research funding programme "LOEWE-Landes-Offensive zur Entwicklung Wissenschaftlich-ökonomischer Exzellenz" of Hesse's Ministry of Higher Education, Research, and the Arts. We are grateful to Guilherme Flach and Marcelo Johan for helping during aDGVM spatialization procedure and to debug of the final 2D-aDGVM. We are also grateful to Gerhard Overbeck, José Pedro Trindade, Fernando Gertum Becker and Steve Higgins for contributions to general discussion, to Ana Luiza Matte for providing and preparing the site maps and to Sandra Müller for generously providing the empirical data for model parameterization and validation.

REFERENCES

Adelmann, W. and A. Zellhuber. 2004. Analysis of environmental conflicts in areas of urban expansion using scenario methods (com versão em português). Pages 60-64 *in* Workshop "Proteção e manejo da vegetação natural da região de Porto Alegre com

- base em pesquisas de padrões e dinâmica da vegetação". PPG-Ecologia, UFRGS, Porto Alegre.
- Allen, R. G., R. Trezza, and M. Tasumi. 2006. Analytical integrated functions for daily solar radiation on slopes. *Agricultural and Forest Meteorology* 139:55-73.
- Beckage, B. and C. Ellingwood. 2008. Fire Feedbacks with Vegetation and Alternative Stable States. *Complex Systems* 18:159-173.
- Beckage, B., L. J. Gross, and W. J. Platt. 2011. Grass feedbacks on fire stabilize savannas. *Ecological Modelling* In Press, Corrected Proof.
- Beckage, B., W. J. Platt, and L. J. Gross. 2009. Vegetation, Fire, and Feedbacks: A Disturbance-Mediated Model of Savannas. *The American Naturalist* 174:805-818.
- Behling, H. 2002. South and southeast Brazilian grasslands during Late Quaternary times: a synthesis. *Palaeogeography, Palaeoclimatology, Palaeoecology*.
- Behling, H., V. D. Pillar, S. C. Müller, and G. E. Overbeck. 2007. Late-Holocene fire history in a forest-grassland mosaic in southern Brazil: Implications for conservation. *Applied Vegetation Science* 10:81-90.
- Behling, H., V. D. Pillar, L. Orlóci, and S. G. Bauermann. 2004. Late Quaternary Araucaria forest, grassland (Campos), fire and climate dynamics, studied by high-resolution pollen, charcoal and multivariate analysis of the Cambará do Sul core in southern Brazil. *Palaeogeography, Palaeoclimatology, Palaeoecology* 203:277-297.
- Bird, M. I. and J. A. Cali. 1998. A million-year record of fire in sub-Saharan Africa. *Nature* 394:767-769.
- Bond, W. J. and J. E. Keeley. 2005. Fire as a global 'herbivore': the ecology and evolution of flammable ecosystems. *Trends in Ecology & Evolution* 20:387-394.
- Bond, W. J., G. F. Midgley, and F. I. Woodward. 2003. The importance of low atmospheric CO₂ and fire in promoting the spread of grasslands and savannas. *Global Change Biology* 9:973-982.

- Bond, W. J., F. I. Woodward, and G. F. Midgley. 2005. The global distribution of ecosystems in a world without fire. *New Phytologist* 165:525-538.
- Brack, P., R. S. Rodrigues, M. Sobral, and S. L. C. Leite. 1998. Árvores e arbustos na vegetação natural de Porto Alegre, Rio Grande do Sul, Brasil. *Iheringia, Sér. Bot.* 51:139-166.
- Caplat, P., M. Anand, and C. Bauch. 2008. Interactions between climate change, competition, dispersal, and disturbances in a tree migration model. *Theoretical Ecology* 1:209-220.
- CENECO/FAURGS. 2004. Diagnóstico Ambiental do Município de Porto Alegre. Relatório 6. Laboratório de Geoprocessamento do Centro de Ecologia, UFRGS. Porto Alegre.
- Chesson, P. and N. Huntly. 1989. Short-term instabilities and long-term community dynamics. *Trends in Ecology & Evolution* 4:293-298.
- Cramer, W., A. Bondeau, F. I. Woodward, I. C. Prentice, R. A. Betts, V. Brovkin, P. M. Cox, V. Fisher, J. A. Foley, A. D. Friend, C. Kucharik, M. R. Lomas, N. Ramankutty, S. Sitch, B. Smith, A. White, and C. Young-Molling. 2001. Global response of terrestrial ecosystem structure and function to CO₂ and climate change: results from six dynamic global vegetation models. *Global Change Biology* 7:357-373.
- D'Odorico, P., F. Laio, and L. Ridolfi. 2006. A Probabilistic Analysis of Fire-Induced Tree-Grass Coexistence in Savannas. *The American Naturalist* 167:E79-E87.
- Danz, N. P., P. B. Reich, L. E. Frelich, and G. J. Niemi. 2011. Vegetation controls vary across space and spatial scale in a historic grassland-forest biome boundary. *Ecography* 34:402-414.
- Duarte, L. S., M. M. G. Santos, S. M. Hartz, and V. D. Pillar. 2006. The role of nurse plants in Araucaria forest expansion over grassland in south Brazil. *Austral Ecology* 31:520-528.

- Fidelis, A., M. D. Delgado-Cartay, C. C. Blanco, S. C. Müller, V. D. Pillar, and J. Pfaenderhauer. 2010. Fire intensity and severity in Brazilian Campos grasslands. *Interciencia (caracas)* 35:739-745.
- Garcia Martinez, P. 2005. Caracterización química y física de los suelos del Morro Santana (Porto Alegre, Rio Grande do Sul, Brasil). Master. TUM, Freising-Weihenstephan.
- Gardner, T. A. 2006. Tree–grass coexistence in the Brazilian cerrado: demographic consequences of environmental instability. *Journal of Biogeography* 33:448-463.
- Geiger, R. 1965. The climate near the ground. 2 edition. Harvard University Press, London.
- Grimm, E. C. 1984. Fire and other factors controlling the big woods vegetation of Minnesota in the mid-nineteenth century. *Ecol. Monog.* 54:291-311.
- Hickler, T., I. C. Prentice, B. Smith, M. T. Sykes, and S. Zaehle. 2006. Implementing plant hydraulic architecture within the LPJ Dynamic Global Vegetation Model. *Global Ecology and Biogeography* 15:567-577.
- Higgins, S. I., W. J. Bond, W. S. W. Trollope, and R. J. Williams. 2008. Physically motivated empirical models for the spread and intensity of grass fires. *International Journal of Wildland Fire* 17:595-601.
- Higgins, S. I., W. J. Bond, S. Winston, and W. Trollope. 2000. Fire, resprouting and variability: a recipe for grass-tree coexistence in savanna. *Journal of Ecology* 88:213-229.
- Higgins, S. I. and M. L. Cain. 2002. Spatially realistic plant metapopulation models and the colonization–competition trade-off. *Journal of Ecology* 90:616-626.
- Higgins, S. I., S. Scheiter, and M. Sankaran. 2010. The stability of African savannas: insights from the indirect estimation of the parameters of a dynamic model. *Ecology* 91:1682-1692.
- Hoffmann, W. A., B. Orthen, and P. K. V. d. Nascimento. 2003. Comparative fire ecology of tropical savanna and forest trees. *Functional Ecology* 17:720-726.

- Jeltsch, F., S. J. Milton, W. R. J. Dean, N. van Rooyen, and K. A. Moloney. 1998. Modelling the impact of small-scale heterogeneities on tree—grass coexistence in semi-arid savannas. *Journal of Ecology* 86:780-793.
- Lehmann, C. E. R., S. A. Archibald, W. A. Hoffmann, and W. J. Bond. 2011. Deciphering the distribution of the savanna biome. *New Phytologist* 191:197-209.
- McGarigal, K. and B. J. Marks. 1995. FRAGSTATS: spatial pattern analysis program for quantifying landscape structure. USDA Forest Service, Pacific Northwest Research Station, Portland, OR, USA.
- Müller, S. C., G. E. Overbeck, J. Pfadenhauer, and V. D. Pillar. 2007. Plant functional types of woody species related to fire disturbance in forest-grassland ecotones. *Plant Ecology* 189:1-14.
- Nimer, E. 1990. Clima. Pages 151-187 in IBGE, editor. *Geografia do Brasil: Região Sul*. IBGE, Rio de Janeiro.
- Oke, T. R. 1987. *Boundary Layer Climates*. 2 edition. Methuen, London.
- Overbeck, G. E., S. C. Müller, A. Fidelis, J. Pfadenhauer, V. D. Pillar, C. C. Blanco, I. I. Boldrini, R. Both, and E. D. Forneck. 2007. Brazil's neglected biome: The South Brazilian *Campos*. *Perspectives in Plant Ecology, Evolution and Systematics* 9:101-116.
- Overbeck, G. E., S. C. Müller, V. D. Pillar, and J. Pfadenhauer. 2006. Floristic composition, environmental variation and species distribution patterns in burned grassland in southern Brazil. *Brazilian Journal of Biology* 66:1073-1090.
- Pickett, S. T. A. and P. White. 1985. *The Ecology of Natural Disturbance and Patch Dynamics*. Academic Press, Orlando, Florida.
- Quadro, M. F. L. d., L. H. R. Machado, S. Calbete, N. N. M. Batista, and G. S. d. Oliveira. 2010. *Climatologia de Precipitação e Temperatura*. in I. F. d. A. Cavalcanti, editor.

Climanálise. Boletim de Monitoramento e Análise Climática. Centro de Previsão de Tempo e Estudos Climáticos - CPTEC/INPE, São Paulo.

- Rothermel, R. C., R. A. Wilson, G. A. Morris, and S. S. Sackett. 1986. Modeling moisture content of fine dead wildland fuels: Input to the BEHAVE fire prediction system. U.S. Department of Agriculture, Forest Service, Intermountain Research Station, Ogden, UT.
- Sankaran, M., N. P. Hanan, R. J. Scholes, J. Ratnam, D. J. Augustine, B. S. Cade, J. Gignoux, S. I. Higgins, X. Le Roux, F. Ludwig, J. Ardo, F. Banyikwa, A. Bronn, G. Bucini, K. K. Caylor, M. B. Coughenour, A. Diouf, W. Ekaya, C. J. Feral, E. C. February, P. G. H. Frost, P. Hiernaux, H. Hrabar, K. L. Metzger, H. H. T. Prins, S. Ringrose, W. Sea, J. Tews, J. Worden, and N. Zambatis. 2005. Determinants of woody cover in African savannas. *Nature* 438:846-849.
- Sarmiento, G. 1992. A conceptual model relating environmental factors and vegetation formations in the lowlands of tropical South America. Pages 583-601 *in* P. A. Furley, J. Proctor, and J. A. Ratter, editors. *Nature and Dynamics of Forest-Savanna Boundaries*. Chapman & Hall, London.
- Scheffer, M. and S. R. Carpenter. 2003. Catastrophic regime shifts in ecosystems: linking theory to observation. *Trends in Ecology & Evolution* 18:648-656.
- Scheiter, S. and S. I. Higgins. 2007. Partitioning of Root and Shoot Competition and the Stability of Savannas. *The American Naturalist* 170:587-601.
- Scheiter, S. and S. I. Higgins. 2009. Impacts of climate change on the vegetation of Africa: an adaptive dynamic vegetation modelling approach. *Global Change Biology* 15:2224-2246.
- Scholes, R. J. and S. R. Archer. 1997. Tree-grass interactions in savannas. *Annual Review of Ecology and Systematics* 28:517-544.

- Silva, L. C. R. and M. Anand. 2011. Mechanisms of Araucaria (Atlantic) forest expansion in southern Brazil Ecosystems (under minor reviews).
- Skarpe, C. 1992. Dynamics of savanna ecosystems. *Journal of Vegetation Science* 3:293-300.
- Staver, A. C., S. Archibald, and S. Levin. 2010. Tree cover in sub-Saharan Africa: rainfall and fire constrain forest and savanna as alternative stable states. *Ecology*.
- Sternberg, L. D. S. L. 2001. Savanna-forest hysteresis in the tropics. *Global Ecology & Biogeography* 10:369-378.
- Turner, M. G. 1989. Landscape ecology: the effect of pattern and process. *Annu. Rev. Ecol. Syst.* 20:171-197.
- van Nes, E. H. and M. Scheffer. 2005. IMPLICATIONS OF SPATIAL HETEROGENEITY FOR CATASTROPHIC REGIME SHIFTS IN ECOSYSTEMS. *Ecology* 86:1797-1807.
- Warman, L. and A. Moles. 2009. Alternative stable states in Australia's Wet Tropics: a theoretical framework for the field data and a field-case for the theory. *Landscape Ecology* 24:1-13.
- Warner, R. R. and P. L. Chesson. 1985. Coexistence Mediated by Recruitment Fluctuations: A Field Guide to the Storage Effect. *The American Naturalist* 125:769-787.
- Watt, A. S. 1947. Pattern and process in the plant community. *Journal of Ecology* 35:1-22.

CAPÍTULO 3 (ARTIGO 2)

Sensitivity of forest-grassland mosaics to changes in climate and atmospheric CO₂³

³ Este manuscrito será submetido para publicação na revista *Global Change Biology*, com Simon Scheiter¹, Steven I. Higgins¹ e Valério D. Pillar como co-autores,

¹Biodiversity and Climate Research Centre (LOEWE BiK-F), Frankfurt, Germany

Abstract

Vegetation has shown to be sensitive to past and recent changes in climate and atmospheric CO₂ levels. IPCC emission scenarios predict drastic changes in climatic and atmospheric conditions. However, the great majority of future predictions from global vegetation models yield potential final vegetation states accordingly, giving less attention to the importance of dynamic interactions at the regional scale in ecotone zones, where contrasting vegetation formations coexist through complex interactions mediated by spatio-temporal ecological processes, such as propagule dispersal and fire. Here we evaluated the sensitivity of forest-grassland mosaics in Southern Brazil to changes in climate from preindustrial to future times using a spatially explicit model that incorporates an adaptive Dynamic Global Vegetation Model (2D-aDGVM), including fire spread behavior and seed dispersal in two dimensions. Results showed that forest-grassland boundaries were sensitive to increasing atmospheric CO₂, temperature and rainfall. Forest expansion in the absence of fire was as fast as the rate of these changes, especially during the final modeled period (2050-2100), when it was also evident in simulations conducted in the presence of frequent fires. Potential vegetation growth and fecundity was enhanced by elevated temperature and atmospheric CO₂ levels and irrespective of plant type physiology (C₃-tree and C₄-grass). However, considering grass-tree interactions under changing climate, the rate of stem growth of C₃-trees was higher than the increment in C₄-grass fine fuel biomass needed to reach a sufficient fire intensity to eliminate the saplings. As climate changed, increasing values of aboveground grass biomass yielded increasing values of fire intensity values, but the proportion of trees killed by fire in burned cells decreased accordingly. This suggests that the photosynthetic advantage of C₃-trees over C₄-grasses in the presence of fire under rising CO₂ levels could also potentially affect the relative stability of forest-grassland boundaries observed until present and maintained under frequent fires.

Key words: Climate change, fire, seed dispersal, forest expansion, demographic model, process-based model, aDGVM, spatially explicit model, subtropical grassland

Introduction

Over the past century, global climatic changes and increasing atmospheric CO₂ levels have been causing vegetation shifts and moving ecosystem boundaries worldwide (Walther et al. 2002, Parmesan 2006). Increasing densities of trees and shrubs have been observed in savannas and grasslands throughout the world, such as in Africa (Roques et al. 2001), Argentina (Cabral et al. 2003) and North America (Van Auken 2000, Bai et al. 2009). Similarly, expansion of forests over grasslands and savannas are occurring in natural mosaics of South Brazil (Oliveira and Pillar 2004, Overbeck et al. 2007), central Brazilian savannas (Silva et al. 2008), North America (Knapp and Soulé 1998, Payette 2007), Australia (Bowman et al. 2001), Africa (Goetze et al. 2006) and Europe (Devi et al. 2008, van Gils et al. 2008).

In fact, shifts in climatic and atmospheric conditions during past glacial and interglacial cycles also showed feedbacks in global vegetation changes (Cerling et al. 1997, Dupont et al. 2000, Dupont et al. 2010). However, the magnitude of recent changes in climatic conditions due to uncontrolled emissions of greenhouse gases by increasing human economic activities over the past two centuries (IPCC 2007) have never occurred over the last 420,000 years (Petit et al. 1999), and may have strong future impacts on managed and unmanaged ecosystems by affecting system productivity (e.g. Izaurralde et al. 2005), disturbance regimes (Bird and Cali 1998) and geographical distribution of biomes (Woodward et al. 2004).

The dependence of plant's photosynthesis and respiration on atmospheric carbon dioxide is one key factor influencing the responses of vegetation to past and recent atmospheric and climatic changes (Drake et al. 1997, Ehleringer et al. 1997, Bennett and Willis 2000). Variations on atmospheric CO₂ levels affect stomatal activity,

evapotranspiration and resource-use efficiency of plants (Drake et al. 1997, Silva et al. 2009). However, differences on photosynthetic pathways between C₃ and C₄ plants yield differentiated responses and asymmetric advantages associated to temperature (Cerling et al. 1997, Ehleringer et al. 1997). Variations on photosynthetic efficiency of plants are caused by interactions of both atmospheric CO₂ levels and temperature. C₃ plants are more sensitive to variations on atmospheric CO₂ levels than C₄, and would be favored in all situations of high CO₂ levels, but are limited under very high temperatures, whereas C₄ would be favored under low CO₂ partial pressure, but in addition to elevated temperatures (Cerling et al. 1997). Such sensitivity of plant-climate interaction to atmospheric CO₂ levels may be the basis for understanding the evolutionary history of C₃ and C₄-dominated ecosystems (Strömberg 2011), as well as their shifts in dominance at the global scale over past glacial and interglacial cycles (Ehleringer et al. 1997, Cowling and Sykes 1999).

In treeline ecotones, like natural forest-grassland mosaics, local factors such as seed dispersal and disturbances interact with regional climate on the complex dynamics of the boundaries. Over millions of years, fire has been one major disturbance influencing vegetation structure and dynamic at the local scale and shaping biomes distribution at the global scale (Bird and Cali 1998, Bond and Keeley 2005). In frequently burned savannas, stability of grass-tree coexistence is promoted by differentiated effects of climate (mainly rainfall) and fire behavior (frequency, intensity and spread) on life-history stages of trees and hence on temporal variability of recruitment rates (Higgins et al. 2000). Where forests face grasslands and savannas, fire delineates sharp boundaries between flammable and fire-sensitive vegetation stands, and has been pointed as one key mechanism promoting their long-term coexistence at the landscape scale when regional climate favors forests (Grimm 1983, Behling et al. 2004, Bowman et al. 2004). However, in such mesic sites, with high rainfall periods, grass productivity is high, and rising atmospheric CO₂ levels are expected to change the threshold at which fire affect biomass and sapling escape due to fertilization effects on

tree recruitment, and hence affecting the local dynamics in these ecotone zones (Bond et al. 2003, Bond 2008).

One hypothesis explaining recent invasion of woody plants in grasslands and savannas is based on the photosynthetic advantage of C₃-trees over C₄-grasses on growth and recovery after fire under rising atmospheric CO₂ levels (Bond and Midgley 2000). Dynamic Global Vegetation Models are especially useful in this case, because they are capable of capturing the transient dynamics of the biosphere in a changing climate, considering the effect of natural disturbances and human activities in shaping vegetation dynamics and distribution. Simulations using DGVMs suggest that CO₂ fertilization effect favours tree recruitment (Bond et al. 2003), and is sufficient to stimulate their geographic expansion (Woodward and Lomas 2004), and therefore shifting the location of ecosystem boundaries and distribution of biomes (Scheiter and Higgins 2009). In addition, rising CO₂ levels enhances fecundity of forest trees (LaDeau and Clark 2001), which may also affect recruitment and dispersal patterns. However, such important local ecological processes such as fire spread behavior and movement of propagules in two dimensions have gained little attention on modelling treeline dynamics with DGVMs in such a regional scale (Cramer et al. 2001, Fisher et al. 2010).

In this paper, we evaluate sensitivity of forest expansion from preindustrial climate to projected climate scenarios using a bidimensional spatially explicit model that incorporates an adaptive Dynamic Global Vegetation Model (aDGVM) (Scheiter and Higgins 2009) to simulate forest-grassland dynamics at a mesic site (precipitation > 1,000 mm). Local factors influencing treeline dynamics, such as seed dispersal and fire, are explored under changing climate and rising atmospheric CO₂ levels.

Materials and methods

Model Description

The model (2D-aDGVM) is a bidimensional spatially explicit model that incorporates an adaptive Dynamic Global Vegetation Model (aDGVM) (Scheiter and Higgins 2009) to simulate dynamics of vegetation stands in a landscape scale, including fire spread behavior and seed dispersal in two dimensions. Detailed descriptions about how vegetation growth, fire and seed dispersal are treated by the model are described as follows.

Vegetation growth

The 2D-aDGVM modelling space is a regular grid of square cells with specified sizes. In daily time-steps at each cell, the aDGVM simulates biophysical, physiological and demographic processes at the leaf, canopy, plant and population level of C₄-grasses and C₃-trees adopting an individual-based approach, as a function of climatic and edaphic conditions, and fire. Competitive interactions between grasses and trees inside the same cell are mediated by light through shading effects, and water competition in different soil layers. Trees are simulated individually and morphologically represented as “typical ones”, whereas for grasses two types of “superindividuals” are considered (grasses between and grasses bellow tree canopies inside the cell), i.e., the aDGVM does not consider different species. For a more detailed description of the aDGVM, see Appendix 1.

Fire

Inside each cell, a semi-empirical aDGVM sub-model simulates fire intensity as a function of fuel biomass, fuel moisture and wind speed; and stem mortality is a function of tree size and fire intensity. A stochastic ignition sequence is calculated annually to determine days when ignition occurs, and is based on the mean annual relative air humidity. If the

potential fire intensity exceeds a pre-defined threshold value in an ignited cell (i.e., the cell has sufficient biomass to burn), the probability of fire spread inside it is calculated locally by

$$p_{fire} = -2.2\theta_{F(grass)} + 1.489 \text{ (Eq. 1)}$$

which is a function of fuel moisture of the resident grass biomass amount $\theta_{F(grass)}$ (this is a modification implemented in the aDGVM, which used to consider a fixed probability of fire spread). In the aDGVM, tree mortality is a function of fire intensity and tree height (Scheiter and Higgins 2009). For a more detailed description of the aDGVM fire sub-model, see Appendix 1.

In the 2D-aDGVM, in an ignition day, the first cell to be ignited is chosen at random from all cells with tree cover <50% to avoid bias on fire frequency due to recurrent failed ignitions eventually occurring in “forested” cells, because the test for a fire to spread inside the first ignited cell is applied once to every ignition event. If ignition is successful (i.e., fire spreads inside the first ignited cell), the probability of fire spread to the surrounding potential burning cells (i.e., those with sufficient biomass to burn) is adjusted with a bias value applied for each of the eight adjacent cells of a new burning one in relation to their orientation towards the prevailing wind (see Supplemental material for a more detailed description of the 2D-aDGVM fire spread rule and parameterization of fire spread probability, as described above).

Seed dispersal

The expected number of seeds N_S landing in a cell is a function of annual seed production Φ_{ij} (calculated by the aDGVM) and its distance from seed sources d_{ij} (distance between two cell’s midpoints), and is calculated by

$$N_s = \sum g_{(d_{ij})} \Phi_{ij} \text{ (Eq. 2)}$$

In Equation (2), $g_{(d_{ij})}$ is the probability density function of each seed to land in a target cell at a certain distance d_{ij} from the source, and is calculated by

$$g_{(d_{ij})} = p_{seed} \frac{1}{\lambda_1} \exp\left(-\frac{d_{ij}}{\lambda_1}\right) + (1 - p_{seed}) \frac{1}{\lambda_2} \exp\left(-\frac{d_{ij}}{\lambda_2}\right) \text{ (Eq. 3)}$$

where p_{seed} is the proportion of seeds dispersed at short distances, λ_1 is the mean distance (m) of short distance dispersal and λ_2 is the mean distance (m) of long distance dispersal. Other spatially explicit models (Higgins and Cain 2002, Caplat et al. 2008) used similar equations, which were referred to as stratified (mixed) kernels, to account for a more flexible way to model short and long distance dispersal (first and second components of Eq. 3, respectively). Finally, seeds dispersed to other cells are subtracted from the cell's resident pool of collected seeds. Seeds arriving from other cells are added to the seed bank, as well as seeds that 'fail' to disperse to other cells. Following, seed decay rate and probability of seed germination are applied daily by the aDGVM (see Appendix 1).

Study site

Data from Morro Santana (30°04'32"S; 51°06'05"W, Porto Alegre, Southern Brazil) were used for the aDGVM parameterization and testing of vegetation growth, structure and biomass dynamic at local soil and current climatic conditions and fire regimes (for more detailed description of the aDGVM parameterization and testing see Supplemental material).

Morro Santana is a granitic hill (altitude max. 311 m a.s.l.) with approximately 1,000 ha. Mean annual precipitation is 1348 mm, with no marked dry season, and average annual temperature is 19.5°C (Nimer 1990). Vegetation cover is a natural mosaic of forest (with species from Semideciduous Seasonal Forest and Atlantic Rain Forest) and “Campos” grasslands (very species rich, dominated by C4 grasses). Analysis from local charcoal and fossil pollen profile and evidences from other sites indicated that grasslands are relicts from Pleistocene and early/mid Holocene drier climatic conditions, and fire has been likely occurring since at least around 9000 yr BP, whereas woody invasion started around 620 and 540 cal yr BP (Behling et al. 2007). At present, fire is a frequent anthropogenic disturbance in the grassland areas, with return intervals of 2–5 years, and a process of forest expansion over grassland is evident (Overbeck et al. 2007).

Simulations

Sensitivity of forest expansion under changing climate and fire regimes

Predictions from IPCC (2007) SRES scenarios show increasing atmospheric CO₂ levels between 540 and 970 p.p.m (parts per million) until 2100, depending on the scenario and model used. Despite several uncertainties on predicting realized changes on climatic variables at the regional scale, an enhancement on the effect of such changes in local temperature and rainfall in Southern Brazil is a consensus (Haylock et al. 2006, Marengo 2007, Marengo and Camargo 2008). For southern Brazil, a comparison of results from different global climate models showed increases in mean temperature ranging between 2 and 3°C considering the climate scenario B2, and between 2 and 5°C for A1, as well as changes in precipitation ranging from -0,5 to +0,5 mm/day, respectively, compared to 1961-1990 values (Marengo 2007). In the present work, we evaluated the sensitivity of vegetation growth and forest expansion under changing climate by comparing simulations using the observed climate normals 1961-1990 (Instituto Nacional de Meteorologia - INMET) and simulations using

projected climate forcing data for temperature, rainfall and atmospheric CO₂ levels from IPCC (2007) SRES A1B scenario (Figure 1) - not the most pessimistic, but also not the most optimistic scenario.

To evaluate sensitivity of forest expansion under changing climate we conducted simulations in an artificial map with 9 km², where vegetation growth was simulated in 30-m sided square cells. Starting landscape cover was represented by a treeline covering 10% of the map with forest and the remaining adjacent 90% with grassland. Topographical variations were ignored (i.e., all cells had horizontal surface). Simulations were conducted from year 1762 to year 2100 using climate normals 1961-1990 (Instituto Nacional de Meteorologia - INMET) and projected climate forcing data for temperature, rainfall and atmospheric CO₂ levels from IPCC (2007) SRES A1B scenario (Figure 1). In the simulations, the first 100 years (during pre-industrial phase) are taken as the spin-up phase to allow the aDGVM to reach an equilibrium state inside each cell, during which fire was set off, when considered. Therefore, simulations were conducted with fire and without fire, and considering the following dispersal parameter values: $p_{seed} = 0.80$; $\lambda_1 = 30$ m; $\lambda_2 = 500$ m.

These dispersal parameter values were chosen after previous simulation experiments with several combinations of possible values for dispersal parameters (not shown), which accounted for the grain size (30 m), for the grid size (9 km²), and for consistency with the literature on frugivores dispersal patterns (e.g. Jordano et al. 2007), as local studies showed that most of forest tree species are zoochorous (including those colonizing grasslands) (Müller and Forneck 2004). This parameterization was conducted starting with one young tree (initial mass = 10 g) located in a central cell, without fire and under current (constant) climate conditions. The final chosen combination of dispersal parameter values (as described before) was the one that best fitted the time needed for a complete tree cover of ca. 1 ha in the absence of fire (40±0.52 years), as predicted by earlier parameterization of the aDGVM in a

single 1-ha cell, by also starting with one young tree and under current local climate (Supplemental material).

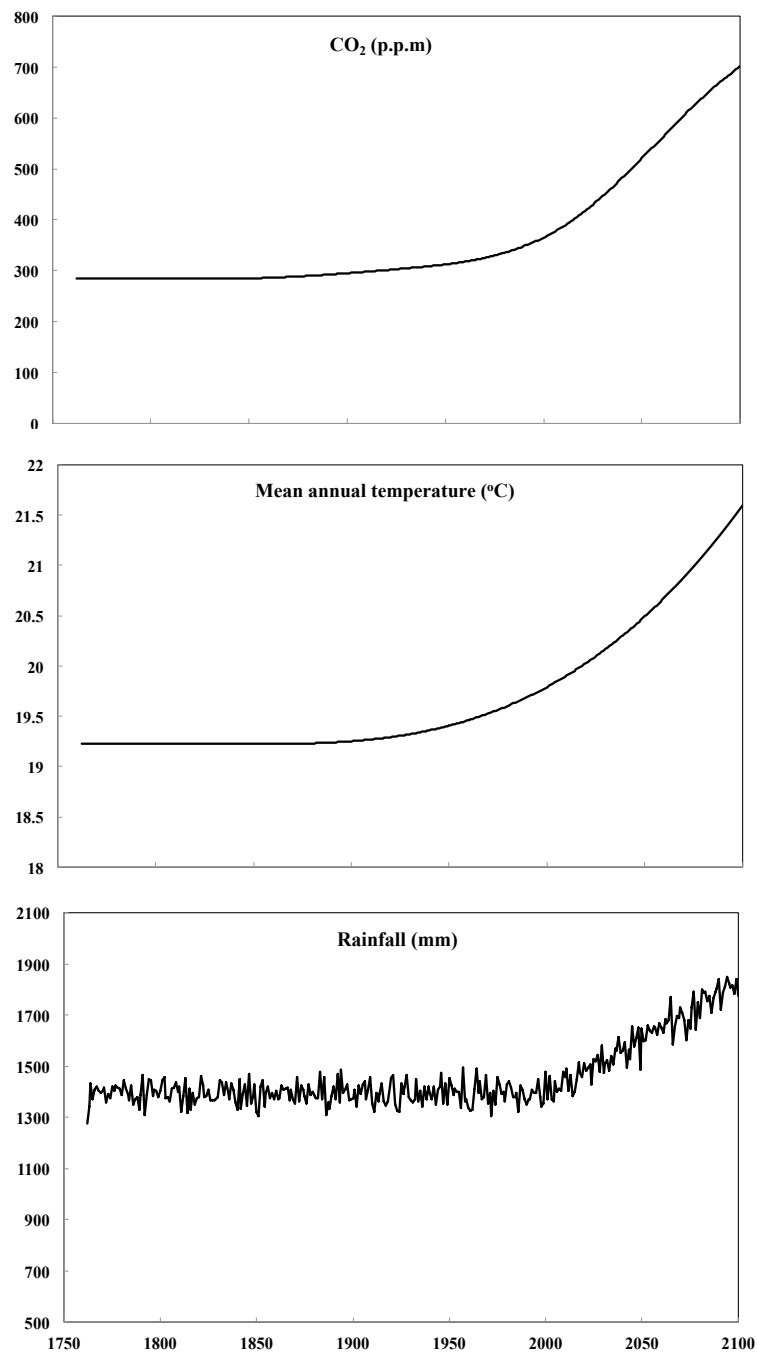


Figure 1. Predicted changes in temperature, rainfall and atmospheric CO₂ in Morro Santana (30°04'32"S; 51°06'05"W, Porto Alegre, Southern Brazil) from projected climate forcing data from IPCC (2007) SRES A1B scenario. Predictions for changes in temperature show only data from annual mean temperature (i.e., annual minimum and maximum temperatures are not shown). Predictions for rainfall show total annual rainfall (mm).

Potential vegetation growth under different climatic conditions

For a more detailed evaluation of the potential effects of climate change on fine-scale processes influencing forest expansion, additional simulations were conducted in an individual cell of 900 m² (i.e., seed dispersal and fire spread in two dimensions were ignored). Therefore, C₃-tree growth and seed production, as well as C₄-grass biomass production under fire effect were explored in the absence of grass-tree competitive interactions and under changing climatic conditions projected from the IPCC (2007) SRES A1B scenario (Fig 1). Simulations evaluating seed production and tree growth were conducted in the absence of fire. Seed production was evaluated by starting simulations with one seedling (initial mass = 10 g). For evaluations of tree growth, individual seeds were allowed to germinate in specified years, which constituted different simulation cases (simulation cases: germinate in 1850, 1900, 1950, 2000, 2050, 2090). Grass biomass production was evaluated by simulations conducted with no trees, and with fire switched on. Biomass production under different fire return intervals were compared. Ten replicates of each simulation case (random initializing seed varying from one to ten) were performed.

Data analysis

To evaluate sensitivity of forest expansion under changing climate, yearly output maps with tree cover of each cell were analyzed from simulations conducted with IPCC (2007) SRES A1B projected climate change scenario (as described above in *Simulations - Sensitivity of forest expansion under changing climate and fire regimes*). In each output map, to get the proportion of cells covered by forest, tree cover values of each cell were converted to zero when < 50% and converted to one when ≥ 50%, representing *grassland* and *forest* cells, respectively. In addition, trade-offs from grass-tree interactions, such as the relationship between aboveground grass biomass (live and dead), fire behavior (fire frequency and intensity) and tree mortality (proportion of trees killed by fire) under changing climate were

also evaluated from yearly outputs from each burned map cell from simulations conducted with fire on. All fire events from the 1900 to 2100 were analyzed. For each 50-year interval (1900-1950, 1950-2000, 2000-2050, 2050-2100), mean values for each fire-exclusion period (Last fire: 1 year, 2 years, 3 years, >3 years) were considered.

To evaluate potential vegetation growth (no grass-tree interactions), yearly outputs for total grass biomass (aboveground and belowground, live and dead) and seed density were analyzed. For evaluations of tree growth, only output data for the first 10 years after germination were considered.

Results

Predicted changes in temperature, rainfall and atmospheric CO₂ at the study site considering IPCC (2007) SRES A1B scenario indicate increasing values from around 1850 and more sharp changes from 2050 to 2100 (Figure 1). Compared to year 2000, the trends in mean temperature and total annual rainfall are expected to be +1.8°C and +300 mm, respectively, at the study site until 2100 (Figure 1). Simulations conducted in the artificial landscape showed that the dynamics of forest-grassland boundary was sensitive to those changes, especially during the final 100 years (Figure 2), i.e., forest expansion was faster from 2050 to 2100 than during previous years. This was more evident in the absence of fire, but could also be noticed in simulations conducted with fire on (Figure 2).

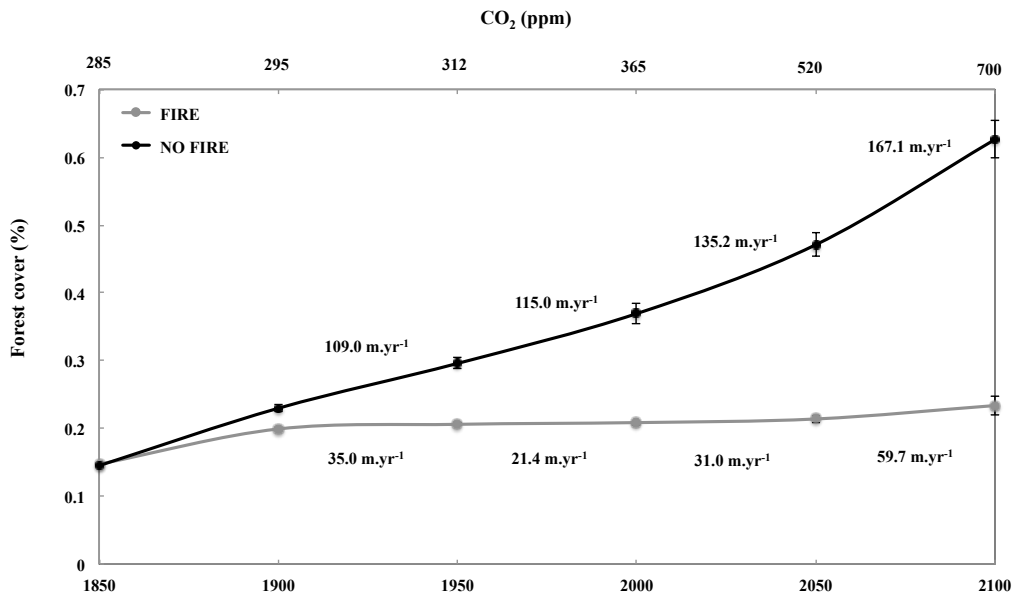


Figure 2. Dynamics of a forest-grassland ecotone under changing climate (IPCC (2007) SRES A1B projected climate scenario) from Morro Santana (30°04'32"S; 51°06'05"W, Porto Alegre, Southern Brazil). The graph shows simulated rates of forest expansion in 50 year-intervals in terms of increments in the proportion of cells with tree cover $\geq 50\%$, considering fire on (grey line) and fire off (dark line). Simulations were conducted in an artificial map with 9 km² (grain size 30 m). Starting landscape cover was a treeline covering 10% of the map with forest and the remaining adjacent 90% with grassland. The graph shows only results after the 100-years spin-up phase. Topographical variations were ignored (i.e., all cells had horizontal surface). Parameters for seed dispersal were: $p_{seed} = 0.80$ (proportion of seeds dispersed short distances from the sources); $\lambda_1 = 30$ m (mean distance for short distance dispersal of seeds); $\lambda_2 = 500$ m (mean distance for long distance dispersal of seeds).

Climate change did not affect significantly the mean fire return interval (1.5 years) considering the total analyzed period (1850-2100) (not shown). However, a closer view on the processes occurring inside the cells showed that although an increasing accumulation of fine fuel biomass (aboveground grass biomass) promoted a general rising on fire intensity values for all fire-return intervals (Figure 3A), an expected increase on tree mortality due to topkill effect related to fire intensity was not observed. On the contrary, the results showed a general decrease in the number of trees killed by fire as climate changed, which was sharper from 2050 to 2100 (black markers in Figure 3B), for all fire-return intervals, except in burned cells after 2 years of fire exclusion (circles in Figure 3B).

The simulations evaluating the potential vegetation growth with no grass-tree interactions conducted in a single cell showed an increasing correlation between grass biomass production and time since last fire, as climate changed, with sharper increase after year 2050 (Figure 4A). This explains the general increasing positive correlation (trendlines in Figure 3A) between aboveground grass biomass and fire intensity in cells burned after higher fire exclusion periods (from 1-year to >3-years of fire exclusion), as well as the decreasing negative correlations with tree mortality as fire exclusion increases (Figure 3B). Seed production of 2100 (4.2 seeds.m⁻²) was almost twice that of 1850 (1.7 seeds.m⁻²) (Figure 4B) and mean growth rate of trees under climatic conditions of 2100 (0.7 m.yr⁻¹) was even higher than twice that of 1850 (0.3 m.yr⁻¹) (Figure 4C).

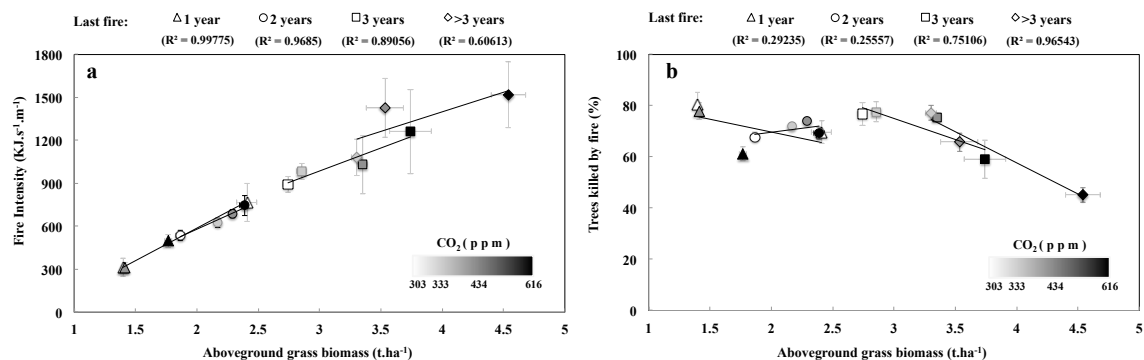
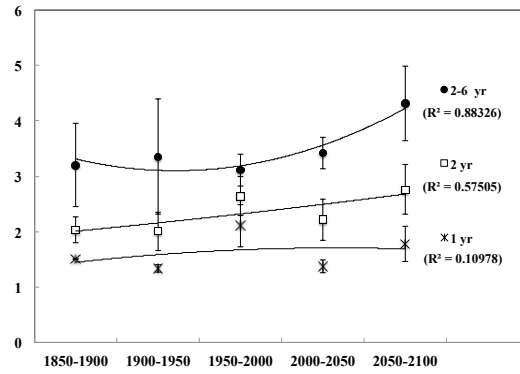
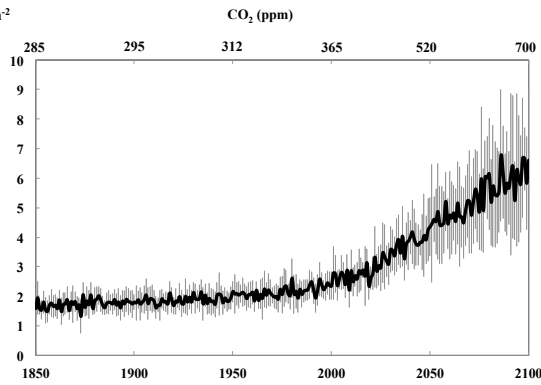


Figure 3. Effects of increasing fine fuel biomass (aboveground live and dead grass biomass) on fire intensity (a) and on the proportion of trees killed by fire (b) from simulations in a forest-grassland ecotone under changing climate (IPCC (2007) SRES A1B projected climate scenario) from Morro Santana (30°04'32"S; 51°06'05"W, Porto Alegre, Southern Brazil). The graphs shows mean and error values from all cells with different fire-exclusion period (Last fire: 1 year, 2 years, 3 years, >3 years) burned during the periods 1900-1950 (303 ppm), 1950-2000 (333 ppm), 2000-2050 (434 ppm) and 2050-2100 (616 ppm), which are indicated by the corresponding increasing CO₂ levels (ppm). Simulations were conducted in an artificial map with 9 km² (grain size 30 m). Starting landscape cover was a treeline covering 10% of the map with forest and the remaining adjacent 90% with grassland. Topographical variations were ignored (i.e., all cells had horizontal surface). Parameters for seed dispersal were: $p_{seed} = 0.80$ (proportion of seeds dispersed short distances from the sources); $\lambda_1 = 30$ m (mean distance for short distance dispersal of seeds); $\lambda_2 = 500$ m (mean distance for long distance dispersal of seeds).

a) Grasses (t.ha⁻¹)



b) Seeds.m⁻²



c) Tree Height (m)

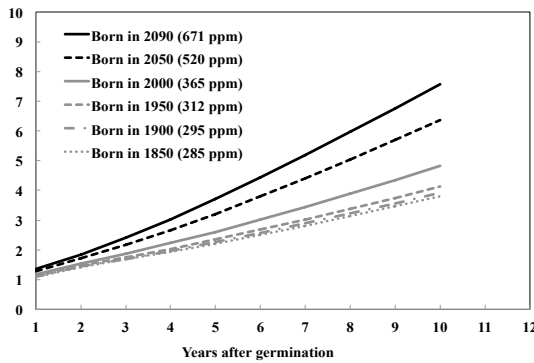


Figure 4. Potential values (no grass-tree interactions) of total grass production (aboveground and belowground biomass) for different fire return intervals (A), seed production (B) and tree height increment (C) under changing climatic conditions in the Morro Santana site (30°04'32"S; 51°06'05"W, Porto Alegre, Southern Brazil) from IPCC SRES A1B projected climate data. Simulations were conducted in a single cell with 900 m² (i.e., seed dispersal and fire spread in two dimensions were ignored). Simulations for evaluation of grass biomass production were conducted with no trees, and with fire on. Simulations for evaluation of seed production and tree growth were conducted with no grasses and no fire. For seed production, simulations started with one seedling (initial mass = 10 g) and for tree growth single seeds were allowed to germinate in specified years, as shown in C. Depicted values are the mean and the standard deviations after 10 replicates of each simulation case (random initializing seed varying from one to ten). In C, standard deviations are not show because the values were < 0.001.

Discussion

Detected trends of increasing temperature (Marengo and Camargo 2008) and rainfall (Haylock et al. 2006) over the last decades (1960 – 2000, 2002) have been reported for Southern Brazil. In addition, the IPCC (2007) A1B emission scenario predicts rising atmospheric CO₂ levels reaching 700 p.p.m (parts per million) in 2100, which will enhance even more the ongoing increases in local temperature and rainfall at the present study site (Figure 1).

Evidences of vegetation sensitivity to past and recent changes in climate from studies with fossil pollen records (e.g. Behling 2002), soil carbon isotopes (Duemig et al. 2008, Silva and Anand 2011) and tree ring analysis (Silva et al. 2009, Oliveira et al. 2010) can help understanding the effects of future climate change on vegetation processes from plant to landscape scales. At sites where at present forests intermingle with ancient grasslands in the highlands of South and Southeast Brazil, such evidences have shown that the expansion of forests started during the Late Holocene with a rate of 30-50 m.yr⁻¹ over the last 10,000 years (Silva and Anand 2011), together with increasing frequencies of anthropogenic fires (Behling 2002, Behling et al. 2007, Duemig et al. 2008). Similar rates were found for riparian forest expansion over savannas in central Brazil by studies with soil carbon isotopes (Silva et al. 2008), and for Semideciduous Seasonal Forest over grasslands from previous simulation experiments conducted for the same study site with the 2D-aDGVM under current climate conditions and frequent fires (from 20±4.4 m.year⁻¹ to 33±4.5 m.year⁻¹) (Chapter 2).

Tree ring analyses suggest that annual tree growth is strongly influenced by climate, and that temperature is the main regional factor affecting cambium activity (Oliveira et al. 2009, Oliveira et al. 2010). In addition, this sensitivity of tree growth to climate is age-dependent, i.e., young trees are more sensitive to climate influence than old ones (Vieira et al. 2009), mainly during the first decades of growth (Silva et al. 2009). Even though the range of responses to climate (mainly temperature and rainfall variations) from field measurements

seems to be species-dependent (Enquist and Leffler 2001, Silva et al. 2009), experimental evidences and simulated predictions support a general tendency of increasing plant efficiency and growth as a consequence of rising atmospheric CO₂ (Drake et al. 1997, Bond et al. 2003).

In the present study, simulations indicated that potential vegetation growth will be enhanced by elevated temperature and atmospheric CO₂ levels under future climate scenarios, when compared to pre-industrial values, and this was so irrespective of plant type physiology (C₃-tree and C₄-grass) (Figure 4). Considering grass-tree interactions in the presence of fire, simulations conducted with other DGVM in mesic savannas (750 mm) in South Africa also predicted increasing growth rates of grass biomass and post-burn stem height of saplings under rising atmospheric CO₂ values, despite the lower differences of tree growth rates for future predictions (0.62 m.yr⁻¹ with 700 ppm) and preindustrial (0.41 m.yr⁻¹ with 270 ppm) CO₂ levels (Bond et al. 2003) when compared to the potential growth rates (no grass-tree interactions and no fire) of seedlings predicted in the present study (Figure 4C). In a scenario of frequent fires, trees growing faster than the biomass accumulation needed to cause their aboveground stem-kill by flames in a future burning (i.e., to reach the escape height) is pointed as the major mechanism conferring advantage to trees over grasses in African savannas, which are favoring an increase in wood density (the “bush encroachment”) by the influence of rising CO₂ levels (Bond and Midgley 2000, Bond et al. 2003). The increasing rates of forest expansion observed under changing climate, mainly during the final 100 years in the study site (2000-2100, Figure 2), may be also attributed to the observed decreasing rates of trees killed by fires (Figure 3) in addition with increasing densities of seeds (Figure 4B) under rising CO₂ levels.

Predicted rates of forest expansion around year 2000 (26.5 ± 2.1 m.yr⁻¹) in the presence of fire and under continuously changing climate found in the present study (Figure 2, grey line) was similar to that found in previous simulations under current invariable climatic conditions as described before (24 ± 3.2 for horizontal surfaces, Chapter 2). These previous

simulations were conducted with the same initial 10% of land covered by forest, but different map size (0.72 km^2) and resolution (5 m), as well as proper seed dispersal parameters ($p_{seed} = 0.95$; $\lambda_1 = 5 \text{ m}$; $\lambda_2 = 10 \text{ m}$). This suggests that the increasing rates of forest expansion during the final 100 years (2000 – 2100) found in the present study under changing climate seems not to be a bias from the dispersal parameter values, map size or resolution, although the combination of these should affect the total time needed for a complete forest cover of the modelling space.

The continuously rising curve of forest cover from simulations conducted without fire (Figure 2, dark line) suggests that forest is the potential vegetation in the present site, as also showed by those other previous simulation experiments under current climate as described before (Chapter 2). However, the relative stability of forest-grassland mosaics promoted by fire (Figure 2, grey line; dark line in Figure 3A and 3B in Chapter 2) suggests that the feedback of higher productive grasslands on higher frequency of fires (Chapter 2) was sufficient to maintain the coexistence of forests and grasslands at the landscape scale under increasing mesic conditions (wetter and warmer) from past to current more forest-prone climate (Behling 2002). In fact, global-scale predictions from other DGVMs estimate forest domain in the absence of fire in Southeastern South America under the current climate (Woodward et al. 2004, Bond et al. 2005), but C_4 -dominated grasslands in the presence of fire (Bond et al. 2005).

Predictions of vegetation responses to other future IPCC emission scenarios in this region indicate a trend toward forests (Woodward and Lomas 2004, Salazar et al. 2007). In addition, as found in the present study, continuously elevated temperature and atmospheric CO_2 levels alone can cause increasing potential vegetation growth, irrespective of plant type physiology (C_3 -tree and C_4 -grass) (Figure 4). All these evidences suggest that the interplay between rainfall, temperature and atmospheric CO_2 levels will be the main driver of future

increasing rates of moving C₃-C₄ ecosystems boundaries and potentially causing regional losses of entire biomes at the regional scale.

Acknowledgements

This research was supported by grants from the Interamerican Institute for Global Change Research (IAI) and from (CAPES, Brazil). We are grateful to Enio Sosinski for gently providing and helping debug the initial source code for the cellular automata structure and to Guilherme Flach and Marcelo Johan for helping during the aDGVM spatialization procedure and debug of the final 2D-aDGVM. We are also grateful to Sandra Müller and Alessandra Fidelis for gently providing the empirical data for the aDGVM parameterization and validation.

References

- Bai, E., T. W. Boutton, X. B. Wu, F. Liu, and S. R. Archer. 2009. Landscape-scale vegetation dynamics inferred from spatial patterns of soil $\delta^{13}\text{C}$ in a subtropical savanna parkland. *Journal of Geophysical Research* **114**:1-10.
- Behling, H. 2002. South and southeast Brazilian grasslands during Late Quaternary times: a synthesis. *Palaeogeography, Palaeoclimatology, Palaeoecology*.
- Behling, H., V. D. Pillar, S. C. Müller, and G. E. Overbeck. 2007. Late-Holocene fire history in a forest-grassland mosaic in southern Brazil: Implications for conservation. *Applied Vegetation Science* **10**:81-90.
- Behling, H., V. D. Pillar, L. Orlóci, and S. G. Bauermann. 2004. Late Quaternary Araucaria forest, grassland (Campos), fire and climate dynamics, studied by high-resolution pollen, charcoal and multivariate analysis of the Cambará do Sul core in southern Brazil. *Palaeogeography, Palaeoclimatology, Palaeoecology* **203**:277-297.
- Bennett, K. D. and K. J. Willis. 2000. Effect of global atmospheric carbon dioxide on glacial–interglacial vegetation change. *Global Ecology and Biogeography* **9**:355-361.
- Bird, M. I. and J. A. Cali. 1998. A million-year record of fire in sub-Saharan Africa. *Nature* **394**:767-769.
- Bond, W. J. 2008. What Limits Trees in C4 Grasslands and Savannas? *Annual Review of Ecology, Evolution, and Systematics* **39**:641-659.
- Bond, W. J. and J. E. Keeley. 2005. Fire as a global 'herbivore': the ecology and evolution of flammable ecosystems. *Trends in Ecology & Evolution* **20**:387-394.
- Bond, W. J. and G. F. Midgley. 2000. A proposed CO₂-controlled mechanism of woody plant invasion in grassland and savannas. *Global Change Biology* **6**:865-869.
- Bond, W. J., G. F. Midgley, and F. I. Woodward. 2003. The importance of low atmospheric CO₂ and fire in promoting the spread of grasslands and savannas. *Global Change Biology* **9**:973-982.
- Bond, W. J., F. I. Woodward, and G. F. Midgley. 2005. The global distribution of ecosystems in a world without fire. *New Phytologist* **165**:525-538.
- Bowman, D. M. J. S., G. D. Cook, and U. Zoppi. 2004. Holocene boundary dynamics of a northern Australian monsoon rainforest patch inferred from isotopic analysis of carbon, (^{14}C and $\delta^{13}\text{C}$) and nitrogen ($\delta^{15}\text{N}$) in soil organic matter. *Austral Ecology* **29**:605-612.
- Bowman, D. M. J. S., A. Walsh, and D. J. Milne. 2001. Forest expansion and grassland contraction within a Eucalyptus savanna matrix between 1941 and 1994 at Litchfield National Park in the Australian monsoon tropics. *Global Ecology and Biogeography* **10**:535-548.
- Cabral, A. C., J. M. De Miguel, A. J. Rescia, M. F. Schmitz, and F. D. Pineda. 2003. Shrub encroachment in Argentinean savannas. *Journal of Vegetation Science* **14**:145-152.
- Caplat, P., M. Anand, and C. Bauch. 2008. Interactions between climate change, competition, dispersal, and disturbances in a tree migration model. *Theoretical Ecology* **1**:209-220.
- Cerling, T. E., J. M. Harris, B. J. MacFadden, M. G. Leakey, J. Quade, V. Eisenmann, and J. R. Ehleringer. 1997. Global vegetation change through the Miocene/Pliocene boundary. *Nature* **389**:153-158.
- Cowling, S. A. and M. T. Sykes. 1999. Physiological Significance of Low Atmospheric CO₂ for Plant-Climate Interactions. *Quaternary Research* **52**:237-242.
- Cramer, W., A. Bondeau, F. I. Woodward, I. C. Prentice, R. A. Betts, V. Brovkin, P. M. Cox, V. Fisher, J. A. Foley, A. D. Friend, C. Kucharik, M. R. Lomas, N. Ramankutty, S. Sitch, B. Smith, A. White, and C. Young-Molling. 2001. Global response of terrestrial ecosystem structure and function to CO₂ and climate change: results from six dynamic global vegetation models. *Global Change Biology* **7**:357-373.

- Devi, N., F. Hagedorn, P. Moiseev, H. Bugmann, S. Shiyatov, V. Mazepa, and A. Rigling. 2008. Expanding forests and changing growth forms of Siberian larch at the Polar Urals treeline during the 20th century. *Global Change Biology* **14**:1581-1591.
- Drake, B. G., M. A. González-Meler, and S. P. Long. 1997. MORE EFFICIENT PLANTS: A Consequence of Rising Atmospheric CO₂? *Annual Review of Plant Physiology and Plant Molecular Biology* **48**:609-639.
- Duemig, A., P. Schad, C. Rumpel, M.-F. Dignac, and I. Kögel-Knabner. 2008. Araucaria forest expansion on grassland in the southern Brazilian highlands as revealed by ¹⁴C and ^δ13C studies. *Geoderma* doi: **10.1016/j.geoderma.2007.06.005**.
- Dupont, L. M., S. Jahns, F. Marret, and S. Ning. 2000. Vegetation change in equatorial West Africa: time-slices for the last 150 ka. *Palaeogeography, Palaeoclimatology, Palaeoecology* **155**:95-122.
- Dupont, L. M., F. SchlÜTz, C. T. Ewah, T. C. Jennerjahn, A. Paul, and H. Behling. 2010. Two-step vegetation response to enhanced precipitation in Northeast Brazil during Heinrich event 1. *Global Change Biology* **16**:1647-1660.
- Ehleringer, J. R., T. E. Cerling, and B. R. Helliker. 1997. C₄ photosynthesis, atmospheric CO₂, and climate. *Oecologia* **112**:285-299-299.
- Enquist, B. J. and A. J. Leffler. 2001. Long-term tree ring chronologies from sympatric tropical dry-forest trees: individualistic responses to climatic variation. *Journal of Tropical Ecology* **17**:41-60.
- Fisher, R., N. McDowell, D. Purves, P. Moorcroft, S. Sitch, P. Cox, C. Huntingford, P. Meir, and F. Ian Woodward. 2010. Assessing uncertainties in a second-generation dynamic vegetation model caused by ecological scale limitations. *New Phytologist* **187**:666-681.
- Goetze, D., B. Hörsch, and S. Porembski. 2006. Dynamics of forest–savanna mosaics in north-eastern Ivory Coast from 1954 to 2002. *Journal of Biogeography* **33**:653-664.
- Grimm, E. C. 1983. Chronology and dynamics of vegetation change in the prairie-woodland region of southern minnesota, U.S.A. *New Phytologist* **93**:311-350.
- Haylock, M. R., T. C. Peterson, L. M. Alves, T. Ambrizzi, Y. M. T. Anunciação, J. Baez, V. R. Barros, M. A. Berlato, M. Bidegain, G. Coronel, V. Corradi, V. J. Garcia, A. M. Grimm, D. KAroly, J. A. Marengo, M. B. Marino, D. F. Moncunill, D. NEchet, J. QUINTANA, E. Rebello, M. Rusticucci, J. L. Santos, I. Trebejo, and L. A. Vincent. 2006. Trends in Total and Extreme South American Rainfall in 1960–2000 and Links with Sea Surface Temperature. *Journal of Climate* **19**:1490-1512.
- Higgins, S. I., W. J. Bond, S. Winston, and W. Trollope. 2000. Fire, resprouting and variability: a recipe for grass-tree coexistence in savanna. *Journal of Ecology* **88**:213-229.
- Higgins, S. I. and M. L. Cain. 2002. Spatially realistic plant metapopulation models and the colonization–competition trade-off. *Journal of Ecology* **90**:616-626.
- IPCC. 2007. *Climate Change 2007: The Physical Science Basis*. Contribution of Working Group I to the Fourth Assessment Report of the Intergovernmental Panel on Climate Change. Cambridge University Press, Cambridge, UK and New York, USA.
- Izaurrealde, R., A. Thomson, N. Rosenberg, and R. Brown. 2005. Climate Change Impacts for the Conterminous USA: An Integrated Assessment. *Climatic Change* **69**:107-126-126.
- Jordano, P., C. García, J. A. Godoy, and J. L. García-Castaño. 2007. Differential contribution of frugivores to complex seed dispersal patterns. *Proceedings of the National Academy of Sciences* **104**:3278-3282.
- Knapp, P. A. and P. T. Soulé. 1998. Recent *Juniperus occidentalis* (Western Juniper) expansion on a protected site in central Oregon. *Global Change Biology* **4**:347-357.
- LaDeau, S. L. and J. S. Clark. 2001. Rising CO₂ Levels and the Fecundity of Forest Trees. *Science* **292**:95-98.

- Marengo J.A. 2007. Cenários de mudanças climáticas para o Brasil em 2100. *Ciência & Ambiente* 34: 97-114.
- Marengo, J. A. and C. C. Camargo. 2008. Surface air temperature trends in Southern Brazil for 1960–2002. *International Journal of Climatology* 28:893-904.
- Müller, S. C. and E. D. Forneck. 2004. Forest-grassland mosaics in the hills of Porto Alegre city: a study case of forest expansion patterns in Santana hill, Rio Grande do Sul, Brazil. Pages 29-37 *in* Workshop - Proteção e manejo da vegetação natural da região de Porto Alegre, com base em pesquisas de padrões e dinâmica da vegetação. Programa de Pós-Graduação em Ecologia/UFRGS, Porto Alegre.
- Nimer, E. 1990. Clima. Pages 151-187 *in* IBGE, editor. Geografia do Brasil: Região Sul. IBGE, Rio de Janeiro.
- Oliveira, J., E. Santarosa, V. Pillar, and F. Roig. 2009. Seasonal cambium activity in the subtropical rain forest tree *Araucaria angustifolia*. *Trees - Structure and Function* 23:107-115-115.
- Oliveira, J. M. and V. D. Pillar. 2004. Vegetation dynamics on mosaics of Campos and Araucaria forest between 1974 and 1999 in Southern Brazil. *Community Ecology* 5:197-202.
- Oliveira, J. M., F. A. Roig, and V. D. Pillar. 2010. Climatic signals in tree-rings of *Araucaria angustifolia* in the southern Brazilian highlands. *Austral Ecology* 35:134-147.
- Overbeck, G. E., S. C. Müller, A. Fidelis, J. Pfadenhauer, V. D. Pillar, C. C. Blanco, I. I. Boldrini, R. Both, and E. D. Forneck. 2007. Brazil's neglected biome: The South Brazilian *Campos*. *Perspectives in Plant Ecology, Evolution and Systematics* 9:101-116.
- Parmesan, C. 2006. Ecological and evolutionary responses to recent climate change. *Annu. Rev. Ecol. Evol. Syst.* 37:637-669.
- Payette, S. 2007. Contrasted dynamics of northern labrador tree lines caused by climate change and migrational lag. *Ecology* 88:770-780.
- Petit, J., J. J., R. D., B. NI, B. JM, B. I, B. M, C. J, D. J, D. G, D. M, K. VM, L. M, L. V, L. C, P. L, R. C, S. E, and S. M. 1999. Climate and atmospheric history of the past 420,000 years from the Vostok Ice Core, Antarctica. *Nature* 300:429-436.
- Roques, K. G., T. G. O'Connor, and A. R. Watkinson. 2001. Dynamics of shrub encroachment in an African savanna: relative influences of fire, herbivory, rainfall and density dependence. *Journal of Applied Ecology* 38:268-280.
- Salazar, L. F., C. A. Nobre, and M. D. Oyama. 2007. Climate change consequences on the biome distribution in tropical South America. *Geophys. Res. Lett.* 34:L09708.
- Scheiter, S. and S. I. Higgins. 2009. Impacts of climate change on the vegetation of Africa: an adaptive dynamic vegetation modelling approach. *Global Change Biology* 15:2224-2246.
- Silva, L. C. R. and M. Anand. 2011. Mechanisms of *Araucaria* (Atlantic) forest expansion in southern Brazil. *Ecosystems* (accepted).
- Silva, L. C. R., M. Anand, J. M. Oliveira, and V. D. Pillar. 2009. Past century changes in *Araucaria angustifolia* (Bertol.) Kuntze water use efficiency and growth in forest and grassland ecosystems of southern Brazil: implications for forest expansion. *Global Change Biology* 15:2387-2396.
- Silva, L. C. R., L. Sternberg, M. Haridasan, W. A. Hoffmann, F. Miralles-Wilhelm, and A. C. Franco. 2008. Expansion of gallery forests into central Brazilian savannas. *Global Change Biology* 14:2108-2118.
- Strömberg. 2011. Evolution of Grasses and Grassland Ecosystems. *Annual Review of Earth and Planetary Science* 39:517-544.
- Van Auken, O. W. 2000. Shrub Invasions of North American Semiarid Grasslands. *Annu. Rev. Ecol. Syst.* 31:197-215.

- van Gils, H., O. Batsukh, D. Rossiter, W. Munthali, and E. Liberatoscioli. 2008. Forecasting the pattern and pace of *Fagus* forest expansion in Majella National Park, Italy. *Applied Vegetation Science* **11**:539-546.
- Vieira, J., F. Campelo, and C. Nabais. 2009. Age-dependent responses of tree-ring growth and intra-annual density fluctuations of *Pinus pinaster* to Mediterranean climate. *Trees - Structure and Function* **23**:257-265-265.
- Walther, G.-R., E. Post, P. Convey, A. Menzel, C. Parmesan, T. J. C. Beebee, J.-M. Fromentin, O. Hoegh-Guldberg, and F. Bairlein. 2002. Ecological responses to recent climate change. *Nature* **416**:389-395.
- Woodward, F. I. and M. R. Lomas. 2004. Vegetation dynamics - simulating responses to climatic change. *Biological Reviews* **79**:643-670.
- Woodward, F. I., M. R. Lomas, and C. K. Kelly. 2004. Global climate and the distribution of plant biomes. *Philosophical Transactions of the Royal Society of London. Series B: Biological Sciences* **359**:1465-1476.

CONSIDERAÇÕES FINAIS

O modelo proposto apresentou uma boa capacidade preditiva para o local de estudo em que foi empregado, principalmente com relação à dinâmica de avanço das bordas florestais. Contudo, alguns aspectos importantes para uma melhor representatividade do sistema não foram contemplados pelo presente trabalho mas podem ser apontados como sugestões futuras para o aprimoramento do modelo proposto. A menor capacidade preditiva de manchas florestais isoladas na matriz campestre atribui-se ao caráter mais aleatório desse processo de estabelecimento das mesmas à medida que aumentam as distâncias das bordas florestais (Matte, 2006). Na escala de paisagem considerada neste trabalho, esse aspecto pode ser melhorado pela implementação de efeitos atratores de “paradouros” naturais para dispersores, como afloramentos rochosos e indivíduos lenhosos isolados na matriz campestre, no favorecimento do adensamento de mais indivíduos lenhosos nesses locais (Duarte, Santos *et al.*, 2006; Carlucci, Duarte *et al.*, 2011), i.e. um *feedback* positivo para o avanço das formações lenhosas. Obviamente, a presença de afloramentos rochosos na paisagem constitui uma característica mais específica dos locais de estudo quando abordados nesta escala, necessitando-se de dados refinados da localização e densidade desses afloramentos. Isto gera a necessidade de uma avaliação custo-benefício entre o esforço amostral para se obter essa informação e a magnitude do incremento da capacidade preditiva do modelo.

Este último aspecto tornar-se-á mais evidente diante de um eventual objetivo futuro de implementação deste modelo numa escala mais ampla (ex. regional). Ainda, numa escala de tal magnitude, como a regional, outros aspectos importantes careceriam da avaliação da necessidade de serem implementados, como por exemplo as variações espaciais na estrutura do solo e disponibilidade de nutrientes, além do sombreamento por outras faces do terreno (Allen, Trezza *et al.*, 2006) e o escoamento superficial das chuvas e talvegues (Matte, 2009), ambos devido ao incremento de topografias mais acidentadas do que aquelas da paisagem

considerada no presente estudo. Finalmente, devido ao caráter determinístico das funções que definem o crescimento da vegetação em função da alometria e fisiologia dos indivíduos, a aplicação do mesmo para outras localidades ainda necessita de uma parametrização com base nos tipos funcionais “médios” ou mais representativos do sistema em questão. Neste sentido, a implementação de outras fisiologias (ex. herbáceas C₃, e CAM), além de um sub-modelo adaptativo para a variação de atributos alométricos e funcionais em função das variações ambientais, permitiria a avaliação dos efeitos das mudanças climáticas futuras na distribuição de determinadas espécies, ou ainda, de diferentes formações lenhosas e herbáceas, em gradientes altitudinais e latitudinais, possibilitando a aplicação do modelo em escalas ainda mais amplas. Não obstante, dentro dos objetivos propostos e considerando os resultados satisfatórios obtidos, conclui-se que a escala de aplicação do modelo foi adequada, assim como a abordagem teórica em que o problema foi abordado. No entanto, diante da exuberante diversidade dos ecossistemas brasileiros e da inerente simplificação advinda da natureza determinística e da representatividade de tipos funcionais considerados no modelo, embora parcialmente superada pela sua característica adaptativa, torna-se necessária a exploração da sua capacidade preditiva em outros sistemas vegetacionais.

Num cenário futuro de incertezas no rumo de decisões que devem partir de uma escala local/regional para o cumprimento de metas de emissões de gases efeito estufa que interferem em processos na escala global, a manutenção da integridade ecológica e da produtividade econômica dos sistemas naturais envolve o conhecimento da interação dos mesmos numa escala de paisagem. No presente trabalho, o entendimento da dinâmica de mosaicos de vegetação considerando a abordagem mais sistêmica de estados estáveis alternativos (Warman e Moles, 2009; Staver, Archibald *et al.*, 2010) parece ser a maneira mais adequada para tratar questões acerca dos mecanismos envolvidos na conservação de ecossistemas de coexistência milenar (Bond e Parr, 2010), como os mosaicos floresta-campo do sul do Brasil. Embora existam evidências de que as paisagens locais tenham sido dominadas por esses

campos relictos num passado distante, a recente intensificação das práticas de uso da terra para fins econômicos, principalmente através do aumento do desmatamento para abertura de fronteiras agropecuárias a partir do século XVII, também favoreceu o aparecimento de áreas abertas de sucessão secundária. Num contexto de paisagens fragmentadas e diante do aumento dos interesses mundiais para a conservação e restauração prioritária das formações florestais, uma distinção equivocada entre campos sucessionais e campos relictos pode trazer sérias conseqüências para esforços futuros de conservação e uso sustentável da biodiversidade das formações campestres naturais (Pillar, Müller *et al.*, 2009; Bond e Parr, 2010). Isto surge do fato de que, diante da tendência geral de crescente invasão de elementos lenhosos sobre as formações abertas, os campos naturais antigos têm permanecido como ecossistemas alternativos nessa paisagem de mosaicos floresta-campo (Pillar e Vélez, 2010). No entanto, as conseqüências dessa nova perspectiva requerem um melhor entendimento das interações positivas e negativas que controlam a resiliência e a relativa estabilidade de ambos os tipos vegetacionais, para que sejam alcançadas estratégias mais adequadas e efetivas para a conservação e uso sustentável de ambos os estados alternativos (floresta e campo) desse complexo *sistema mosaico*.

REFERÊNCIAS BIBLIOGRÁFICAS

- ALLEN, R. G.; TREZZA, R.; TASUMI, M. Analytical integrated functions for daily solar radiation on slopes. **Agricultural and Forest Meteorology**, v. 139, n. 1-2, p. 55-73, 2006. ISSN 0168-1923. Disponível em: < <http://www.sciencedirect.com/science/article/B6V8W-4KCRS6D-1/2/be4eaf544ca3e4c64544167afbe585da> >.
- BACHELET, D. et al. **MC1: a dynamic vegetation model for estimating the distribution of vegetation and associated ecosystem fluxes of carbon, nutrients, and water**. USDA Forest Service, Pacific Northwest Station General Technical Report PNW-GTR-508. 2001.
- BAI, E. et al. Landscape-scale vegetation dynamics inferred from spatial patterns of soil $\delta^{13}C$ in a subtropical savanna parkland. **Journal of Geophysical Research**, v. 114, n. G01019, p. 1-10, 2009.
- BECKAGE, B.; ELLINGWOOD, C. Fire Feedbacks with Vegetation and Alternative Stable States. **Complex Systems**, v. 18, p. 159-173, 2008.
- BECKAGE, B.; GROSS, L. J.; PLATT, W. J. Grass feedbacks on fire stabilize savannas. **Ecological Modelling**, v. In Press, Corrected Proof, 2011. ISSN 0304-3800. Disponível em: < <http://www.sciencedirect.com/science/article/B6VBS-52FBNVK-1/2/82951d7c23eb4685072a598e834f9390> >.
- BECKAGE, B.; PLATT, W. J.; GROSS, L. J. Vegetation, Fire, and Feedbacks: A Disturbance-Mediated Model of Savannas. **The American Naturalist**, v. 174, n. 6, p. 805-818, 2009. ISSN 00030147. Disponível em: < <http://www.jstor.org/stable/10.1086/648458> >.
- BEHLING, H. South and southeast Brazilian grasslands during Late Quaternary times: a synthesis. **Palaeogeography, Palaeoclimatology, Palaeoecology**, 2002. Disponível em: < D:\Users\José Pedro\Papers\science_Behling2002SS.pdf >.
- BEISNER, B.; HAYDON, D.; CUDDINGTON, K. Alternative stable states in ecology. **Frontiers in Ecology and the Environment**, v. 1, n. 7, p. 376-382, 2003. Disponível em: < <http://www.esajournals.org/doi/abs/10.1890/1540-9295%282003%29001%5B0376%3AASSIE%5D2.0.CO%3B2> >.
- BOLDRINI, I. I.; EGGERS, L. Directionality of succession after grazing exclusion in grassland in the south of Brazil. **Coenoses**, Gorizia, v. 12, n. 02/Mar, p. 63-66, 4/23/2002 1997.
- BOLDRINI, I. I. et al. Biodiversidade dos campos do planalto das araucárias. In: BOLDRINI, I. I. (Ed.). **Relatório Técnico do PROBIO** Brasília: MMA, v.30, 2009. p.38-94.
- BOLDRINI, I. L. A flora dos campos do Rio Grande do Sul. In: PILLAR, V. D.; MÜLLER, S. C., et al (Ed.). **Campos Sulinos: Conservação e uso sustentável fa biodiversidade**. Brasília: MMA, 2009. cap. 4, p.63-77. ISBN 978-85-7738-117-3.
- BOND, W. J. What Limits Trees in C4 Grasslands and Savannas? **Annual Review of Ecology, Evolution, and Systematics**, v. 39, n. 1, p. 641-659, 2008/12/01 2008. ISSN 1543-

592X. Disponível em: < <http://dx.doi.org/10.1146/annurev.ecolsys.39.110707.173411> >. Acesso em: 2011/02/10.

BOND, W. J.; MIDGLEY, G. F. A proposed CO₂-controlled mechanism of woody plant invasion in grassland and savannas. **Global Change Biology**, v. 6, p. 865-869, 2000.

BOND, W. J.; MIDGLEY, G. F.; WOODWARD, F. I. The importance of low atmospheric CO₂ and fire in promoting the spread of grasslands and savannas. **Global Change Biology** v. 9, p. 973-982, 2003.

BOND, W. J.; PARR, C. L. Beyond the forest edge: Ecology, diversity and conservation of the grassy biomes. **Biological Conservation**, v. 143, n. 10, p. 2395-2404, 2010. ISSN 0006-3207. Disponível em: < <http://www.sciencedirect.com/science/article/B6V5X-4Y6K07J-1/2/6159006726b9d9eee674c5ce56e21572> >.

BOWMAN, D. M. J. S. **Australian rainforests: islands of green in a land of fire**. Cambridge, UK: Cambridge University Press, 2000.

CABRAL, A. C. et al. Shrub encroachment in Argentinean savannas. **Journal of Vegetation Science**, v. 14, p. 145-152, 2003.

CARLUCCI, M. B.; DUARTE, L. D. S.; PILLAR, V. D. Nurse rocks influence forest expansion over native grassland in southern Brazil. **Journal of Vegetation Science**, v. 22, n. 1, p. 111-119, 2011. ISSN 1654-1103. Disponível em: < <http://dx.doi.org/10.1111/j.1654-1103.2010.01229.x> >.

CRAMER, W. et al. Global response of terrestrial ecosystem structure and function to CO₂ and climate change: results from six dynamic global vegetation models. **Global Change Biology**, v. 7, n. 4, p. 357-373, 2001. ISSN 1365-2486. Disponível em: < <http://dx.doi.org/10.1046/j.1365-2486.2001.00383.x> >.

DRAKE, B. G.; GONZÁLEZ-MELER, M. A.; LONG, S. P. MORE EFFICIENT PLANTS: A Consequence of Rising Atmospheric CO₂? **Annual Review of Plant Physiology and Plant Molecular Biology**, v. 48, n. 1, p. 609-639, 1997/06/01 1997. ISSN 1040-2519. Disponível em: < <http://dx.doi.org/10.1146/annurev.arplant.48.1.609> >. Acesso em: 2011/07/18.

DUARTE, L. S. et al. The role of nurse plants in Araucaria forest expansion over grassland in south Brazil. **Austral Ecology**, v. 31, p. 520-528, 2006.

DUEMIG, A. et al. Araucaria forest expansion on grassland in the southern Brazilian highlands as revealed by ¹⁴C and ^δ¹³C studies. **Geoderma**, v. doi: 10.1016/j.geoderma.2007.06.005., 2008.

FISHER, R. et al. Assessing uncertainties in a second-generation dynamic vegetation model caused by ecological scale limitations. **New Phytologist**, v. 187, n. 3, p. 666-681, 2010. ISSN 1469-8137. Disponível em: < <http://dx.doi.org/10.1111/j.1469-8137.2010.03340.x> >.

GOETZE, D.; HÖRSCH, B.; POREMBSKI, S. Dynamics of forest–savanna mosaics in north-eastern Ivory Coast from 1954 to 2002. **Journal of Biogeography**, v. 33, n. 4, p. 653-664, 2006. ISSN 1365-2699. Disponível em: < <http://dx.doi.org/10.1111/j.1365-2699.2005.01312.x> >.

HIGGINS, S. I. et al. Fire, resprouting and variability: a recipe for grass-tree coexistence in savanna. **Journal of Ecology**, v. 88, p. 213-229, 2000.

HIGGINS, S. I.; SCHEITER, S.; SANKARAN, M. The stability of African savannas: insights from the indirect estimation of the parameters of a dynamic model. **Ecology**, v. 91, n. 6, p. 1682-1692, 2010/06/01 2010. ISSN 0012-9658. Disponível em: < <http://dx.doi.org/10.1890/08-1368.1> >. Acesso em: 2011/02/22.

IPCC. Climate Change 2007: The Physical Science Basis. Contribution of Working Group I to the Fourth Assessment Report of the Intergovernmental Panel on Climate Change. Cambridge, UK and New York, USA: Cambridge University Press, 2007.

KLEIN, R. M. Southern Brazilian phytogeographic features and the probable influence of Upper Quaternary climate changes in the floristic distribution. **Boletim Paranaense de Geociências**, v. 33, p. 67-88, 1975.

LANGEVELDE, F. V. et al. Effects of fire and herbivory on the stability of savanna ecosystems. **Ecology**, v. 84, n. 2, p. 337-350, 2003.

LEITE, P. F.; KLEIN, R. M. Vegetação. In: IBGE (Ed.). **Geografia do Brasil: Região Sul.** Rio de Janeiro: Instituto Brasileiro de Geografia e estatística, v.2, 1990. p.113-150.

LINDMAN, C. A. M. **A Vegetação no Rio Grande do Sul.** São Paulo/Belo Horizonte: EDUSP/Itatiaia, 1906.

MATTE, A. L. Padrões espaciais de manchas florestais em mosaicos de floresta-campo nos morros de Porto Alegre, RS. Salão de Iniciação Científica 2006. Porto Alegre, Brazil. UFRGS/PROPESQ. p.461.

_____. **Padrões de distribuição, estrutura e contexto de manchas florestais em um mosaico de campo e floresta no planalto sul brasileiro.** 2009. 73 Instituto de Biociências. Programa de Pós-Graduação em Ecologia, Universidade Federal do Rio Grande do Sul, Porto Alegre.

MÜLLER, S. C. **Padrões de espécies e tipos funcionais de Plantas lenhosas em bordas de floresta e Campo sob influência do fogo.** 2005. 135 (Tese de Doutorado). Programa de Pós-Graduação em Ecologia, Universidade Federal do Rio Grande do Sul, Porto Alegre.

OLIVEIRA, J. M.; PILLAR, V. D. Vegetation dynamics on mosaics of Campos and Araucaria forest between 1974 and 1999 in Southern Brazil. **Community Ecology**, v. 5, n. 2, p. 197-202, 2004.

OLIVEIRA-FILHO, A. T.; FONTES, M. A. L. Patterns of floristic differentiation among Atlantic Forest in Southeastern Brazil and the influence of climate. **Biotropica**, v. 32, n. 4b, p. 793-810, 2000.

OVERBECK, G. E. et al. Brazil's neglected biome: The South Brazilian *Campos*. **Perspectives in Plant Ecology, Evolution and Systematics**, v. 9, p. 101-116, 2007.

PARMESAN, C. Ecological and evolutionary responses to recent climate change. **Annu. Rev. Ecol. Evol. Syst.**, v. 37, p. 637-669, 2006.

PENG, C. From static biogeographical model to dynamic global vegetation model: a global perspective on modelling vegetation dynamics. **Ecological Modelling**, v. 135, n. 1, p. 33-54, 2000. ISSN 0304-3800. Disponível em: <

<http://www.sciencedirect.com/science/article/B6VBS-41JKVRY-3/2/1d9e41397cadd1432876a49e44737565> >.

PILLAR, V. D. Dinâmica de expansão florestal em mosaicos de floresta e campos no sul do Brasil. In: CLAUDINO-SALES, V. (Ed.). **Ecosistemas brasileiros: manejo e conservação**. Fortaleza: Expressão Gráfica e Editora, 2003. p.209-216.

PILLAR, V. D. et al. **Campos Sulinos: Conservação e Uso Sustentável da Biodiversidade**. Brasília: MMA, 2009. 403p.

PILLAR, V. D.; QUADROS, F. L. F. Grassland-forest boundaries in southern Brazil. **Coenoses**, v. 12, p. 119-126, 1997.

PILLAR, V. D.; VÉLEZ, E. Extinção dos Campos Sulinos em unidades de conservação: um fenômeno natural ou um problema ético? **Natureza e Conservação**, v. 8, p. 84-88, 2010.

PINILLOS, M. et al. Understanding forest-grassland mosaics: Three case studies on the basaltic plateaus in humid subtropical Brazil. **Ecotrópicos**, v. 22, n. 2, p. 110-128, 2009.

PIVELLO, V. R.; NORTON, G. A. FIRETOOL: An expert system for the use of prescribed fires in cerrado (Brazilian savanna) conservation areas. **Journal of Applied Ecology**, v. 33, p. 348-356, 1996.

RAMBO, B. **A fisionomia do Rio Grande do Sul**. Porto Alegre: Selbach, 1956.

ROQUES, K. G.; O'CONNOR, T. G.; WATKINSON, A. R. Dynamics of shrub encroachment in an African savanna: relative influences of fire, herbivory, rainfall and density dependence. **Journal of Applied Ecology**, v. 38, p. 268-280, 2001. Disponível em: < C:\Meus documentos\Revisões bibliográficas\Dinamica\Roquesetal01_shrubEncroachmentSavanaFire.pdf >.

SANKARAN, M. et al. Determinants of woody cover in African savannas. **Nature**, v. 438, n. 7069, p. 846-849, 2005. ISSN 0028-0836. Disponível em: < <http://dx.doi.org/10.1038/nature04070> >.

SANKARAN, M.; RATNAM, J.; HANAN, N. P. Tree-grass coexistence in savannas revisited – insights from an examination of assumptions and mechanisms invoked in existing models. **Ecology Letters**, v. 7, n. 6, p. 480-490, 2004. ISSN 1461-0248. Disponível em: < <http://dx.doi.org/10.1111/j.1461-0248.2004.00596.x> >.

SARMIENTO, G. **The Ecology of Neotropical Savannas**. Harvard University Press, 1984.

_____. A conceptual model relating environmental factors and vegetation formations in the lowlands of tropical South America. In: FURLEY, P. A.; PROCTOR, J., *et al* (Ed.). **Nature and Dynamics of Forest-Savanna Boundaries**. London: Chapman & Hall, 1992. p.583-601.

SATO, H.; ITOH, A.; KOHYAMA, T. SEIB-DGVM: A new Dynamic Global Vegetation Model using a spatially explicit individual-based approach. **Ecological Modelling**, v. 200, n. 3-4, p. 279-307, 2007. ISSN 0304-3800. Disponível em: < <http://www.sciencedirect.com/science/article/B6VBS-4M57HDN-3/2/e90c068b3eb97dd86f90c03b6fe4f02b> >.

SCHEFFER, M. et al. Catastrophic shifts in ecosystems. **Nature**, v. 413, n. 6856, p. 591-596, 2001. ISSN 0028-0836. Disponível em: < <http://dx.doi.org/10.1038/35098000> >.

SCHEITER, S.; HIGGINS, S. I. Impacts of climate change on the vegetation of Africa: an adaptive dynamic vegetation modelling approach. **Global Change Biology**, v. 15, n. 9, p. 2224-2246, 2009. ISSN 1365-2486. Disponível em: < <http://dx.doi.org/10.1111/j.1365-2486.2008.01838.x> >.

SCHOLES, R. J.; ARCHER, S. R. Tree-grass interactions in savannas. **Annual Review of Ecology and Systematics**, v. 28, p. 517-544, 1997.

SILVA, L. C. R.; ANAND, M. Mechanisms of Araucaria (Atlantic) forest expansion in southern Brazil **Ecosystems (under minor reviews)**, 2011.

SILVA, L. C. R. et al. Past century changes in Araucaria angustifolia (Bertol.) Kuntze water use efficiency and growth in forest and grassland ecosystems of southern Brazil: implications for forest expansion. **Global Change Biology**, v. 15, n. 10, p. 2387-2396, 2009. ISSN 1365-2486. Disponível em: < <http://dx.doi.org/10.1111/j.1365-2486.2009.01859.x> >.

SILVA, L. C. R. et al. Expansion of gallery forests into central Brazilian savannas. **Global Change Biology**, v. 14, n. 9, p. 2108-2118, 2008. ISSN 1365-2486. Disponível em: < <http://dx.doi.org/10.1111/j.1365-2486.2008.01637.x> >.

STAVER, A. C.; ARCHIBALD, S.; LEVIN, S. Tree cover in sub-Saharan Africa: rainfall and fire constrain forest and savanna as alternative stable states. **Ecology**, 2010. ISSN 0012-9658. Disponível em: < <http://dx.doi.org/10.1890/10-1684.1> >. Acesso em: 2011/03/08.

TEIXEIRA, M. B. et al. Vegetação. In: IBGE (Ed.). **Levantamento de recursos naturais (Folha SH.22 Porto Alegre e parte das Folhas SH.21 Uruguaiana e SI.22 Lagoa Mirim)**. Rio de Janeiro: IBGE, v.33, 1986. p.541-632.

VAN AUKEN, O. W. Shrub Invasions of North American Semiarid Grasslands. **Annu. Rev. Ecol. Syst.**, v. 31, p. 197-215, 2000.

VÉLEZ, E. et al. Um panorama sobre as iniciativas de conservação dos Campos Sulinos. In: PILLAR, V. D.; MÜLLER, S. C., *et al* (Ed.). **Campos Sulinos: Conservação e uso sustentável da biodiversidade**. Brasília: MMA, 2009. cap. 28, p.356-379.

WALKER, B. H.; NOY-MEIR, I. Aspects of the Stability and Resilience of Savanna Ecosystems. In: HUNTLEY, B. J. e WALKER, B. H. (Ed.). **Ecology of tropical Savannas**. Berlin: Springer-Verlag, v.42, 1982. p.556-590.

WALTER, H. **Ecology of Tropical and Subtropical Vegetation**. Edinburgh: Oliver & Boyd, 1971.

WALTHER, G.-R. et al. Ecological responses to recent climate change. **Nature**, v. 416, n. 6879, p. 389-395, 2002. ISSN 0028-0836. Disponível em: < <http://dx.doi.org/10.1038/416389a> >.

WARMAN, L.; MOLES, A. Alternative stable states in Australia's Wet Tropics: a theoretical framework for the field data and a field-case for the theory. **Landscape Ecology**, v. 24, n. 1, p. 1-13, 2009. ISSN 0921-2973. Disponível em: < <http://dx.doi.org/10.1007/s10980-008-9285-9> >.

WHITTAKER, R. H. **Communities and Ecosystems**. London: McGraw-Hill Book Co., 1971.

_____. **Classification of Plant Communities**. Dr. W. Junk bv Publishers, 1978.

WOODWARD, F. I.; LOMAS, M. R.; KELLY, C. K. Global climate and the distribution of plant biomes. **Philosophical Transactions of the Royal Society of London. Series B: Biological Sciences**, v. 359, n. 1450, p. 1465-1476, 2004. Disponível em: < <http://rstb.royalsocietypublishing.org/content/359/1450/1465.abstract> >.

APÊNDICE 1

aDGVM:

An adaptive dynamic global vegetation model for tropical ecosystems.

Version 1.0⁴

⁴ Este apêndice apresenta a descrição detalhada do modelo aDGVM e corresponde ao Apêndice S1 do material complementar de Scheiter and Higgins (2009).

**aDGVM:
An adaptive dynamic global vegetation
model for tropical ecosystems.
Version 1.0**

Simon Scheiter¹ and Steven I. Higgins²

26th November 2008

Supplementary material S1 for: Scheiter, S. & Higgins, S.I. Impacts of climate change on the vegetation of Africa: an adaptive dynamic vegetation modelling approach.

¹ Lehrstuhl für Vegetationsökologie
Technische Universität München
85350 Freising-Weihenstephan, Germany
E-mail: scheiter@em.uni-frankfurt.de
Phone: +49 (0)69 798 40167, Fax: +49 (0)69 798 40169

² Institut für Physische Geographie
Johann Wolfgang Goethe-Universität Frankfurt am Main
60438 Frankfurt am Main, Germany
E-mail: higgins@em.uni-frankfurt.de

Contents

1	Introduction	3
2	Modelling concepts	4
3	Input data	6
4	Leaf photosynthesis	7
4.1	Photosynthesis sub-model	7
4.2	Stomatal conductance sub-model	9
4.3	Linking photosynthesis and stomatal conductance	10
5	Individual plant model	11
5.1	Biomass pools of a plant	11
5.2	Plant allometry	12
5.3	Canopy photosynthesis and stomatal conductance	13
5.4	Respiration sub-model	15
5.5	Carbon balance and allocation	16
5.6	Leaf phenology	18
5.7	Biomass turnover and decomposition	20
5.8	Evapotranspiration	20
6	Stand scale dynamics	21
6.1	Total evapotranspiration and soil water balance	21
6.2	Light competition	22
6.3	Tree population dynamics	24
6.3.1	Reproduction and seed bank model	24
6.3.2	Death process	25
6.4	Grass fires and tree topkill	25
7	Synthesis of sub-models	27
8	Programming	29
9	Model parameters	29
	References	37

1 Introduction

Tropical regions are dominated by grasslands, savannas and forests. The factors that determine whether savannas, forests or grasslands dominate a given location have long intrigued ecologists and biogeographers (Sarmiento 1984; Scholes and Archer 1997; Higgins *et al.* 2000; House *et al.* 2003; Sankaran *et al.* 2004). Recent studies have argued that progress can be made by integrating demographic or disturbance based theories of savanna dynamics with resource or competition based theories (Sankaran *et al.* 2005). For instance models have been developed (Scheiter and Higgins 2007) that allow one to understand, in a theoretical sense, the conditions under which grasslands, forests or savannas exist. Although useful in a heuristic sense this model and other similar models are not explicitly based on bio-physical mechanisms, with the consequence that they cannot predict vegetation states as a function of climatic and edaphic conditions.

How climate influences vegetation, can in principle, be addressed by a class of models called dynamic global vegetation models (DGVMs, Figure 1). Several models of this class have been proposed and used (e.g. Lüdeke *et al.* 1994; Cramer *et al.* 2001; Moorcroft *et al.* 2001; Arora 2003; Bonan *et al.* 2003; Sitch *et al.* 2003; Hély *et al.* 2006; Hickler *et al.* 2006; Schaphoff *et al.* 2006; Sato *et al.* 2007) to simulate the response of vegetation to environmental conditions by simulating bio-physical, physiological and demographic mechanisms. However, these models have not been developed and tested in tropical regions (House *et al.* 2003, but see Moorcroft *et al.* 2001 for an exception) and therefore poorly represent processes that are known to be important in these systems. Thus, transitional zones such as savannas have been identified as being subjected to high uncertainties (Hickler *et al.* 2006). For instance, existing DGVMs often describe fire by simply correlating litter to a fire frequency and by assuming that fire removes a constant fraction of standing biomass (Thonicke *et al.* 2001; Venevsky *et al.* 2002). One consequence of such fire models is that existing DGVMs underestimate the extent of savannas and often predict grasslands or forests in regions where savannas are observed (Cramer *et al.* 2001). Further, most existing DGVMs are not individual-based which means that those models cannot explicitly simulate the effect of fire on the horizontal structure of tree populations and the impact of climate change on a plant level.

In the following we present an individual-based vegetation model that is based on the bio-physical, physiological and demographic processes that are assumed to determine tropical vegetation. The model only needs general soil and climate data as input and thus, the model allows us to predict, using readily available environmental data, whether the environmental conditions at a study site define a savanna, grassland, deciduous woodland or an evergreen forest.

This manuscript is structured as follows. First, we outline the basic model structure. Then we provide a detailed description of the input data and the different sub-models.

Finally, we describe how the sub-models are linked together in our model implementation.

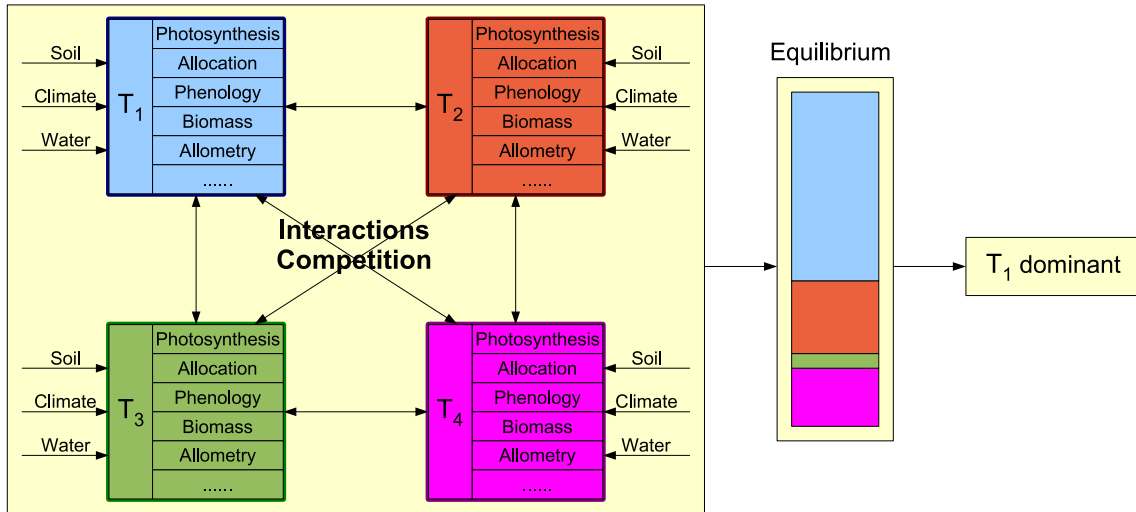


Figure 1: Basic structure of a DGVM. The models define different vegetation types which are characterized by different model parameters and by their response to environmental variables. Depending on inter- and intra-specific competition and interactions, the model converges towards an equilibrium state, characterized by the relative abundance of different vegetation types. Potentially, one of them is dominant and suppresses the others.

2 Modelling concepts

The sections that follow provide detailed descriptions of the sub-models while this section outlines the basic features of the model's structure. The model simulates biophysical, physiological and demographic processes at the leaf, canopy, plant, population and ecosystem level (Figure 2). The model includes several sub-models that represent plant growth and inter- and intra-specific competition for light and moisture. The model also considers how demographic processes and disturbance may influence vegetation development. The model strives to represent these processes in a mechanistic way. However, we wish to emphasize the semantic point that few models are truly mechanistic. For instance, the rates of many processes in the model are temperature dependent and we represent these temperature dependencies using statistically estimated functions.

The model simulates two life forms, grasses and trees. Apart from the fact that we simulate grasses as using the C₄ photosynthetic pathway and trees as using the C₃ pathway, we assume that both are regulated by the same biophysical processes. The rates of the biophysical processes are determined by generally available soil and climate data (Global Soil Data Task Group 2000; New *et al.* 2002).

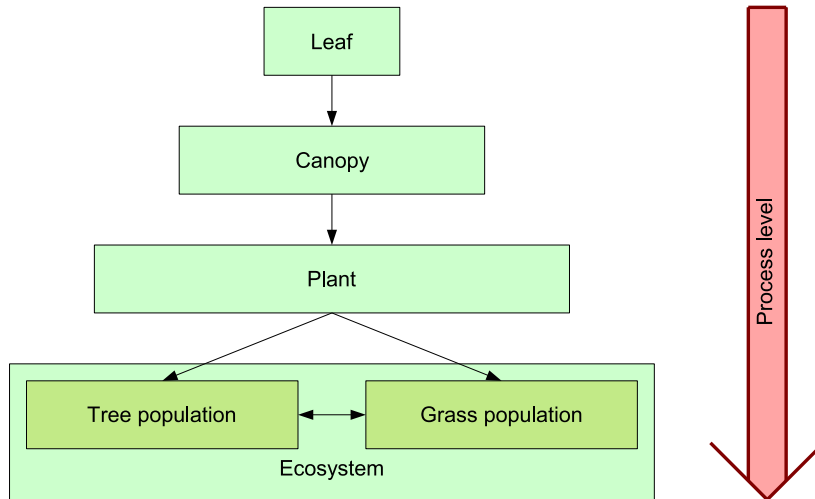


Figure 2: The different process levels of the model.

At the leaf level the model simulates photosynthetic and respiration rates by linking sub-models for photosynthesis and stomatal conductance. For photosynthesis, we follow Collatz *et al.* (1991, 1992)’s implementation of the Farquhar *et al.* (1980) photosynthesis model for C_3 and C_4 plants. We use the stomatal conductance sub-model proposed by Ball *et al.* (1987) and link it to photosynthesis using a diffusion gradient definition of photosynthesis.

The leaf level processes are scaled to the whole plant level. A plant is defined by its different biomass pools and by allometric equations that relate biomass in these pools to height, basal area, canopy area, leaf area index and rooting depth. Using light availability (which is influenced by the leaf area index) and water availability (determined by rooting depth and soil water content) we scale the leaf level photosynthetic rate to the canopy level photosynthetic rate (Schulze *et al.* 1994; Ronda *et al.* 2001; Arora 2002). Photosynthetic carbon gain is reduced by growth respiration, while all living biomass pools are affected by maintenance respiration (Arora 2003). Hence, canopy photosynthesis and respiration together define the net carbon gain of the plant. Carbon gain is allocated to living biomass compartments of the plant, following the allocation concept of Tilman (1988) and Friedlingstein *et al.* (1999), which assumes that the carbon gain is preferentially allocated to the compartment that most limits growth. A plant has two phenological states, active and dormant. We use a simplified version of the phenology models proposed by Lüdeke *et al.* (1994) and Givnish (2002) to simulate the transitions between these two states. Transitions between dormant and active state occur when the potential carbon gain exceeds or falls below the costs of photosynthesis. Plant material is lost due the senescence of leaf and root material.

The next level is the population level. The population structure we consider includes a continuous layer of grass and a more or less discontinuous layer of trees. We do

not simulate different species; we assume that the biomass is adequately described by a “typical” tree and by a “typical” grass species. We simulate a grass population consisting of two super-individuals representing grass below and between tree canopies. For the grass population we ignore population structure and demography and assume that grasses are adequately described by these two immortal super-individuals. In contrast, the tree population is individual-based and we keep track of attributes of each individual tree. For trees, we explicitly simulate reproduction and mortality of each individual. Reproduction is controlled by temperature, soil moisture and the carbon status, while mortality is controlled by the tree’s carbon status. Intra-specific (grass-grass and tree-tree) interactions are influenced by light and water competition. Inter-specific (grass-tree) interactions are mediated by shading effects and competition for water in different soil layers (Walter 1971). Finally, fire shapes both the grass biomass and the tree population and hence inter-specific interactions. We use a semi-empirical fire model proposed by Higgins *et al.* (2008) that estimates the fire intensity as a function of available fuel biomass, moisture content and windspeed and that explicitly simulates the fire damage suffered by individual trees (Higgins *et al.* 2000).

The grass and tree populations are embedded in a sub-model that describes micro-climatic conditions and soil moisture availability. The soil moisture levels are determined by rainfall and evapotranspiration. We simulate stochastic sequences of daily rainfall using the mean and variance of observed rain, following New *et al.* (2002). Evapotranspiration is calculated following Jones (1992) and Allen *et al.* (1998). Radiation is computed using Allen *et al.* (1998)’s guidelines.

The model provides output data from each process levels. Specifically, the model calculates the biomasses of grasses and trees, treecover, number of trees and the size structure of the tree population. The fire sub-model reports the frequency, intensity and timing of fire and data on the effect of fire on the vegetation.

3 Input data

For the model to be flexible enough to simulate vegetation at arbitrary locations, we use only generally available site specific soil and climate data as input data. Soil data were obtained from a global 5×5 minute data set of selected soil characteristics (Global Soil Data Task Group 2000). We used the soil nitrogen S_N , soil carbon S_C , wilting point θ_{wp} and field capacity θ_{fc} from this data set. Climate data were obtained from New *et al.* (2002)’s global 10×10 minute data set of mean monthly surface climate data. We used precipitation (given by the mean value r_m and the coefficient of variance r_{cv}), wet-day frequency w_f , days with frost d_f , mean temperature \bar{T} , diurnal temperature range T_Δ , relative humidity h_s , sunshine percentage p_s , wind speed u_{ref} and elevation Z from this data set (Table 1).

These input data are used to calculate secondary atmospheric characteristics of the study site, needed to calculate radiation, photosynthesis and evapotranspiration. We use Allen *et al.* (1998)'s guidelines to calculate atmospheric pressure P , minimum and maximum temperature T_{min} and T_{max} , day temperature T , average saturation vapor pressure e^A , saturation vapor pressure e^S , slope of the vapor pressure curve s , vapor pressure deficit h_{vpd} , psychrometric constant γ , density of air ρ_{air} , photosynthetic active radiation Q_p and the net radiation Q_0 (Table 1). The rainfall algorithm (New *et al.* 2002) generates a time series of daily rainfall F_i for each year from the parameters r_m and r_{cv} (section “*Total evapotranspiration and soil water balance*”).

Characteristics of the input data from the database and other variables characterizing the environment are summarized in Table 1. Should alternative soil or climate datasets for specific study sites be available, e.g. the IPCC (2007) SRES climate projections, they can be used as an alternative input data source.

4 Leaf photosynthesis

The following sections describe how we estimate the monthly leaf-level photosynthetic and respiration rates of the study site from temperature, relative humidity, atmospheric pressure, wind speed, soil nitrogen, soil carbon and photosynthetic active radiation. We link sub-models for photosynthesis and for stomatal conductance.

4.1 Photosynthesis sub-model

In principle we follow Collatz *et al.* (1991, 1992)'s implementation of the Farquhar *et al.* (1980) model of leaf photosynthesis to generate the (bio-physical) gross and net photosynthetic rates A_0^b and A_n^b (units $\mu\text{mol m}^{-2}\text{s}^{-1}$). An empirical function derived by Woodward *et al.* (1995) from data presented by Woodward and Smith (1994b, a) allows the estimation of the maximum light saturated rate of photosynthesis A_{max} from the soil carbon content S_C (g m^{-2}) and the soil nitrogen content S_N (g m^{-2}) as

$$A_{max} = \begin{cases} 50 \cdot 0.999927^{S_C} & \text{when } S_N > 600 \\ 50 \cdot 0.999927^{S_C} \cdot 0.00166 \cdot S_N & \text{when } S_N < 600. \end{cases} \quad (1)$$

Equation (1) is valid for soil carbon content $S_C \leq 30000 \text{ g m}^{-2}$. We assume that A_{max} for C_4 plants relates to S_N and S_C in the same way as A_{max} for C_3 plants does. However, following Collatz *et al.* (1992) we assume that A_{max} for C_4 photosynthesis is only a fraction $A_R = 0.435$ of A_{max} for C_3 photosynthesis.

The maximum light saturated rate of photosynthesis A_{max} is used to estimate the

maximum carboxylation rate V_{max} ($\mu\text{mol m}^{-2}\text{s}^{-1}$) as

$$V_{max} = 2^{0.1(T-25)} A_{max} A_S \frac{1}{(1 + e^{0.3(13-T)}) (1 + e^{0.3(T-36)})}, \quad (2)$$

where T is the (leaf) temperature (Collatz *et al.* 1992) and A_S is a global scaling factor for both C_3 and C_4 photosynthesis (Collatz *et al.* 1992).

The internal CO_2 partial pressure is defined as c_i . For C_3 plants, c_i is taken to be 70% of its atmospheric partial pressure (Woodward *et al.* 1995). For C_4 plants, c_i represents the bundle sheath value. There is no consensus on how to chose c_i and we estimated c_i to be eight times the atmospheric partial pressure of CO_2 even though in our simulations, photosynthesis is not sensitive to the bundle sheath value as photosynthesis is not CO_2 limited. The CO_2 compensation point is defined as

$$\Gamma_* = \frac{O_i}{2\tau}, \quad (3)$$

where τ describes the partitioning of RuBP to the carboxylase or oxygenase reactions of Rubisco and O_i is the intercellular partial pressure of oxygen (assumed to be 21 kPa). Further, K_c is the Michaelis constant for CO_2 and K_o is the O_2 inhibition constant. We use the function

$$f_{25}(T) = K_{25} Q_{10}^{\frac{T-25}{10}} \quad (4)$$

to describe the response of K_c , K_o and τ to temperature T . Here, K_{25} and Q_{10} are empirically determined parameters specific for K_c , K_o and τ (see Table 2).

The gross rate of photosynthesis A_0 is calculated, following Collatz *et al.* (1991) for C_3 plants and Collatz *et al.* (1992) for C_4 plants, as the minimum of three potentially limiting assimilation rates. The Rubisco limited assimilation rate J_c is defined as

$$J_c = \frac{V_{max}(c_i - \Gamma_*)}{c_i + K_c(1 + O_i/K_o)} \quad (5)$$

$$J_c = V_{max} \quad (6)$$

for C_3 and C_4 respectively. When light is limiting, the efficiency of CO_2 fixation is limited by the quantum yield. The light limited assimilation rate J_e is defined as

$$J_e = a\alpha Q_0 \frac{c_i - \Gamma_*}{c_i + 2\Gamma_*} \quad (7)$$

$$J_e = a\alpha Q_0 \quad (8)$$

for C_3 and C_4 respectively. Here Q_0 is the incident quantum flux density ($\mu\text{mol m}^{-2}\text{s}^{-1}$) that a leaf receives, a is the leaf absorptance and α is the intrinsic quantum yield of

photosynthesis (see Table 2). When light and Rubisco do not limit the assimilation rate, then it is assumed that the capacity for the export of the products of photosynthesis is limiting for C₃ plants. This transport limited assimilation rate J_s is approximated as

$$J_s = \frac{V_{max}}{2}. \quad (9)$$

For C₄ plants, when light and Rubisco are not limiting it is assumed that CO₂ concentrations limit the assimilation rate. This CO₂ limited rate J_p is approximated as

$$J_p = \frac{\kappa C_i}{P} \quad (10)$$

(Woodward and Smith 1994b). The term κ is the empirically defined initial slope of the response of CO₂ to photosynthesis (units $\mu\text{mol m}^{-2} \text{s}^{-1}$) and P is the atmospheric pressure (Pa). In summary, the gross rate of (bio-physical) photosynthesis A_0^b is

$$A_0^b = \min(J_c, J_e, J_s) \quad (11)$$

$$A_0^b = \min(J_c, J_e, J_p) \quad (12)$$

for C₃ plants and for C₄ plants. The net rate of (bio-physical) photosynthesis A_n^b is

$$A_n^b = A_0^b - R_{mLs}, \quad (13)$$

where

$$R_{mLs} = rV_{max} \quad (14)$$

is the single leaf maintenance respiration rate. Here, r is a proportion assumed to be 0.015 for C₃-photosynthesis and 0.025 for C₄-photosynthesis (Collatz *et al.* 1991, 1992) and V_{max} is the maximum carboxylation rate from Equation (2). All parameters and variables for this section are summarized in Table 2.

4.2 Stomatal conductance sub-model

The CO₂ assimilation rate is coupled to stomatal conductance using Ball *et al.* (1987)'s empirical model. The model relates the response of stomatal conductance g_s ($\mu\text{mol m}^{-2}\text{s}^{-1}$) to the net rate of CO₂ uptake A_n :

$$g_s = m \frac{A_n h_s P}{c_s} + b. \quad (15)$$

The terms m and b are empirically derived parameters (see Table 3), h_s is the relative humidity (expressed as unitless ratio), P is the atmospheric pressure (Pa) and c_s is the

partial pressure of CO₂ at the leaf surface, calculated as

$$c_s = c_a - \frac{1.4A_n P}{g_b}. \quad (16)$$

Here, c_a is the atmospheric partial pressure of CO₂ (Pa) and g_b is the leaf boundary layer conductance, estimated as

$$g_b = 0.271 \cdot 10^6 \sqrt{\frac{u(z)}{D_L}}, \quad (17)$$

where, $u(z)$ is the wind speed (ms⁻¹) at height z (m) above the ground and D_L is the characteristic leaf dimension (Jones 1992). We calculate the windspeed $u(z)$ from the reference windspeed u_{ref} (m s⁻¹), measured at height z_{ref} (m) above the ground as

$$u(z) = u_{ref} \frac{\ln(z - z_d) - \ln(z_0)}{\ln(z_{ref} - z_d) - \ln(z_0)}. \quad (18)$$

Here, z_d is the displacement height (m) and z_0 is the roughness length (m) (Jones 1992). Both z_0 and z_d are functions of the aerodynamic properties of the vegetation and following Jones (1992) we simply assume $z_d = 0.86\bar{H}$ and $z_0 = 0.06\bar{H}$. For these purposes we assume mean vegetation height \bar{H} is 1.5m. The reference height z_{ref} is 10 m and the windspeed u_{ref} is read from a database. Variables of this section are summarized in Table 3.

4.3 Linking photosynthesis and stomatal conductance

The leaf photosynthesis and conductance sub-models are interdependent. The photosynthesis model requires estimates of c_i , which is determined by stomatal conductance. The stomatal model, in turn requires estimates of A_n , which also depends on c_i . The system of equations is closed by noting that A_n can also be defined in terms of the CO₂ diffusion gradient

$$A_n^d = \frac{g_s(c_s - c_i)}{1.6P}. \quad (19)$$

When solving for A_n we iteratively seek the value of c_i that satisfies both Equation (19) and the equations

$$A_n^b = \min(J_c, J_e, J_s) - R_{mLs}, \quad (20)$$

$$A_n^b = \min(J_c, J_e, J_p) - R_{mLs}, \quad (21)$$

for C_3 and C_4 plants given by Equations (11) or (12) and (13), hence, we solve the equation

$$c_i^* = \min_{c_i > 0} |A_n^b - A_n^d|. \quad (22)$$

5 Individual plant model

In this section we describe how we model individual plants. Here, we do not differentiate between trees and grasses and we assume that apart from differences in the photosynthetic pathways and plant specific parameters, grasses and tree have the same physiological properties and are influenced by the same biophysical processes.

5.1 Biomass pools of a plant

Each individual consists of eight different biomass pools. The biomass pools are divided into living and dead biomass pools. The living biomass pools are root biomass B_R , stem biomass B_S and leaf biomass B_L . The dead biomass pools are standing dead stem and leaf biomass B_{Ss} and B_{Ls} , stem and leaf litter B_{Sd} and B_{Ld} and dead root biomass B_{Rd} . Figure 3 illustrates the geometry of a plant in its environment and Table 4 provides a summary of the biomass compartments.

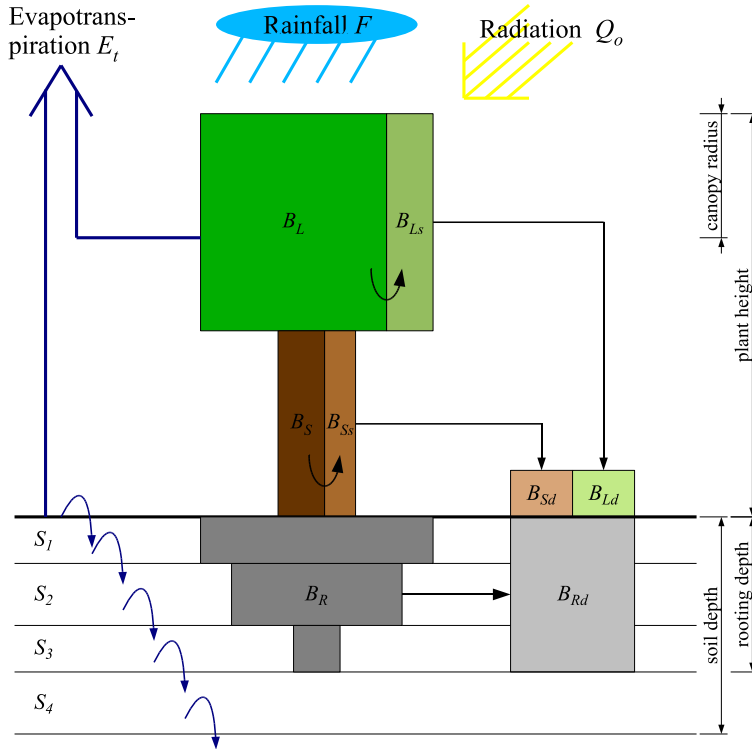


Figure 3: The figure depicts the different biomass pools and allometric properties of a single individual in its environment.

We motivate this biomass partitioning as follows. The living biomass pools differ in their functions. Leaf biomass is responsible for photosynthesis and carbon gain, root biomass is responsible for water and nutrient uptake, stem biomass creates the infrastructure needed for leaves to capture light effectively. Roots and stems store resources of the plant, especially for re-allocation of leaf biomass after dormancy or after fire (Wolfson 1999; Higgins *et al.* 2000; Hoffmann and Solbrig 2003) and act to buffer the plant against disturbance. The splitting of biomass also allows the simulation of how competition for water and light, herbivory or fire can influence the plant (Scheiter and Higgins 2007). The differentiation of dead biomass pools is important for light competition, fire and for the carbon accounting of the ecosystem.

5.2 Plant allometry

Stem biomass B_S and leaf biomass B_L (kg/plant for trees and kg/m² for grasses) are translated into height H (m) using the relationships

$$H = H_1 \cdot (B_S + B_L)^{H_2} \quad (23)$$

$$H = H_1 \cdot B_L^{H_2} \quad (24)$$

for trees (Equation 23) and grasses (Equation 24). The parameters H_1 and H_2 for trees (Equation 23) were taken from Higgins *et al.* (2007) and the parameters for grasses (Equation 24) were taken from Arora and Boer (2005). For trees, we follow Higgins *et al.* (2007) to calculate the stem diameter d_s (cm) from height H (m) as

$$d_s = \frac{d_{s1}}{d_{s2}} H. \quad (25)$$

The canopy area of a plant is given by

$$C = \pi(H\gamma_c)^2, \quad (26)$$

where γ_c is the ratio of stem height to canopy radius. We estimated $\gamma_c = 0.37$ for trees and $\gamma_c = 0.4$ for grasses. The leaf area index L is defined as

$$L = \frac{B_L A_{SL}}{C}. \quad (27)$$

Here, A_{SL} is the specific leaf area and we use $A_{SL}=10.9$ m² kg⁻¹ for grass and $A_{SL}=10$ m² kg⁻¹ for trees (Scholes and Walker 1993). The rooting depth D_{root} is assumed to be defined by the biomass needed to construct a narrow cylinder with radius r_r (0.5cm for

grasses and 1.5cm for trees) and assuming the density of root biomass is $\rho_r = 10^2 \text{ kg m}^{-3}$,

$$D_{cyl} = \frac{B_R}{\rho_r r_r^2 \pi}. \quad (28)$$

Rooting depth is limited by the maximum rooting depth of the plant D_{mrd} and by the soil depth D_{soil} , hence

$$D_{root} = \min(D_{mrd}, D_{soil}, D_{cyl}). \quad (29)$$

Variables and constants of this section are listed in Table 5.

5.3 Canopy photosynthesis and stomatal conductance

To estimate the whole plant's carbon gain, the leaf level estimates of A_0 and g_s generated in section 4 (“*Leaf photosynthesis*”) need to be scaled up to the canopy scale. We assume that the quantum flux density Q in the canopy exponentially decays with leaf layer l following Beer's law (Jones 1992)

$$Q(l) = Q_0 e^{-kl}. \quad (30)$$

Here, Q_0 is the quantum flux density incident on the canopy and k is the canopy extinction coefficient ($k = 0.5$). Hence, the light received by an unshaded plant (Q_{sum}) is given by the integral

$$Q_{sum} = Q_0 \int_0^L e^{-kl} dl, \quad (31)$$

where L is the leaf area index of the canopy, Equation (27). We follow Sellers *et al.* (1992) in assuming that light is the primary determinant of how photosynthesis scales through the canopy. This assumption implies that light limited canopy photosynthesis A_c can be defined as

$$A_c = A_0 Q_i \int_0^L e^{-kl} dl. \quad (32)$$

Here, Q_i is an additional factor that describes the potential light availability of the plant. For a single unshaded plant, Q_i is equal to one, however, in presence of other competitor plants, Q_i can be less than one, as the light environment of the target plant might be modified by competitor plants (see section 6.2, “*Light competition*”).

Canopy photosynthesis and stomatal conductance are limited by the soil moisture content (Schulze *et al.* 1994). To simulate this effect, we first define a soil moisture index $G(\theta_i)$ for each soil layer i as

$$G(\theta_i) = 2\beta(\theta_i) - \beta^2(\theta_i), \quad (33)$$

where

$$\beta(\theta_i) = \max \left(0, \min \left(1, \frac{\theta_i - \theta_{wp}}{\theta_{fc} - \theta_{wp}} \right) \right). \quad (34)$$

Here, θ_i is the soil moisture content of soil layer i and θ_{wp} and θ_{fc} are wilting point and field capacity (Ronda *et al.* 2001). We assume that water availability G_w of a plant is given as the weighted mean value of the soil moisture indexes $G(\theta_i)$ of all soil layers where the plant has roots,

$$G_w = \frac{1}{D_{root}} \sum_i d_i G(\theta_i), \quad (35)$$

Here, d_i is the thickness of soil layer i . The light and water limited rate of canopy photosynthesis A_{cs} is then defined as

$$A_{cs} = A_0 Q_i G_w \int_0^L e^{-kl} dl. \quad (36)$$

Canopy stomatal conductance g_s^c is calculated using the Ball-Berry equation (Ball *et al.* 1987)

$$g_s^c = m \frac{(A_{cs} - R_{mL}) h_s P}{c_s^c} + b, \quad (37)$$

where b , m and h_s are defined as in Equation (15) and Table 3. The partial pressure of CO₂ of the canopy is given as

$$c_s^c = c_a - \frac{1.4 A_{cs} P}{g_b^c} \quad (38)$$

as in Equation (16) except that the canopy boundary layer conductance g_b^c (m s⁻¹) is used,

$$g_b^c = \frac{u_{ref} K^2}{\ln^2 \left(\frac{z_{ref} - z_d}{z_0} \right)}. \quad (39)$$

Here, K is the von Karman constant ($K = 0.41$) while u_{ref} , z_{ref} , z_d and z_0 are defined as in Equation (18). To compute z_0 and z_d we use the plant height H . The canopy maintenance respiration R_{mL} in Equation (37) is defined as

$$R_{mL} = r A_{cs}, \quad (40)$$

where r is a constant defined in Equation (14) and Table 2. Maintenance respiration is determined by canopy light extinction and it is also influenced by soil moisture conditions, since there is evidence that maintenance respiration rates are closely related to carbon assimilation rates (Thornley and Cannell 2000). See Table 6 for a summary

of variables and constants used in this section.

5.4 Respiration sub-model

Respiration is poorly understood and there is no consensus on how it should be modeled (Thornley and Cannell 2000). We distinguish between growth respiration R_g and maintenance respiration R_m . Growth respiration R_g , which we define as the cost of producing new tissue, is calculated as

$$R_g = \sigma A_{cs} \mathcal{C}, \quad (41)$$

where σ is a constant proportion, assumed to be 0.35 (Arora 2003), and \mathcal{C} is the canopy area of the plant as defined in Equation (26). The leaf level photosynthetic rate A_{cs} and the leaf level respiration rate R_{mL} are transformed from $\mu\text{mol m}^{-2}\text{s}^{-1}$ to kg/day/plant by multiplication of leaf level rates with $44e^{-9} \cdot (12/44) \cdot 3600 \cdot p_s \cdot 24$, where p_s is the percentage of sunshine per day.

Maintenance respiration R_m is the cost of keeping live tissue functional and is estimated as the sum of leaf respiration R_{mL} , stem respiration R_{mS} and root respiration R_{mR} , hence, $R_m = R_{mL} + R_{mS} + R_{mR}$. We assume that the total leaf biomass is alive and canopy maintenance respiration is given by $R_{mL} = r A_{cs}$, as defined in Equation (40). For stem biomass we assume that a fraction β_S is living sapwood and subjected to maintenance respiration. The remaining biomass is dead heartwood, that does not respire. We assume that roots consist of fine roots, sapwood and heartwood. Fine roots are most active and hence, are the most important source of respiration. Since we know little about fine root dynamics, we simply assume that fine root respiration can be estimated as a function of leaf respiration (Thornley and Cannell 2000). More specifically, we assume that fine root respiration is equal to leaf maintenance respiration R_{mL} . From the root biomass which is not in fine roots, a fraction β_R is sapwood and subjected to maintenance respiration. The remaining root biomass is heartwood and not subjected to respiration. The parameters β_S and β_R effectively scale the total respiration $R_m + R_g$ and hence, the ratio between respiration and photosynthesis (carbon use efficiency). Empirical estimates suggest that carbon use efficiency in tropical vegetation lies between 0.35 and 0.6 (Scholes and Walker 1993; Thornley and Cannell 2000; DeLucia *et al.* 2007).

Stem and root maintenance respiration R_{mS} and R_{mR} (kg d^{-1}) are calculated as a function of the carbon content and carbon to nitrogen ratios of roots or stem (Arora 2003):

$$R_{mS} = \beta_N \frac{\beta_R B_S}{v_S} f(T) \quad (42)$$

$$R_{mR} = \beta_N \frac{\beta_S (B_R - B_L)}{v_R} f(T) + R_{mL}. \quad (43)$$

Here, β_N is a constant respiration rate, B_L , B_S and B_R are the leaf, stem and root biomasses (kg) and v_S and v_R are the C:N ratios of the stems and roots (see Table 7). The function

$$f(T) = (3.22 - 0.046T)^{\frac{T-20}{10}} \quad (44)$$

allows us to simulate that respiration rates depend on temperature (Tjoelker *et al.* 2001). Table 7 summarizes parameters and variables of this section.

5.5 Carbon balance and allocation

The difference between canopy photosynthesis and respiration rates from the above sections defines the net carbon gain C_Δ (kg per day) of the plant,

$$C_\Delta = A_{cs}C - R_g. \quad (45)$$

Vegetation models differ greatly in how they simulate carbon allocation to living biomass pools, probably because no allocation sub-model provides a generally applicable abstraction of this complex process. We follow the allocation concepts of Tilman (1988) and Friedlingstein *et al.* (1999). The allocation model assumes that the greatest part of the carbon gain is directed to the compartment that most limits growth. That is, if light is limiting growth, then allocation is directed towards stems. If water is limiting, allocation is directed towards roots. When photosynthesis is limiting after the plant has moved from the dormant to the active state or after a fire, then allocation is directed to leaf biomass. The realized proportions of carbon gain directed to roots, shoots and leaves a_R , a_S and a_L are given as

$$a_R = \frac{1 + a_{0R} - G_w}{3 + a_{0R} + a_{0S} - Q_i - G_w - C_i}, \quad (46)$$

$$a_S = \frac{1 + a_{0S} - Q_i}{3 + a_{0R} + a_{0S} - Q_i - G_w - C_i}, \quad (47)$$

$$a_L = \frac{1 - C_i}{3 + a_{0R} + a_{0S} - Q_i - G_w - C_i}. \quad (48)$$

The parameters a_{0R} , a_{0S} and a_{0L} describe the proportional allocation to roots, shoots and leaves when resources are not limiting, G_w and Q_i describe water and light availability (Equations 32 and 35) and

$$C_i = \frac{B_L}{a_{0L}(B_R + B_S + B_L)} \quad (49)$$

describes the deviance of leaf biomass from the fraction of leaf biomass in the non-limiting case, a_{0L} . Figure 4 depicts how the allocation model behaves in different situations and Table 8 summarizes the variables and parameters used in this section.

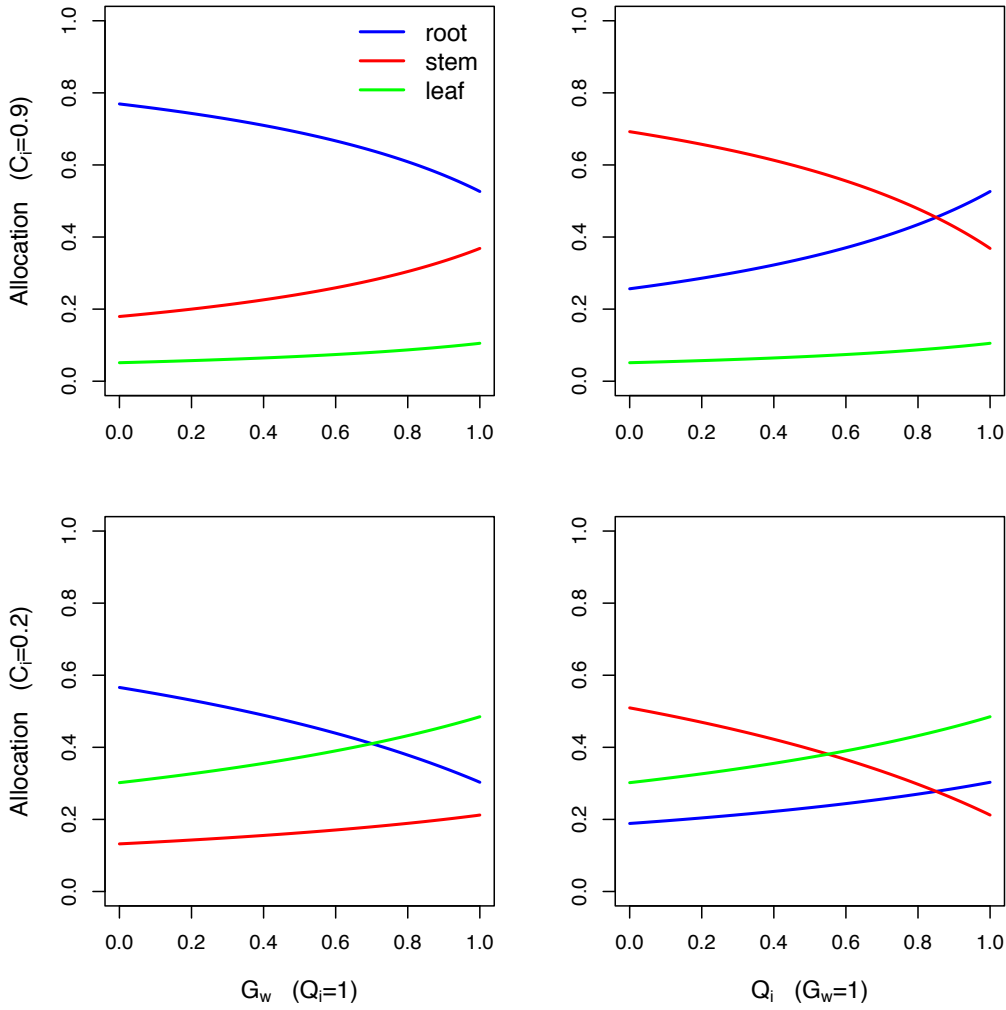


Figure 4: The panels depict how the plant's carbon gain C_{Δ} is allocated to different plant compartments, when light is highly available ($Q_i = 1$, left column) or when water is highly available ($G_w = 1$, right column) in response to light or water availability (variable G_w or Q_i). Further, the panels depict differences in allocation when leaf biomass is high ($C_i = 0.9$) or when leaf biomass is low ($C_i = 0.2$).

5.6 Leaf phenology

As it is the case for respiration and allocation, ignorance of the underlying processes means that there is no consensus on how leaf phenology (hereafter simply referred to as phenology) should be modeled. In existing DGVMs it is typically assumed that phenology is controlled by temperature or soil moisture (Cramer *et al.* 2001). However, phenology has a large impact on the global carbon cycle as the growing season length is a major determinant of a plant's water uptake and carbon gain (Jolly and Running 2004). We use a simplified version of Lüdeke *et al.* (1994)'s and Givnish (2002)'s phenological model. The phenology model is resource based which means that the model allows the simulation of transitions between a dormant and an active state in response to resource availability and environmental conditions. The model assumes that switches between dormant and active states are determined by photosynthetic carbon gain and the respirative costs of carbon gain. These costs and benefits are indexed as

$$A_{index} = A_0 (G_i + T_i) - R_{mL}. \quad (50)$$

The benefits are a function of A_0 and the costs are a function of leaf level maintenance respiration R_{mL} . A soil moisture index defined as

$$G_i = \frac{2}{3}\theta_4 + \frac{1}{3}G_w \quad (51)$$

is used to weight A_0 . Here, θ_4 is the water content of the fourth soil layer (20cm to 30cm) and G_w is the average water available to plants, defined by the water content of all soil layers in which the plant has roots (Equation 35). By using this definition of G_i we can assume that the phenology is primarily determined by water and that single precipitation events, which strongly influence the water content of the upper soil layer, are less likely to influence phenology than deeper soil layers (Jolly and Running 2004). Additionally, the index G_i allows plants with different rooting depth to respond differently to soil moisture availability. Plants with shallow roots use only water in the highly variable upper soil layers, and sensitivity analyses (not shown) indicate that the dynamics of the upper soil layers are best represented by the fourth soil layer (20cm to 30cm). Plants with deep roots have access to the less dynamic deeper soil layers, which are adequately described by the mean soil water content G_w . It should be noted that the definition of G_i is dependent on the number and depth of soil layers included and would require a re-calibration should the number of soil layers be changed.

Phenology is also controlled by temperature as photosynthesis A_0 and respiration R_{mL} respond to temperature. Further, T_i is a temperature index, defined as $T_i = 0$

when the minimum monthly temperature T_{min} is above a threshold T_* and as

$$T_i = 2.5 \left(\frac{T_{min}}{T_*} - 1 \right) \quad (52)$$

when T_{min} is below T_* (Table 9). In tropical regions, phenology is generally not influenced by temperature, however, at high altitudes T_i might play a role.

The A_{index} controls leaf phenology by determining when a plant shifts the phenological state. When A_{index} becomes negative a plant moves from the growing phase into a standby phase. After d_{neg} successive days of negative A_{index} , the plant moves into a phase of leaf abscission and dormancy. A return to the growing phase occurs after d_{pos} successive days of positive A_{index} . Both the transition from the growing phase to the dormancy phase and the transition from the dormancy phase to the growing phase take place instantaneously but they affect the biomass pools in different ways. While moving from the growing phase to the dormant phase, photosynthesis is not possible and only a proportion ζ_L of leaf biomass remains alive. The rest accumulates in the dead biomass pools (Table 9 defines the constants). When a plant turns from the dormant into the growing phase, photosynthesis is possible again, allowing carbon gain (see Figure 5). We assume that the phenological sequence is influenced by frost. On days with frost, the counter d_{neg} is advanced by one which means that given the same distribution of G_i , the plants at sites with frost have a shorter growing season length.

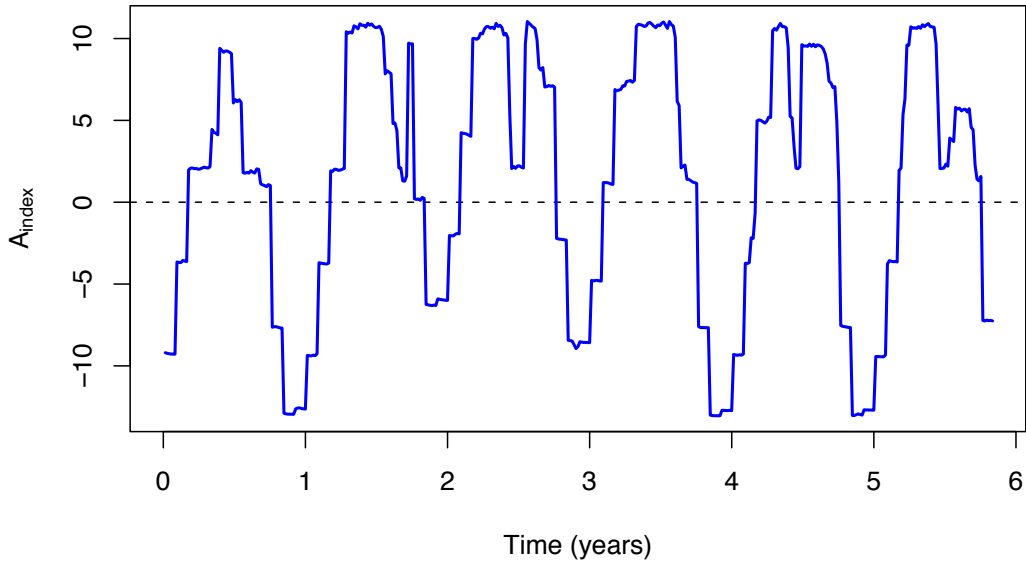


Figure 5: The cost-benefit index of photosynthesis, A_{index} , defines the phenological state of the plant: the plant moves to the active state after d_{pos} successive days of positive A_{index} and it moves to the dormant state after d_{deg} successive days of negative A_{index} .

5.7 Biomass turnover and decomposition

The living plant compartments (leaf, stem and root biomass) are affected by turnover, that is the continuous death of living biomass. The turnover rates are determined by longevities ω_L , ω_S and ω_R of leaf, stem and root biomass. The biomass removed by turnover accumulates in the standing dead biomass compartments.

Dead biomass is continuously influenced by the transition from standing to lying dead biomass and by decomposition. During the transition, proportions ξ_L and ξ_S of standing dead leaf and stem biomass permanently turn into litter and accumulate to the lying dead biomass compartments. Decomposition removes a fraction defined by the longevity ω_D of dead material. The decomposed biomass is lost for the system. The turnover and decomposition parameters we used (Table 10) are taken from Scholes and Walker (1993) and Gill and Jackson (2000). Figure 6 summarizes the biomass accounting of plants.

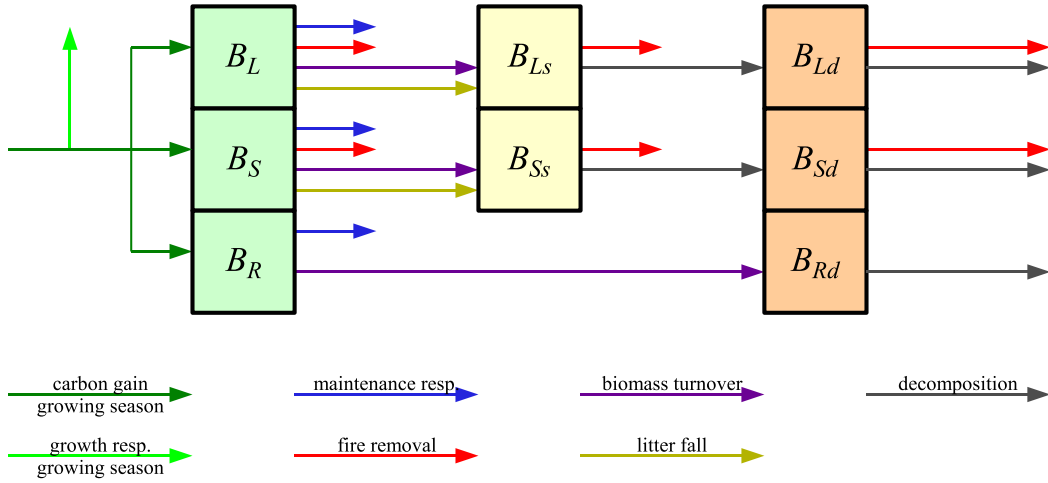


Figure 6: The diagram depicts the biomass pools of a plant and the processes that modify biomass: carbon gain, respiration, decomposition, turnover, litter fall and fire.

5.8 Evapotranspiration

The plant's evapotranspiration is calculated using the Penman-Monteith equation (Jones 1992; Allen *et al.* 1998),

$$E_t^p = \frac{sQ_0 + 86400\rho_{air}c_p h_{vpd}g_b^c}{\lambda \left(s + \gamma \left(1 + \frac{g_b^c}{g_s^c} \right) \right)}. \quad (53)$$

Here s is the slope of vapor pressure curve, Q_0 is the net radiation, ρ_{air} is the density of air, c_p is the specific heat of moist air, h_{vpd} is the saturation vapor pressure deficit, g_b^c is the canopy boundary layer conductance from Equation (39), λ is the latent heat of air, γ is the psychrometric constant and g_s^c is the canopy stomatal conductance from Equation (37). We use Allen *et al.* (1998)'s detailed guide to the computation of the components of E_t^p .

6 Stand scale dynamics

The stand structure we consider follows the definition of a savanna, that is a continuous layer of grasses and a discontinuous layer of trees (Huntley and Walker 1982; Scholes and Walker 1993). The tree population is described using an individual-based structure that allows us to simulate reproduction, establishment and mortality of single trees. The population structure of the grass layer is ignored and we consider only biomass of two super-individuals (Scheffer *et al.* 1995) representing grass under and grass between the canopies of trees. Hence, we assume that the grass layer is adequately described by biomass and that vegetative reproduction buffers the biomass dynamics from demographic events.

Variables describing the tree population are the number of trees n_t , the size S of the study site and the proportional tree cover Υ , defined as the sum of the canopy areas of all trees taller than half a meter without competitor, divided by the size of the study site, S (Table 11).

6.1 Total evapotranspiration and soil water balance

Vegetation and soil characteristics, are used to calculate the total evapotranspiration rate E_t ($\text{m s}^{-1} \text{m}^{-2}$) of the system. Total evapotranspiration is given as the sum of soil evaporation E_t^s , grass evapotranspiration E_t^g and tree evapotranspiration E_t^t . Soil evaporation is given as

$$E_t^s = \frac{0.0864}{2.45} \frac{1}{g_b^s} \exp(-4.28 + 11.97 \min(0.35, \theta_1)) h_{vpd}, \quad (54)$$

where g_b^c is the boundary layer conductance of the soil (Equation 39) and θ_1 is the water content of the upper soil layer. Grass evapotranspiration E_t^g is defined as the weighted mean value of evapotranspiration rates of grass between and grass under the canopies of trees, calculated with Equation (53). Tree evapotranspiration E_t^t is given as the mean

value of evapotranspiration of all trees,

$$E_t^t = \frac{1}{S} \sum_{i=1}^{n_t} E_i^p. \quad (55)$$

The rainfall algorithm (New *et al.* 2002) generates a time series of daily rainfall F_i for each year of the simulation. It assumes that monthly rainfall is a gamma-distributed random variable and that the mean rainfall event size is monthly rainfall r_m divided by the mean number of rain days per month w_f . Monthly parameters for the gamma distribution and for rainy days per month are provided by New *et al.* (2002). We assume that daily rainfall is an exponentially distributed random number with mean equalling the mean event size.

Rainfall and evapotranspiration are used to drive a multi-layer, tipping bucket model of soil moisture content. All soil layers are assumed to have the same wilting point θ_{wp} and field capacity θ_{fc} , while they may differ in thickness d_i (Table 12). Rainfall is tipped from one layer into a lower layer when the soil moisture content of a soil layer exceeds its field capacity θ_{fc} . Evapotranspiration causes moisture to move from deeper soil layers to higher soil layers and finally from the top-soil into the atmosphere. Upper soil layers are assumed to dry out first, and we assume that a soil layer cannot be dried beyond its wilting point θ_{wp} .

6.2 Light competition

The light competition algorithm estimates the relative light availability Q_i (Equation 32) of a single grass or tree individual (which we call the target plant and index with “ t ”), depending on its neighbor plants (competitors, indexed with “ c ”). Light competition occurs within and between the grass and the tree populations. Unshaded plants receive the incident photosynthetically active radiation ($Q_i = 1$). If a plant is shaded by a competitor (either another tree or grass) then light availability Q_i and as consequence the photosynthetic rate A_{cs} are reduced. Light competition is often described by using a linear function of competitor abundance (Bond *et al.* 1995; Case 2000). We follow this approach and simply assume that light availability of the target plant is reduced as a linear function of the competitor height. The light competition model is only a coarse approximation of the real situation, as we assume that a tree has either no competitor tree or exactly one competitor tree. Of course, this is an oversimplification of the reality, but light models that consider shading effects of several trees in a three-dimensional environment (e.g. Chave 1999; Shabanov *et al.* 2000) are computationally expensive.

The light environment of trees is influenced by grasses and by a competitor tree. Whether a tree has a competitor tree or not is assigned at the beginning of a tree’s life

by randomly assigning a neighbor contingent on the treecover and the number of trees. More explicitly, a tree has a competitor with probability $e_1 - e_2 \Upsilon - n_t / e_3$. This ensures, that in sparse populations, most of the trees do not have a competitor while in a dense tree population, there is a high probability that trees have a competitor. Should a tree have a competitor, the identity of the competitor is randomly drawn from the current tree population.

Whether the light availability of the target tree is influenced by the competitor tree or not depends on the tree heights of the target tree, H_t , and its competitor tree, H_c . If the target tree is taller than the competitor, then the target tree has full light availability and $Q_i = 1$. When the target tree is smaller than the competitor, then Q_i is scaled by the linear function

$$Q_{comp} = \mu_c \frac{H_t}{H_c} + (1 - \mu_c) \quad (H_t < H_c) \quad (56)$$

where μ_c is a parameter that measures the maximum influence of the competitor on the light environment of the target tree. Analogously, we use a factor

$$Q_{grass} = \mu_g \frac{H_t}{H_g} + (1 - \mu_g) \quad (H_t < H_g) \quad (57)$$

to simulate the influence of the grasses on trees (this only applies when $H_t < H_g$, i.e. in the tree seedling phase). Here, μ_g measures the maximum influence of grasses on trees and H_g is the height of grass between tree canopies. For grass on tree competition, we use grass between tree canopies as the competitor. The light availability of trees is then given by

$$Q_i = Q_{comp} Q_{grass}. \quad (58)$$

The light environment of grasses is assumed to be influenced by two factors: by the shading effects of trees (only for sub-canopy grass) and by shading of dead grass biomass. The shading effect of trees is given by

$$Q_{tree} = \mu_t \frac{H_g}{H_t} + (1 - \mu_t) \quad (H_g < H_t) \quad (59)$$

and the shading effect of dead biomass is

$$Q_{dead} = \mu_d \frac{B_L}{B_{Ls}} + (1 - \mu_d) \quad (B_L < B_{Ls}). \quad (60)$$

Here, μ_t and μ_d measure the maximum influence of trees and dead grass biomass on the light environment of grasses, H_t and H_g are the mean tree height and the grass height and B_L and B_{Ls} are live and standing dead grass leaf biomasses. The light availability

of grasses is given by

$$Q_i = Q_{tree} Q_{dead}. \quad (61)$$

Table 13 defines the constants of this section.

6.3 Tree population dynamics

The sections 5 (“*Individual plant model*”) and 6.2 (“*Light competition*”) described the processes that influence the growth of single individuals. In this section we discuss birth and death processes that change the size n_t of the tree population (Table 14 summarizes the constants).

6.3.1 Reproduction and seed bank model

To simulate seed production and germination, we simulate a seed bank. The seed bank accumulates the seed production of all trees. The number of seeds produced by each tree depends on environmental conditions as well as on the plants carbon balance. We assume that to be able to produce seeds, a tree must have a positive carbon balance C_Δ and it must be adult, which means older than A_a years (we assume $A_a = 10$ years). Then, the number of seeds produced by a tree is given by

$$\phi_i = \left\lfloor \frac{C_\Delta}{B_{seed}} \right\rfloor. \quad (62)$$

Here, $B_{seed} = 1\text{g}$ (Hovestadt *et al.* 1999) is the seed weight and C_Δ is the carbon gain (Equation 45). Equation (62) implies, that trees with low net carbon gain only produce few seed while adult trees with high carbon gain produce many seeds. To mimic the fact that seed production is variable and linked to environmental conditions, we assume that C_Δ in Equation (62) is the total carbon gain on the first day of the month with the highest potential photosynthetic rate A_0 . The total number Φ of seeds in the seed bank is given by summing over the seed production ϕ_i of all trees. Hence, no dispersal process is simulated. Trial simulations suggest that the seed production rate does not limit reproduction and population growth in this model. Seeds are assumed to have short survival times, specifically we assume that the annual mortality rate ϕ_{mort} of seeds is 70% (Higgins *et al.* 2000).

Seeds cannot germinate until the next wet season, thus the seed bank buffers the population dynamics. We assume, that seeds can germinate when the counter of wet days d_{wet} reaches 3 days. Here, a wet day is defined as a day without frost where the soil moisture of the upper soil layer θ_1 reaches the field capacity θ_{fc} . When the soil moisture of the upper soil layer does not reach the field capacity then the counter d_{wet} is reduced by one. On each day fulfilling the condition $d_{wet} = 3$, a proportion ϕ_{sprout} of the seeds Φ are available for germination but the germination probability of these

seeds is only ϕ_{germ} . This mechanism prevents all seeds from germinating at once and introduces a stochastic element to the timing and number of germinations.

6.3.2 Death process

Grasses are assumed to be immortal. We consider three additive factors that determine the probability that a tree dies. (1) When a tree is in the active state and the carbon balance of a tree is negative ($C_{\Delta} < 0$), then the death probability is increased by P_{carb} . (2) When a tree has a competitor tree then the death probability is increased by P_{comp} . (3) On days with frost, the probability for tree mortality is increased by P_{frost} . Each day, the probabilities of the three mortality processes are used to determine the total mortality probability P_{death} of the tree. When a uniformly distributed random number between zero and one is less than P_{death} , then the tree is deleted from the population and the biomass is added to the dead biomass pools.

6.4 Grass fires and tree topkill

Grass fires are a characteristic feature of savannas. Fires remove grass biomass and also induce topkill (stem mortality) in trees. The potential fire intensity I ($\text{kJ s}^{-1}\text{m}^{-1}$) is predicted using Higgins *et al.* (2008)'s semi-empirical model of grass fire intensity,

$$I(B_F, \theta_F) = hB_F \frac{\arctan(u_{ref})cf(B_F, a_w)}{Q_m\theta_F + Q_v(1 - \theta_F)}. \quad (63)$$

Here, B_F is the average fuel biomass (kg m^{-2}), θ_F is the fuel moisture, Q_m and Q_v are heats of preignition of moisture and fuel, c is regression parameter, u_{ref} is the wind speed (m s^{-1}) and h is the heat yield of fuel consumed (typically 16890 kJ kg^{-1}). Further,

$$f(B_F, a_w) = \frac{B_F}{B_F + a_w} \quad (64)$$

is a sigmoidal function of fuel biomass and a_w is a regression parameter estimated from data on fire behavior. To estimate the fuel biomass B_F and the moisture content θ_F , we divide the biomass into live biomass B_{live} which is moist and dead biomass B_{dead} which is dry. Live fuel biomass B_{live} is given by the grass leaf biomass B_L^g and by one half of the grass standing dead biomass B_{Ls}^g ,

$$B_{live} = B_L^g + \frac{1}{2}B_{Ls}^g. \quad (65)$$

Live tree biomass does not contribute to B_{live} . Dead fuel biomass B_{dead} is given by the leaf litter of all trees, B_{Ld}^t , as well as by grass lying dead biomass B_{Ld}^g and one half of

the grass standing dead biomass B_{Ls}^g ,

$$B_{dead} = B_{Ld}^g + \frac{1}{2}B_{Ls}^g + B_{Ld}^t. \quad (66)$$

The moisture content of live fuel is assumed to equal the air humidity h_s that is, $\theta_{live} = h_s$. For dead biomass the moisture content quickly decreases by an exponential function (Cheney and Sullivan 1997)

$$\theta_{dead} = h_s \cdot \theta_r^T, \quad (67)$$

where θ_r ($=0.95$) describes how fast biomass dries out and T is the number of days since litter fall, that is the last transition from the active to the dormant state. Total fuel biomass is given as

$$B_F = B_{live} + B_{dead} \quad (68)$$

and fuel moisture is given as the mean value

$$\theta_F = \frac{B_{live}\theta_{live} + B_{dead}\theta_{dead}}{B_{live} + B_{dead}}. \quad (69)$$

For a fire to spread, two conditions must be fulfilled; first, an ignition must take place and second, the potential fire intensity I must exceed a minimum intensity of $300 \text{ kJ s}^{-1}\text{m}^{-1}$ (van Wilgen and Scholes 1997). An annual stochastic ignition sequence is generated in the beginning of each year. The number of ignitions is limited by the random variable $i_1\Upsilon - i_2$ which imitates that fuel biomass in tree stands with high canopy cover is shaded and dries out slower. The probability that a fire spreads in case of an ignition event and an appropriate fire intensity is $p_{fire} = 1.5\%$.

Fire consumes the total grass and tree litter as well as all standing dead grass biomass. Fire removes most of the live aboveground grass biomass compartments B_S^g and B_L^g ,

$$B_S^{g'} = \psi_g B_S^g \quad (70)$$

$$B_L^{g'} = \psi_g B_L^g. \quad (71)$$

Here ψ_g is the proportion of grass biomass that survives a fire. Fire might induce topkill of trees. Following Higgins *et al.* (2000) the probability of topkill is an empirically derived function of fire intensity I and tree height H (Figure 7),

$$P_{topkill}(H, I) = \frac{\exp(D_1 - D_2 \ln(H) + D_3 \sqrt{I})}{1 + \exp(D_1 - D_2 \ln(H) + D_3 \sqrt{I})}. \quad (72)$$

A tree is subjected to topkill when a uniformly distributed random number between zero and one is less than the tree's topkill probability $P_{topkill}(H, I)$. Topkilled trees retain only a proportions ψ_{ts} and ψ_{tl} of their stem and leaf biomass:

$$B_S^{t'} = \psi_{ts} B_S^t, \quad (73)$$

$$B_L^{t'} = \psi_{tl} B_L^t. \quad (74)$$

Topkilled tree stems usually resprout from rootstocks (Hoffmann and Solbrig 2003). For savanna trees the probability of resprouting is high (Higgins *et al.* 2000). Fire mostly affects the trees in the juvenile state and prevents them from reaching the adult state. Adults are unaffected by fire, because they are, according to Equation (72) too large to be topkilled. Table 15 provides a summary of the parameters and variables of the fire model.

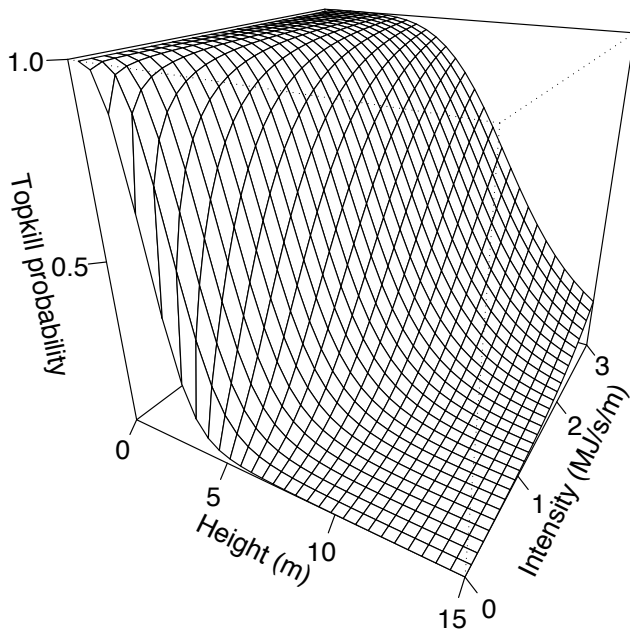


Figure 7: The figure depicts the topkill probability of a single tree as a function of tree height and fire intensity. Small trees have a high topkill probability while tall trees might only be topkilled by intense fires.

7 Synthesis of sub-models

Figure 8 depicts a flow diagram for the model. First, environmental data of the defined study site are read from data bases and site characteristics, such as radiation, potential leaf level photosynthesis and respiration are calculated. Further, the grass and tree populations are initialized. At the beginning of each simulation year, we generate a stochastic rain sequence and a stochastic fire ignition sequence for the year. For each

day in the year, we first calculate the net radiation. Then we run the death process for trees and eventually remove dead trees. Then, we calculate the components of evapotranspiration (trees, grasses and soil) and update the soil water content of the different layers using precipitation and evapotranspiration. The next step is to run the grass and tree physiology. We first calculate the carbon balance and the potential carbon gain using light and water availability. The carbon balance defines whether the plant is in the active or in the dormant state. In the active state, carbon gain is allocated to the live plant compartments using the allocation sub-model. Finally, we remove biomass by decomposition, respiration and turnover. For trees, we run the reproduction process, that is, we determine the seed production and eventually add individuals into the tree population, when environmental conditions allow germination. At the end of each simulation day, we check if a fire spreads and if yes, we remove aboveground grass biomass and, in the case of topkill, aboveground biomass of selected trees. Finally, the model writes the desired output data to a file.

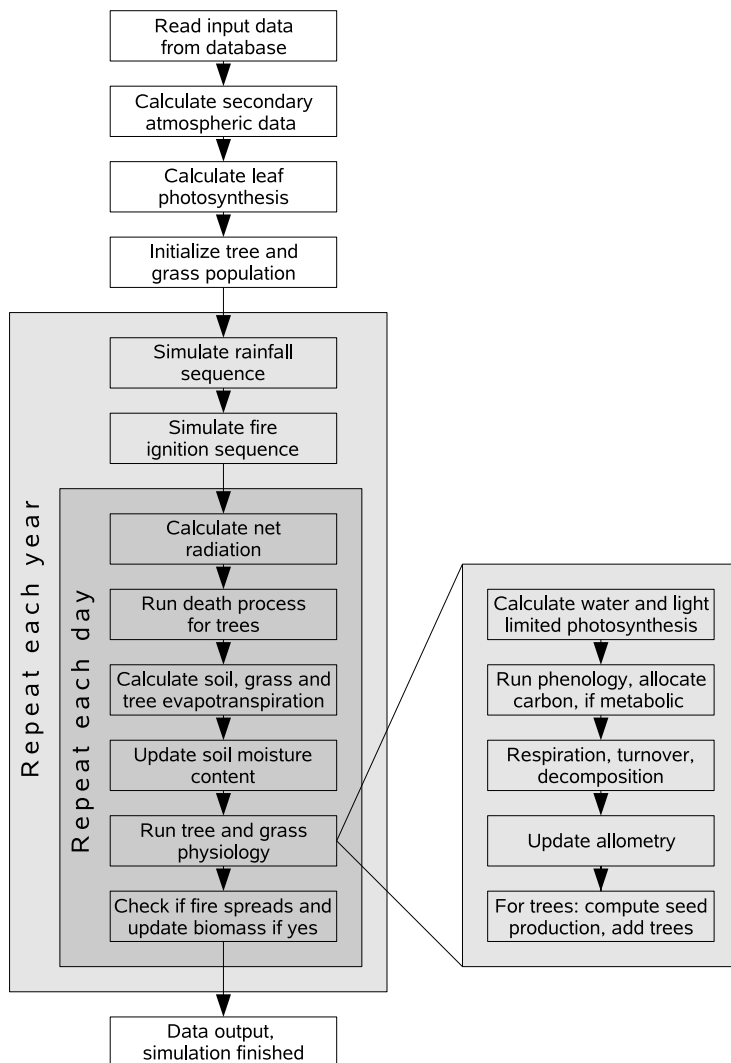


Figure 8: The figure depicts a flow diagram of the different components used in the model.

8 Programming

This model is implemented in C++ and has been compiled on the Linux operating system using both the GNU-compiler and the Intel compilers. Simulations were conducted on the Linux cluster provided by the Leibnitz-Rechenzentrum in Munich (www.lrz-muenchen.de).

9 Model parameters

Table 1: Input data from databases and secondary environmental variables. In Tables 1-15 the notation “prop” indicates a value between zero and one and “variable” indicates that this parameter is a modelled variable.

Name	Description	Value	Units
T_{Δ}	Daily temperature range	database	°C
\bar{T}	Mean day temperature	database	°C
w_f	Wet day frequency	database	frequency
r_m	Mean value of rain	database	mm/month
r_{cv}	Coefficient of variance of rain	database	%
p_s	Percentage of sunshine per day	database	%
h_s	Relative humidity	database	%
d_f	Frost days per month	database	days/month
u_{ref}	Reference wind speed	database	m/s
Z	Elevation	database	m
S_N	Soil nitrogen content	database	g/m ²
S_C	Soil carbon content	database	g/m ²
θ_{fc}	Field capacity	database	mm
θ_{wp}	Wilting point	database	mm
P	Atmospheric partial pressure	variable	Pa
T	Day temperature	variable	°C
T_{min}	Minimum temperature	variable	°C
T_{max}	Maximum temperature	variable	°C
s	Slope of vapor pressure curve	variable	kPa/C
γ	Psychrometric constant	variable	kPa/C
e^A	Actual vapor pressure	variable	kPa
e^S	Saturation vapor pressure	variable	kPa
ρ_{air}	Density of air	variable	g/m ³
h_{vpd}	Saturation vapor pressure deficit	variable	kPa
Q_p	Photosynthetically active radiation	variable	$\mu\text{mol}/\text{m}^2\text{s}$
Q_0	Net radiation	variable	$\mu\text{mol}/\text{m}^2\text{s}$
F_i	Simulated precipitation at day i	variable	mm

Table 2: Photosynthesis sub-model.

Name	Description	Value C ₃	Value C ₄	Units
A_{max}	Maximum light saturated photosynthesis	variable	variable	$\mu\text{mol}/\text{m}^2\text{s}$
A_0	Gross photosynthetic rate	variable	variable	$\mu\text{mol}/\text{m}^2\text{s}$
A_n	Net photosynthetic rate	variable	variable	$\mu\text{mol}/\text{m}^2\text{s}$
A_0^b	Gross photosynthesis (bio-physical)	variable	variable	$\mu\text{mol}/\text{m}^2\text{s}$
A_n^b	Net photosynthesis (bio-physical)	variable	variable	$\mu\text{mol}/\text{m}^2\text{s}$
A_n^d	Net photosynthesis (diffusion)	variable	variable	$\mu\text{mol}/\text{m}^2\text{s}$
V_{max}	Maximum carboxylation rate	variable	variable	$\mu\text{mol}/\text{m}^2\text{s}$
A_R	Scaling factor for C ₄ photosynthesis	1	39/90	unitless
A_S	Scaling factor for V_{max}	2	2	unitless
R_{mLs}	Constant leaf level respiration rate	0.82	1.36	$\mu\text{mol}/\text{m}^2\text{s}$
c_a	Atmospheric partial pressure of CO ₂	38.1	38.1	Pa
c_i	Internal CO ₂ pressure (C ₃ only)	$0.7c_a$	—	Pa
c_i	Bundle sheath value (C ₄ only)	—	$8c_a$	Pa
K_c	Michaelis constant for CO ₂	variable	variable	Pa
K_o	O ₂ inhibition constant	variable	variable	Pa
τ	Fraction of RuBP to reaction of rubisco	variable	variable	prop
$f_{25}(T)$	Temperature function for K_c , K_o , τ	variable	variable	unitless
K_{25,K_c}	Constant for f_{25} for K_c	30	140	Pa
Q_{10,K_c}	Constant for f_{25} for K_c	2.1	2.1	Pa
K_{25,K_o}	Constant for f_{25} for K_o	30	34	Pa
Q_{10,K_o}	Constant for f_{25} for K_o	1.2	1.2	Pa
$K_{25,\tau}$	Constant for f_{25} for τ	2600	2600	Pa
$Q_{10,\tau}$	Constant for f_{25} for τ	0.57	0.67	Pa
O_i	Intercellular partial pressure of oxygen	21	21	kPa
Γ_*	CO ₂ compensation point	variable	variable	Pa
J_c	Rubisco limited assimilation rate	variable	variable	$\mu\text{mol}/\text{m}^2\text{s}$
J_e	Light limited assimilation rate	variable	variable	$\mu\text{mol}/\text{m}^2\text{s}$
J_s	Transport limited assimilation rate for C ₃	variable	—	$\mu\text{mol}/\text{m}^2\text{s}$
J_p	CO ₂ limited assimilation rate for C ₄	—	variable	$\mu\text{mol}/\text{m}^2\text{s}$
a	Leaf absorbance of incident flux	0.86	0.80	unitless
α	Intrinsic quantum yield of photosynthesis	0.08	0.067	unitless
κ	Initial slope of response of CO ₂	—	$0.7 \cdot 10^6$	$\mu\text{mol}/\text{m}^2\text{s}$
V_{max}^c	Initial estimation for V_{max}	0.8	0.4	$\mu\text{mol}/\text{m}^2\text{s}$
r	Respiration as fraction of V_{max}	0.015	0.025	prop
c_p	Specific heat of moist air	$1.013 \cdot 10^{-3}$	$1.013 \cdot 10^{-3}$	MJ/kgdegC
λ	Latent heat of air	2.45	2.45	MJ/kg

Table 3: Stomatal conductance sub-model.

Name	Description	Value C ₃	Value C ₄	Units
g_s	Leaf level stomatal conductance	variable	variable	$\mu\text{mol}/\text{m}^2\text{s}$
m	Empirical parameter for g_s	9	4	unitless
b	Empirical parameter for g_s	0.01	0.04	$\mu\text{mol}/\text{m}^2\text{s}$
g_b	Leaf level boundary layer conductance	variable	variable	m
c_s	Partial pressure of CO ₂ at leaf surface	variable	variable	Pa
D_L	Characteristic leaf dimension	0.02	0.005	m
\bar{H}	Mean vegetation height	1.5	1.5	m
$u(z)$	Wind at height z from ground level	variable	variable	m/s
z_d	Displacement height	$0.86\bar{H}$	$0.86\bar{H}$	m
z_0	Roughness length	$0.06\bar{H}$	$0.06\bar{H}$	m
z_{ref}	Reference height	10	10	m

Table 4: Biomass pools of a plant.

Name	Description	Value	Units
B_R	Live root biomass	variable	kg/plant
B_S	Live stem biomass	variable	kg/plant
B_L	Live leaf biomass	variable	kg/plant
B_{Ss}	Standing dead stem biomass	variable	kg/plant
B_{Ls}	Standing dead leaf biomass	variable	kg/plant
B_{Rd}	Dead root biomass	variable	kg/plant
B_{Sd}	Lying dead stem biomass	variable	kg/plant
B_{Ld}	Lying dead leaf biomass	variable	kg/plant

Table 5: Allometric constants and variables.

Name	Description	Value C ₃	Value C ₄	Units
H	Height of plant	variable	variable	m
H_1	Linear factor for height calculation	1.3	3.5	unitless
H_2	Exponent for height calculation	0.392	0.5	unitless
d_s	Stem diameter	variable	variable	cm
d_{s1}	Parameter to calculate stem diameter	2.797	—	unitless
d_{s2}	Parameter to calculate stem diameter	200	—	unitless
C	Canopy area of plant	variable	variable	m ²
γ_c	Ratio of canopy radius to height	0.37	0.4	prop
L	Leaf area index	variable	variable	unitless
A_{SL}	Specific leaf area	10	10.9	m ² /kg
D_{root}	Rooting depth	variable	variable	m
D_{mrd}	Maximum rooting depth	2	0.3	m
D_{soil}	Soil depth	2	2	m
D_{cyl}	Depth of cylindrical root	variable	variable	m
ρ_r	Density of root biomass	100	100	kg/m ³
r_r	Minimum root radius	0.015	0.005	m

Table 6: Canopy scaling.

Name	Description	Value	Units
Q_{sum}	Light received by a plant	variable	$\mu\text{mol}/\text{m}^2\text{s}$
$Q(l)$	Light distribution in canopy	variable	$\mu\text{mol}/\text{m}^2\text{s}$
Q_i	Light availability index of plants	variable	prop
k	Canopy extinction coefficient	0.5	unitless
θ_i	Soil moisture content in layer i	variable	mm
$G(\theta_i)$	Soil water availability in layer i	variable	%
$\beta(\theta_i)$	Soil moisture function for G_i	variable	%
d_i	Thickness of soil layer i	defined	m
G_w	Water availability index of plants	variable	%
A_c	Light stressed canopy photosynthesis	variable	$\mu\text{mol}/\text{m}^2\text{s}$
A_{cs}	Water and light stressed canopy photosynthesis	variable	$\mu\text{mol}/\text{m}^2\text{s}$
g_s^c	Canopy level stomatal conductance	variable	$\mu\text{mol}/\text{m}^2\text{s}$
g_b^c	Canopy boundary layer conductance	variable	$\mu\text{mol}/\text{m}^2\text{s}$
c_s^c	Canopy partial pressure of CO ₂	variable	Pa
K	Von Karman constant	0.41	unitless

Table 7: Respiration sub-model.

Name	Description	Value C ₃	Value C ₄	Units
β_N	Respiration rate for roots and stems	0.218	0.218	kg C/kg N
β_S	Fraction of sapwood in stems	2.5	15	%
β_R	Fraction of sapwood in roots	2.5	15	%
v_S	C to N ratio for stems	150	120	prop
v_R	C to N ratio for roots	60	120	prop
$f(T)$	Temperature function for respiration	variable	variable	unitless
σ	Growth respiration constant	0.35	0.35	prop
R_g	Growth respiration	variable	variable	$\mu\text{mol}/\text{m}^2\text{s}$
R_m	Total maintenance respiration	variable	variable	kg/d plant
R_{mL}	Leaf maintenance respiration	variable	variable	kg/d plant
R_{mS}	Stem maintenance respiration	variable	variable	kg/d plant
R_{mR}	Root maintenance respiration	variable	variable	kg/d plant

Table 8: Carbon allocation sub-model.

Name	Description	Value C ₃	Value C ₄	Units
C_Δ	Net carbon gain of plant	variable	variable	kg/d plant
a_R	Proportion of carbon allocated to roots	variable	variable	%
a_S	Proportion of carbon allocated to stem	variable	variable	%
a_L	Proportion of carbon allocated to leaf	variable	variable	%
a_{0R}	Not-limited carbon gain allocated to roots	0.35	0.4	%
a_{0S}	Not-limited carbon gain allocated to stem	0.35	0	%
a_{0L}	Not-limited carbon gain allocated to leaf	0.3	0.6	%
C_i	Limitation factor of photosynthesis	variable	variable	prop

Table 9: Phenology sub-model.

Name	Description	Value C ₃	Value C ₄	Units
A_{index}	Stress index controlling phenology	variable	variable	unitless
G_i	Water availability index for phenology	variable	variable	prop
T_i	Temperature index for phenology	variable	variable	prop
T_*	Threshold temperature for phenology	15	15	°C
d_{neg}	Counter for days with negative C balance	7	5	d
d_{pos}	Counter for days with positive C balance	10	7	d
ζ_L	Remaining leaf biomass after litter fall	0.1	0.1	prop

Table 10: Decomposition and mass turnover.

Name	Description	Value C ₃	Value C ₄	Units
ω_R	Longevity of root biomass	9125	384	d
ω_S	Longevity of stem biomass	9125	384	d
ω_L	Longevity of leaf biomass	451	417	d
ω_D	Longevity of dead biomass	1408	577	d
ξ_L	Standing to lying dead grass biomass	0	$7.5 \cdot 10^{-2}$	%

Table 11: Evapotranspiration and population properties.

Name	Description	Units
Υ	Treecover	prop
n_t	Number of trees	number
S	Size of study site	m ²
E_t	Total evapotranspiration	mm/day
E_t^s	Soil evapotranspiration	mm/day
E_t^p	Single plant evapotranspiration	mm/day
E_t^g	Total grass evapotranspiration	mm/day
E_t^t	Total tree evapotranspiration	mm/day

Table 12: Size of soil layers.

Name	Description	Value	Cumul.	Units
d_1	Layer S_1	5	5	cm
d_2	Layer S_2	5	10	cm
d_3	Layer S_3	10	20	cm
d_4	Layer S_4	10	30	cm
d_5	Layer S_5	10	40	cm
d_6	Layer S_6	20	60	cm
d_7	Layer S_7	20	80	cm
d_8	Layer S_8	20	100	cm
d_9	Layer S_9	25	125	cm
d_{10}	Layer S_{10}	25	150	cm
d_{11}	Layer S_{11}	25	175	cm
d_{12}	Layer S_{12}	25	200	cm

Table 13: Light competition.

Name	Description	variable	Units
e_1	Probability function for competitor tree	1.1	unitless
e_2	Probability function for competitor tree	1.5	unitless
e_3	Probability function for competitor tree	1000	unitless
Q_{comp}	Shading effect of competitor tree	variable	prop
Q_{grass}	Shading effect of grasses on trees	variable	prop
Q_{tree}	Shading effect of trees on grasses	variable	prop
Q_{dead}	Shading effect of dead grass	variable	prop
μ_c	Maximum effect of Q_{comp}	0.35	prop
μ_g	Maximum effect of Q_{grass}	0.25	prop
μ_t	Maximum effect of Q_{tree}	0.4	prop
μ_d	Maximum effect of Q_{dead}	0.5	prop
H_t	Height of target tree	variable	m
H_c	Height of competitor tree	variable	m
H_g	Height of grasses	variable	m

Table 14: Reproduction and mortality sub-model.

Name	Description	Value	Units
B_{seed}	Weight of tree seed	1	g
A_a	Minimum age of trees for seed production	10	years
ϕ_i	Seed production of tree i	variable	seeds
Φ	Seed production of all trees	variable	seeds
ϕ_{mort}	Mortality rate of seed per year	70	%
ϕ_{sprout}	Proportion of seed that sprouts per day	10	%
ϕ_{germ}	Germination probability of seed	25	%
d_{wet}	Number of wet days needed for germination	3	days
P_{carb}	Mortality rate: carbon deficiency	0.1	%
P_{comp}	Mortality rate: competitor	0.1	%
P_{frost}	Mortality rate: frost	0.1	%
P_{death}	Total mortality rate of trees	variable	%

Table 15: Fire sub-model.

Name	Description	Value	Units
I	Fire intensity	variable	kJ/s m
h	Heat yield of grass	16890	kJ/kg
c	Regression parameter	301	unitless
a_w	Regression parameter	119.7	unitless
Q_m	Heat of preignition	$2.6 \cdot 10^6$	J/g
Q_v	Heat of preignition	160749	J/g
B_F	Fuel biomass	variable	kg/m^2
B_{live}	Living fuel biomass	variable	kg
B_{dead}	Dead fuel biomass	variable	kg
θ_F	Fuel moisture	variable	%
θ_{live}	Moisture of living fuel biomass	variable	%
θ_{dead}	Moisture of dead fuel biomass	variable	%
θ_r	Drying of dead fuel biomass	0.95	prop
T	Days since litter fall	variable	days
i_1	Fire ignition probability function	0.08333	unitless
i_2	Fire ignition probability function	0.1	unitless
p_{fire}	Fire probability	1	%
$P_{topkill}$	Topkill probability of trees	variable	%
D_1	Regression parameter for topkill	4.3	unitless
D_2	Regression parameter for topkill	5.003	unitless
D_3	Regression parameter for topkill	0.004408	unitless
ψ_g	Grass survival after fire	0.1	%
ψ_{ts}	Tree stem survival after fire	1	%
ψ_{tl}	Tree leaf survival after fire	0.1	%

References

- Allen, R., Pereira, L., Raes, D., and M., S. (1998). *Crop evapotranspiration: Guidelines for computing crop water requirements*. Irrigation & Drainage, Paper 56, FAO, Rome, Italy.
- Arora, V. (2002). Modeling vegetation as a dynamic component in soil-vegetation-atmosphere transfer schemes and hydrological models. *Reviews of Geophysics*, **40**(2), 1006.
- Arora, V. (2003). Simulating energy and carbon fluxes over winter wheat using coupled land surface and terrestrial ecosystem models. *Agricultural and Forest Meteorology*, **118**, 21–47.
- Arora, V. and Boer, G. (2005). A parameterization of leaf phenology for the terrestrial ecosystem component of climate models. *Global Change Biology*, **11**, 39–59.
- Ball, J., Woodrow, I., and Berry, J. (1987). *Progress in Photosynthesis Research*, chapter A model predicting stomatal conductance and its contribution to the control of photosynthesis under different environmental conditions, pages 221–224. Nijhoff, Dordrecht.
- Bonan, G. B., Levis, S., Sitch, S., Vertenstein, M., and Oleson, K. W. (2003). A dynamic global vegetation model for use with climate models: concepts and description of simulated vegetation dynamics. *Global Change Biology*, **9**(11), 1543–1566.
- Bond, W. J., Maze, K., and Desmet, P. (1995). Fire life-histories and the seeds of chaos. *Ecoscience*, **2**(3), 252–260.
- Case, T. J. (2000). *An Illustrated Guide to Theoretical Ecology*. Oxford University Press.
- Chave, J. (1999). Study of structural, successional and spatial patterns in tropical rain forests using troll, a spatially explicit forest model. *Ecological Modelling*, **124**(2-3), 233–254.
- Cheney, P. and Sullivan, A. (1997). *Grassfires: Fuel, Weather and Fire Behaviour*. CSIRO Publishing, Collingwood, Australia.
- Collatz, G., Ball, J., Grivet, C., and Berry, J. (1991). Physiological and environmental regulation of stomatal conductance, photosynthesis and transpiration: a model that includes a laminar boundary layer. *Agriculture and Forest Meteorology*, **54**, 107–136.

- Collatz, G., Ribas-Carbo, M., and Berry, J. (1992). Coupled photosynthesis-stomatal conductance model for leaves of C₄ plants. *Australian Journal of Plant Physiology*, **19**, 519–538.
- Cramer, W., Bondeau, A., Woodward, F. I., Prentice, I. C., Betts, R. A., Brovkin, V., Cox, P. M., Fisher, V., Foley, J. A., Friend, A. D., Kucharik, C., Lomas, M. R., Ramankutty, N., Sitch, S., Smith, B., White, A., and Young-Molling, C. (2001). Global response of terrestrial ecosystem structure and function to CO₂ and climate change: results from six dynamic global vegetation models. *Global Change Biology*, **7**(4), 357–373.
- DeLucia, E. H., Drake, J. E., Thomas, R. B., and Gonzalez-Meler, M. (2007). Forest carbon use efficiency: is respiration a constant fraction of gross primary production? *Global Change Biology*, **13**(6), 1157–1167.
- Farquhar, G. D., Caemmerer, S. V., and Berry, J. A. (1980). A biochemical-model of photosynthetic CO₂ assimilation in leaves of C₃ species. *Planta*, **149**(1), 78–90.
- Friedlingstein, P., Joel, G., Field, C. B., and Fung, I. Y. (1999). Toward an allocation scheme for global terrestrial carbon models. *Global Change Biology*, **5**(7), 755–770.
- Gill, R. A. and Jackson, R. B. (2000). Global patterns of root turnover for terrestrial ecosystems. *New Phytologist*, **147**(1), 13–31. 2056.
- Givnish, T. J. (2002). Adaptive significance of evergreen vs. deciduous leaves: Solving the triple paradox. *Silva Fennica*, **36**(3), 703–743.
- Global Soil Data Task Group (2000). *Global Gridded Surfaces of Selected Soil Characteristics (International Geosphere-Biosphere Programme - Data and Information System)*. Data set. Available on-line [<http://www.daac.ornl.gov>] from Oak Ridge National Laboratory Distributed Active Archive Center, Oak Ridge, Tennessee, U.S.A.
- Hély, C., Bremond, L., Alleaume, S., Smith, B., Sykes, M. T., and Guiot, J. (2006). Sensitivity of African biomes to changes in the precipitation regime. *Global Ecology and Biogeography*, **15**(3), 258–270.
- Hickler, T., Prentice, I. C., Smith, B., Sykes, M. T., and Zaehle, S. (2006). Implementing plant hydraulic architecture within the LPJ dynamic global vegetation model. *Global Ecology and Biogeography*, **15**(6), 567–577.
- Higgins, S., Bond, W., Trollope, W., and Williams, R. (2008). Physically motivated empirical models for the spread and intensity of grass fires. *International Journal of Wildland Fire*, **17**, 595–601.

- Higgins, S. I., Bond, W. J., and Trollope, W. S. (2000). Fire, resprouting and variability: a recipe for grass-tree coexistence in savanna. *Journal of Ecology*, **88**, 213–229.
- Higgins, S. I., Bond, W. J., February, E. C., Bronn, A., Euston-Brown, D. I. W., Enslin, B., Govender, N., Rademan, L., O'Regan, S., Potgieter, A. L. F., Scheiter, S., Sowry, R., Trollope, L., and Trollope, W. S. W. (2007). Effects of four decades of fire manipulation on woody vegetation structure in savanna. *Ecology*, **88**(5), 1119–1125.
- Hoffmann, W. A. and Solbrig, O. T. (2003). The role of topkill in the differential response of savanna woody species to fire. *Forest Ecology and Management*, **180**, 273–286.
- House, J., Archer, S., Breshears, D., and NCEAS-Tree-Grass-Interaction-Participants (2003). Conundrums in mixed woody-herbaceous plant systems. *Journal of Biogeography*, **30**, 1763–1777.
- Hovestadt, T., Yao, P., and Linsenmair, E. (1999). Seed dispersal mechanisms and the vegetation of forest islands in a West African forest-savanna mosaic (Comoé National Park, Ivory Coast). *Plant Ecology*, **144**, 1–25.
- Huntley, B. and Walker, B. (1982). *Ecology of Tropical Savannas*. Springer-Verlag Berlin.
- IPCC (2007). *Climate Change 2007: The Physical Science Basis. Contribution of Working Group I to the Fourth Assessment Report of the Intergovernmental Panel on Climate Change*. Cambridge University Press, Cambridge, United Kingdom and New York, NY, USA.
- Jolly, W. M. and Running, S. W. (2004). Effects of precipitation and soil water potential on drought deciduous phenology in the kalahari. *Global Change Biology*, **10**(3), 303–308.
- Jones, H. (1992). *Plants and microclimate: a quantitative approach to environmental plant physiology*. 2nd edn. Cambridge University Press.
- Lüdeke, M., Badeck, F., Otto, R., Häger, C., Dönges, S., Kindermann, J., Würth, G., Lang, T., Jäkel, U., Klaudius, A., Range, P., Habermehl, S., and Kohlmaier, G. (1994). The Frankfurt Biosphere Model. A global process oriented model for the seasonal and longterm CO₂ exchange between terrestrial ecosystems and the atmosphere. Part 1: Model description and illustrating results for the vegetation types cold deciduous and boreal forests. *Climate Research*, **4**, 143–166.

- Moorcroft, P. R., Hurtt, G. C., and Pacala, S. W. (2001). A method for scaling vegetation dynamics: The ecosystem demography model (ED). *Ecological Monographs*, **71**(4), 557–585.
- New, M., Lister, D., Hulme, M., and Makin, I. (2002). A high-resolution data set of surface climate over global land areas. *Climate Research*, **21**(1), 1–25.
- Ronda, R. J., de Bruin, H. A. R., and Holtslag, A. A. M. (2001). Representation of the canopy conductance in modeling the surface energy budget for low vegetation. *Journal of Applied Meteorology*, **40**(8), 1431–1444.
- Sankaran, M., Jayashree, R., and Hanan, N. P. (2004). Tree-grass coexistence in savannas revisited - insights from an examination of assumptions and mechanisms invoked in existing models. *Ecology Letters*, **7**, 480–490.
- Sankaran, M., Hanan, N. P., Scholes, R. J., Ratnam, J., Augustine, D. J., Cade, B. S., Gignoux, J., Higgins, S. I., Roux, X. L., Ludwig, F., Ardo, J., Banyikwa, F., Bronn, A., Bucini, G., Caylor, K. K., Coughenour, M. B., Diouf, A., Ekaya, W., Feral, C. J., February, E. C., Frost, P. G. H., Hiernaux, P., Hrabar, H., Metzger, K. L., Prins, H. H. T., Ringrose, S., Sea, W., Tews, J., Worden, J., and Zambatis, N. (2005). Determinants of woody cover in African savannas. *Nature*, **438**(7069), 846–849.
- Sarmiento, G. (1984). *The Ecology of Neotropical Savannas*. Harvard University Press, Cambridge, MA.
- Sato, H., Itoh, A., and Kohyama, T. (2007). SEIB-DGVM: A new dynamic global vegetation model using a spatially explicit individual-based approach. *Ecological Modelling*, **200**(3-4), 279–307.
- Schaphoff, S., Lucht, W., Gerten, D., Sitch, S., Cramer, W., and Prentice, I. C. (2006). Terrestrial biosphere carbon storage under alternative climate projections. *Climatic Change*, **74**(1-3), 97–122.
- Scheffer, M., Baveco, J., DeAngelis, D., Rose, K., and van Nes, E. (1995). Super-individuals a simple solution for modelling large populations on an individual basis. *Ecological Modelling*, **80**(2-3), 161–170.
- Scheiter, S. and Higgins, S. (2007). Partitioning of root and shoot competition and the stability of savannas. *American Naturalist*, **170**(4), 587–601.
- Scholes, R. and Walker, B. (1993). *An African Savanna-Synthesis of the Nylsvley study*. Cambridge University Press.

- Scholes, R. J. and Archer, S. R. (1997). Tree-grass interactions in Savannas. *Annual Review of Ecology, Evolution, and Systematics*, **28**, 517–544.
- Schulze, E. D., Kelliher, F. M., Körner, C., Lloyd, J., and Leuning, R. (1994). Relationships among maximum stomatal conductance, ecosystem surface conductance, carbon assimilation rate, and plant nitrogen nutrition: A global ecology scaling exercise. *Annual Review of Ecology and Systematics*, **25**, 629–662.
- Sellers, P., Berry, J., Collatz, G., Field, C., and Hall, F. (1992). Canopy reflectance, photosynthesis, and transpiration. III. a reanalysis using improved leaf models and a new canopy integration scheme. *Remote Sensing of Environment*, **42**, 187–216.
- Shabanov, N. V., Knyazikhin, Y., Baret, F., and Myneni, R. B. (2000). Stochastic modeling of radiation regime in discontinuous vegetation canopies. *Remote Sensing of Environment*, **74**(1), 125–144.
- Sitch, S., Smith, B., Prentice, I. C., Arneth, A., Bondeau, A., Cramer, W., Kaplan, J. O., Levis, S., Lucht, W., Sykes, M. T., Thonicke, K., and Venevsky, S. (2003). Evaluation of ecosystem dynamics, plant geography and terrestrial carbon cycling in the LPJ dynamic global vegetation model. *Global Change Biology*, **9**(2), 161–185.
- Thonicke, K., Venevsky, S., Sitch, S., and Cramer, W. (2001). The role of fire disturbance for global vegetation dynamics: coupling fire into a dynamic global vegetation model. *Global Ecology and Biogeography*, **10**(6), 661–677.
- Thornley, J. H. M. and Cannell, M. G. R. (2000). Modelling the components of plant respiration: Representation and realism. *Annals of Botany*, **85**(1), 55–67.
- Tilman, D. (1988). *Plant Strategies and the Dynamics and Structure of Plant Communities*. Princeton University Press.
- Tjoelker, M. G., Oleksyn, J., and Reich, P. B. (2001). Modelling respiration of vegetation: evidence for a general temperature-dependent Q_{10} . *Global Change Biology*, **7**(2), 223–230.
- van Wilgen, B. and Scholes, R. (1997). *Fire in Southern African Savannas*, chapter The vegetation and fire regimes of southern hemisphere Africa, pages 27–46. Witwatersrand University Press, Johannesburg, South Africa.
- Venevsky, S., Thonicke, K., Sitch, S., and Cramer, W. (2002). Simulating fire regimes in human-dominated ecosystems: Iberian peninsula case study. *Global Change Biology*, **8**(10), 984–998.

- Walter, H. (1971). *Ecology of Tropical and Subtropical Vegetation*. Oliver and Boyd, Edinburgh.
- Wolfson, M. (1999). *Veld management in South Africa*, chapter The response of forage plants to defoliation: Grasses, pages 91–103. University of Natal, Scottsville.
- Woodward, F. and Smith, T. (1994a). *Ecophysiology of Photosynthesis*, chapter Predictions and measurements of the maximum photosynthetic rate, A_{max} , at the global scale, pages 491–509. Springer, Berlin.
- Woodward, F. and Smith, T. (1994b). Global Photosynthesis and Stomatal Conductance: Modelling the Controls by Soil and Climate. *Advances in Botanical Research*, **20**, 1–41.
- Woodward, F. I., Smith, T. M., and Emanuel, W. R. (1995). A global land primary productivity and phytogeography model. *Global Biogeochemical Cycles*, **9**(4), 471–490.